STUDY OF AC-DC CONVERTER-FED BATTERY CHARGING CIRCUITS

A Thesis Submitted

in Partial Fulfilment of the Requirements

for the Degree of

MASTER OF TECHNOLOGY

by

RAKESH BAIRATHI

to the

DEPARTMENT OF ELECTRICAL ENGINEERING
INDIAN INSTITUTE OF TECHNOLOGY, KANPUR

APRIL, 1993.

CERTIFICATE

It is certified that the work contained in the thesis entitled STUDY OF AC-DC CONVERTER-FED BATTERY CHARGING CIRCUITS by RAKESH BAIRATHI, has been carried out under my supervision, and that this work has not been submitted elsewhere for the award of a degree.

Dr. S. R. Doradla
Professor
Department of Electrical Engineering
Indian Institute of Technology
Kanpur - 208016
INDIA

April, 1993.

ABSTRACT

The performance study of three-phase, phase-controlled converters for battery charging circuits is carried out for both constant load current and pulsating load current conditions. It includes fully controlled, and half controlled symmetrical and asymmetrical converters. A generalized computer programme is developed to obtain input source and output load performance characteristics of phase-controlled converters for given circuit parameters. The characteristic curves $\omega L/R$ versus firing angle α are obtained for different values of normalized battery voltage. These curves enable the selection of minimum inductance to ensure continuous conduction. Additional inductance is, however, required to be added to the load circuit if the output current ripple is to be restricted within certain limits. Experimental oscillograms are also obtained for half controlled converters.

The performance of single-phase PWM ac-dc bridge converter using three PWM control schemes namely EPWM, SPWM and SEPWM is also studied. A working model of single-phase ac-dc bridge converter using MOSFETs is fabricated and tested with these PWM control techniques. The SEPWM combines the good features of EPWM and SPWM. It has, however, the drawback that the battery charging circuit needs to be initially started with SPWM. The transfer characteristics of SEPWM shows that it appears to be attractive for power supply applications.

ACKNOWLEDGEMENTS

I wish to record my deep sense of gratitude to Professor S.R. DORADLA for his guidance througput the course of this thesis.

I am grateful to Mr. G.S.N. Raju, Mr. V.R. Kanetkar and Mr. V.V. Deshpande, from whom I am greatly benefitted through discussions and with whom working was a pleasure.

I extend my thanks to Mr. Om Prakas Arora and Mr. R.S. Verma of Power Electronics Lab. for their timely help in providing components, test instruments etc.

My sincere thanks to Mr. L.S. Bajpai for devoting his time in typing this thesis.

RAKESH BAIRATHI

CONTENTS

CHAPTER - 1

INTRODUCTION

Ideally, the voltage supplied by the electric supply authority should be a perfect sinewave without any harmonics, at its nominal frequency of 50 Hz and at its nominal magnitude. But in practice, however, voltage can significantly dipout from the ideal condition due to the power line disturbances like overvoltage, undervoltage, outage, voltage spikes, chopped voltage waveform, harmonics and electromagnetic interference.

The effect of such power line disturbances on the sensitive equipment depends on the following factors :

(1) type and magnitude of the power line disturbance
(2) type of equipment.

When the magnitude of power line disturbances cross the limit, for which the equipment is designed, equipment may tripout. In case of critical applications where such a tripping or shutdown is unacceptable, the backup is provided by means of uninterruptible supplies (UPS).

For supplying very critical loads such as computers, life-care and medical equipment, telecommunication equipment, alarm systems and safety lighting it may be necessary to use UPS. These

provide protection against power outages, as well as voltage regulation during power line overvoltage and undervoltage conditions. They are also excellent in terms of suppressing incoming line transient and harmonic disturbances.

UPS essentially consits of rectifier, battery and inverters. In the normal mode of operation, the power to the inverter is drawn from the supply source via the rectifier. In case of line outage, the power comes from the battery bank.

There are many different types of battery systems. Of these, the conventional lead-acid batteries are commonly used for the UPS applications. In the normal mode when the line voltage is present the battery is trickle charged to offset the slight self-discharge by the battery. In the event of a line outage, the battery supplies the load. Once the line voltage is restored, the battery in UPS is brought back to its fully charged state. The usable life of all batteries is principally governed by the electrical conditions imposed upon them. The charging conditions are particularly important in this respect.

For supplying dc power to the inverter and for keeping the battery charged, the naturally commutated, phase-controlled thyristor circuits are in wide use to produce the necessary controlled dc power.

Many circuits are available for battery charging. They are based on either line commutation or forced commutation. But the circuit choice is affected by the need to maintain continuous

current with reduced ripples in the dc side and harmonic current in ac with improved input power factor.

The discontinuity of load current affects the shape of the load voltage waveform. This is highly undesirable for battery charging circuits. The supply current harmonics cause problem on the power system, including excessive neutral current, transformer hot spot, and instrumentation inaccuracies. They present problems to other loads connected on the same line bus to voltage distortion, and from radiated interference into communication circuits [1].

AC-DC converter is used as a front end converter in battery charger and uninterruptible power supplies. The commonly used line commutated thyristor converters in these applications suffer from three common drawbacks :

(i) they produce low frequency harmonics at the source terminals
(ii) operate at low power factor for large firing angles
(iii) their output voltage and current consists of ripple.

The harmonic contents decrease and the frequency of dominant harmonics increases as the converter pulse number is increased. At low power levels only two-pulse converters are used. In medium and high power applications, three-pulse, six-pulse and even twelve-pulse converters are used.

The low frequency harmonics in the output voltage deteriorate the performance of the load. When used in a closed loop system, with a linear controller, the transient response becomes sluggish, making it necessary to use more sophisticated controllers [2]. The magnitude of ripple and region of discontinuous conduction increases with the decrease in converter pulse number.

The solution for the improvement of power factor and reduction of harmonics on ac side, lies in the development of improved converter control methods and topologies. The methods employing line commutation consist of controlled flywheeling in fully controlled converters [3] - [6], sequence control [7] - [8], bias voltage control [9].

The methods employing line commutation have been preferred because of lower cost, weight, volume and improved reliability. They also allow substantial improvement in power factor and reduction in low frequency harmonics. But the improvement is far less than what could be achieved by employing forced commutation.

Forced commutation methods employ some kind of pulse width modulation (PWM). The PWM techniques employed in forced commutated thyristors converters are single pulse modulation [10], equal PWM [11] - [14], sinusoidal PWM [15] - [16], selective harmonics elimination [17] - [18] and current controlled PWM [19]. The sinusoidal PWM gives the highest power factor and least harmonic contents in the source current, the equal PWM has the least ripple

on the dc side. The selective harmonic elmination method is suitable where certain undesirable harmonics should be reduced to practically zero.

The availability of self-commutated devices and the improvement in their power handling capability has renewed interest in PWM ac-to-dc converters. As the gate turn-off thyristors (GTO) are now available with high power handling capacity [22], the GTO-based converters are prefered over forced commutated thyristor converters. The converter built using self-commutated devices do not require forced commutation circuits. Thus it saves the associated cost, weight, volume and loss. Because of higher switching speeds of power transistors and MOSFETs, the PWM converter can be operated at unity power factor, with negligible harmonics in source current and low ripple in the output current.

In Chapter 2 four converters are considered for detailed studies. These are three-phase fully controlled converter and three-phase half controlled converters. In the latter case, both symmetrical and asymmetrical configuration with one and two diodes are considered. Since these converters invariably form the front end converters in UPS, the studies presented in the thesis will be useful while designing the UPS system. Further, these converters are widely used as battery charging circuits. The studies relating to supply current harmonics, minimum inductance, ripple in the output current and voltage will be highly useful for such applications. Although these converters are widely used, the

comparative performance study of these converters is lacking in the literature. The half controlled converter circuits have been rigged up in the laboratory and experimental results are also obtained.

A generalized computer programme is developed which calculates the performance characteristics of converters for continuous constant and pulsating load current for any feasible load circuit parameters. Since the programme accepts the circuit data either in per unit or actual values, it is possible to obtain the performance for any circuit parametrs.

Chapter 3 deals with the pulsewidth modulation schemes. Single-phase ac to dc MOSFET-based converter is considered. Equal pulsewidth modulation (EPWM) and sinusoidal pulsewidth modulation (SPWM) control schemes are implemented. Another pulsewidth modulation scheme SEPWM is proposed in this thesis. It combines the good features of both EPWM and SPWM schemes. The performance studies are presented for the single-phase ac-dc converter with these three control schemes. The converter is simulated using SPICE simulation package before it is built in the laboratory. The experimental results from laboratory setup are obtained to verify the basic principles of pulsewidth modulation schemes presented in this thesis.

Lastly, Chapter 4 presents conclusions and scope of future work.

CHAPTER - 2

STUDY OF PHASE-CONTROLLED AC-DC CONVERTERS FOR BATTERY CHARGING CIRCUITS

2.1 INTRODUCTION

This chapter describes the circuit operation and performance of polyphase controlled converters. These circuits are used to convert polyphase ac voltage to a constant or adjustable dc voltage for battery charging circuits. In such converters thyristors are turned off by line commutation. When an incoming thyristor is turned on, it immediately reverse-biases the outgoing thyristor and turns it off. Phase-controlled converters are therefore simple and less expensive and are extensively used in industries.

There are a number of controlled rectifier circuits, some fed from a single-phase supply and others from a three-phase supply. The controlled rectifier circuits are classified as fully-controlled and half-controlled rectifiers. Fig. 2.1 shows some fully-controlled single-phase and three-phase converters. It includes bridge and midpoint configurations. Fig. 2.2 shows half-controlled single-phase and three-phase converters. The phase-controlled converters independent of pulse number can be representedby a simple line diagram. The line diagram for the fully-controlled and half-controlled rectifiers are shown in Fig. 2.3(a) and 2.3(b) respectively. V_o and I_o denote the average

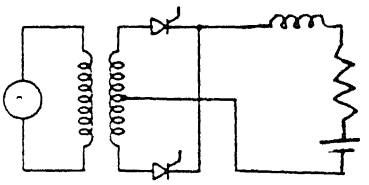

(a) 2 pulse midpoint rectifier

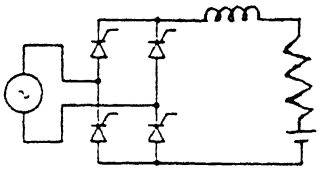

(b) 2 pulse bridge rectifier

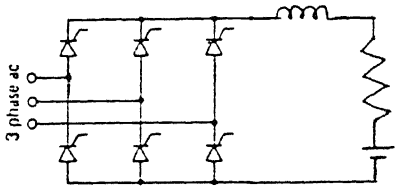

(c) 6-pulse bridge rectifier

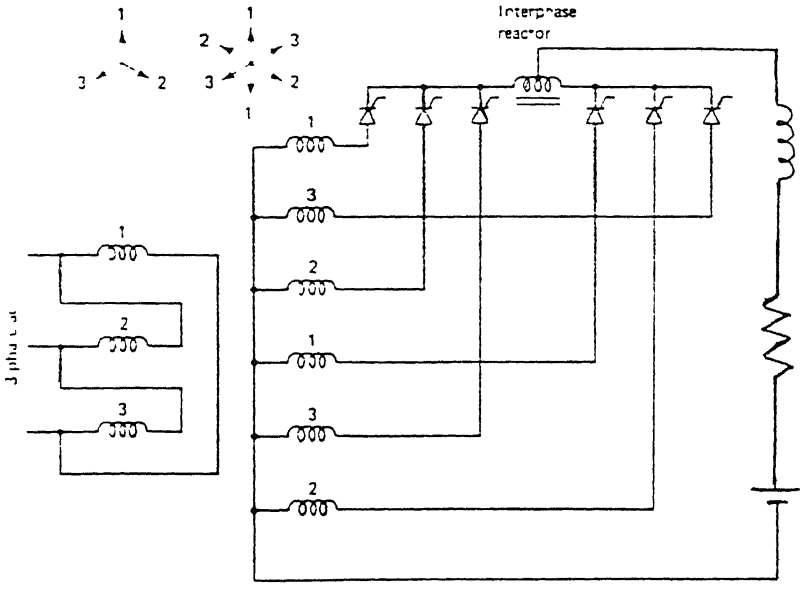

(d) 6-pulse midpoint rectifier with interphase reactor

Fig. 2.1 fully-controlled converters

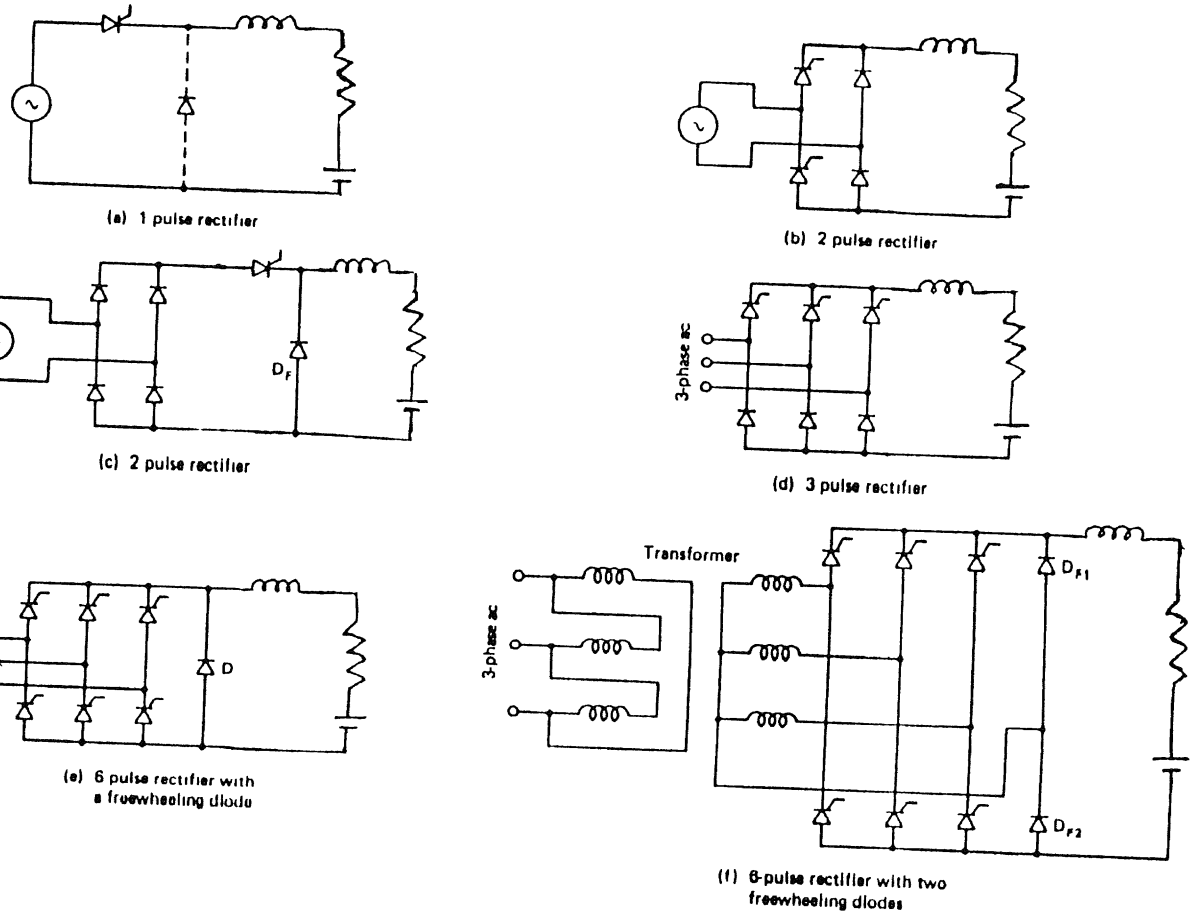

Fig. 2.2 half-controlled converters

values of the converter output voltage and load current respectively. The variation of V_o with the firing angle α, assuming continuous current conduction for fully controlled and half controlled converters are shown in Figs. 2.3(c) and (d) respectively. In case of half controlled converters the load voltage follows the segments of ac supply voltage or becomes zero under the conditions of continuous load current. When the load current becomes discontinuous, the output voltage comprises of segments of ac supply and battery voltages or zero voltage. The discontinuous load current is undesirable in battery charging circuits. An external load inductance is required to maintain continuous load current.

Phase-controlled converters are available in high voltage and current ratings. They are, therefore,used in high power applications. In applications such as UPS, thyirstor converters are widely used in the front end converters even in medium power levels. In this chapter the performance of the phase-controlled converters used for battery charging circuit have been studied. The following assumptions are made :

(i) the power switches are ideal

(ii) the source is ideal with no source inductance

(iii) the circuit is analyzed only for positive mean dc output voltage.

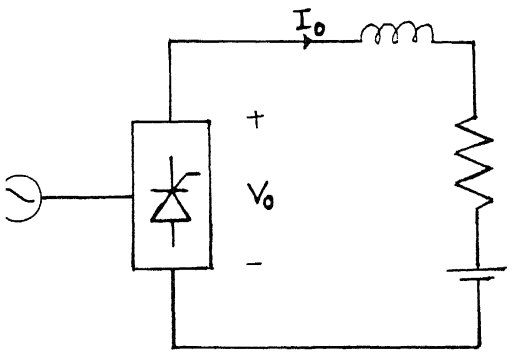

(a)

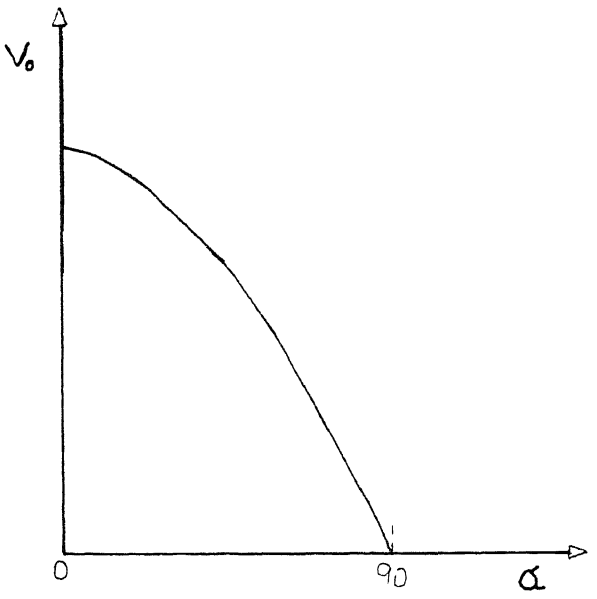

(c)

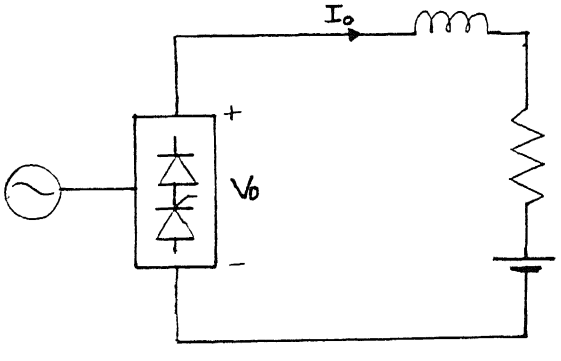

(b)

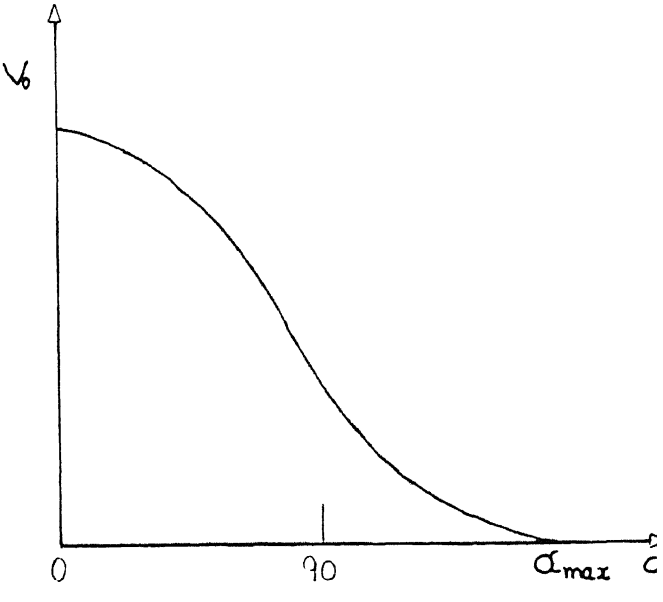

(d)

Fig. 2.3 *Line* - diagram and output characteristics of phase-controlled converters (a) Fully controlled converter (b) half controlled converter (c) output voltage of fully controlled converter (d) output voltage of half controlled converter.

2.2 BRIEF DESCRIPTION OF PHASE-CONTROLLED THREE-PHASE CONVERTERS

2.2.1 Fully Controlled Bridge Converter (FCC)

The circuit diagram of the commonly used three-phase fully controlled bridge is shown in Fig. 2.4. It uses six thyristors fired in sequence every 60°, and each thyristor conducts for 120° interval. The voltage across the output terminals of the bridge consists of dc voltage and ac ripples. The frequency of the lowest harmonic is six times the supply frequency at all trigger angles. The output voltage can be varied from its maximum positive value to maximum negative value by varying the firing angle from zero to 180°. Since only positive output voltage is considered, the firing angle is varied from 0° to 90°. The output voltage waveforms for different firing angles are shown in Fig. 2.5. The line-to-line voltage appears across the dc terminals of the converter.

2.2.2 Half Controlled Symmetrical Bridge Converter (HFC)

The circuit diagram of the symmetrical half controlled bridge converter is shown in Fig. 2.6. It uses three thyristors and three diodes, each thyristor-diode pair conducts for 120° duration. The thyristors are fired at every 120° interval. The output voltage waveform repeats for every 120°. For firing angle $\alpha > 60$, the output voltage comprises of line-to-line voltage for interval $(\frac{7\pi}{6} - \alpha)$ and zero value due to the conduction of both devices in the same lags for the interval of $(\alpha - \frac{\pi}{3})$. The output voltage can be varied from its maximum value to zero by varying

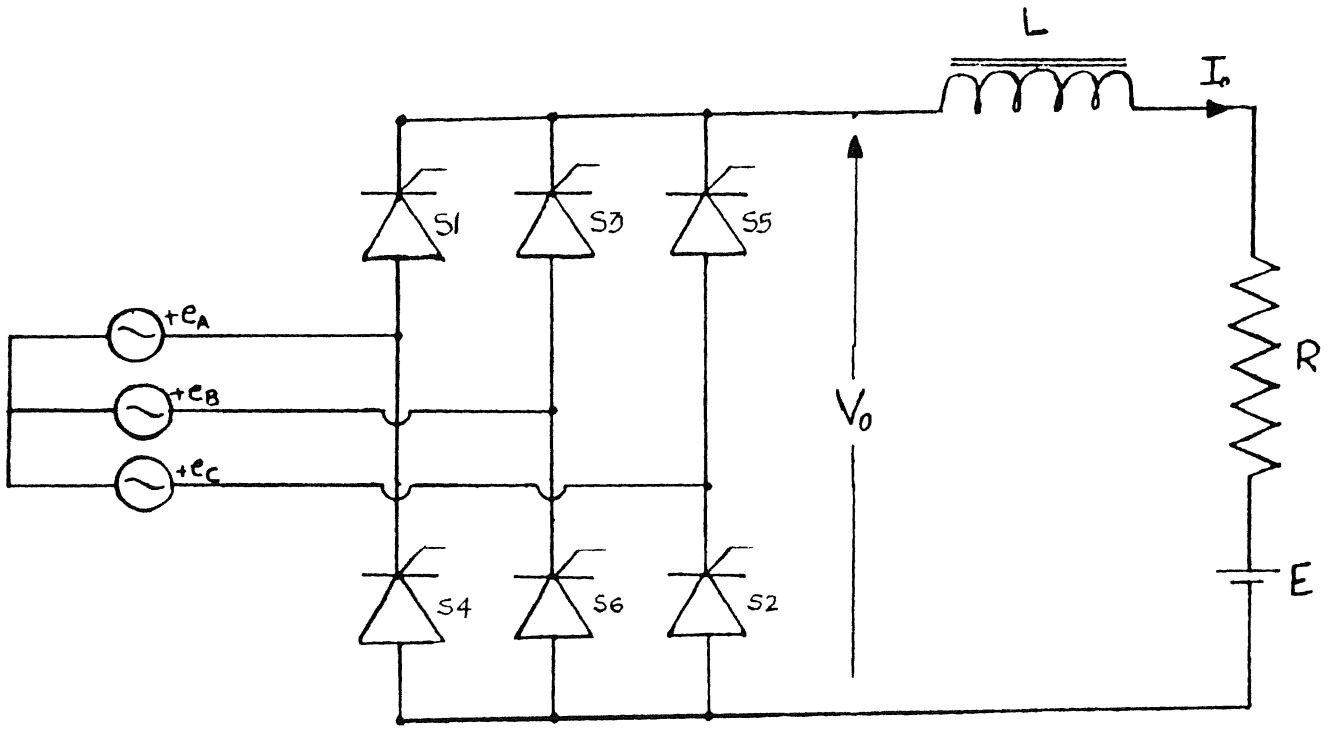

Fig. 2.4 three-phase fully-controlled converter

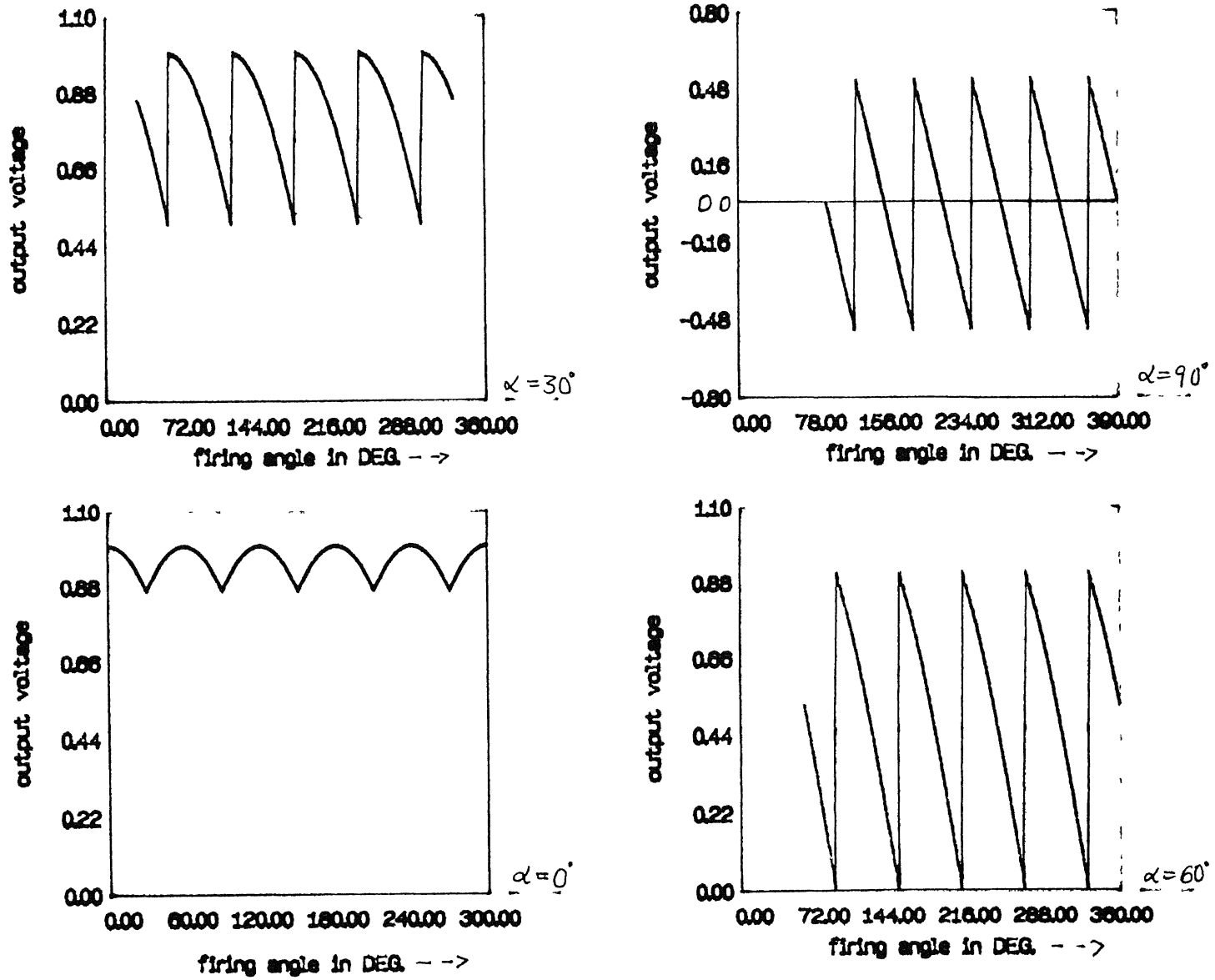

Fig. 2.5 output voltage waveforms associated with fully-controlled converter

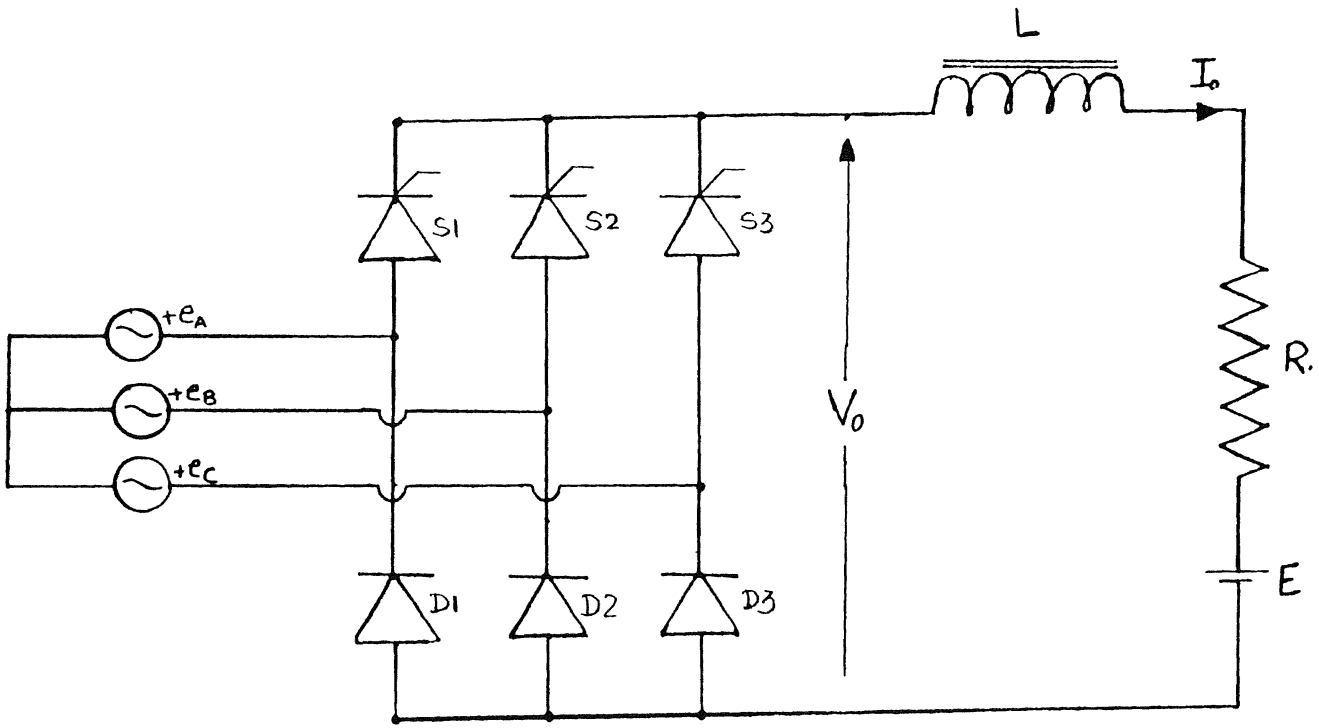

Fig. 2.6 three-phase half-controlled symmetrical converter

the firing angle from 0° to 180°. The output voltage waveforms for different firing angle are shown in Fig. 2.7.

2.2.3 Half-Controlled Asymmetrical Bridge Converters

(a) Asymmetrical bridge with one diode (HFAS-1D)

The circuit diagram of HSAS - 1D is shown in Fig. 2.8. The circuit operates as a fully controlled bridge converter when the firing angle $\alpha \leq 60$. The freewheeling diode begins to conduct for α greater than 60°. The control range of firing angle is from zero to 120°. Figure 2.9 shows the output voltage waveforms for different values of α. When the firing angle α is less than 60°, the output voltage consists of segments of ac line-to-line voltage. When the firing angle lies between 60° and 120°, the line-to-line voltage appears across the output terminal for the interval of $(\frac{2\pi}{3} - \alpha)$. During the interval $(\alpha - \frac{\pi}{3})$, the output voltage becomes zero due to the conduction of freewheeling diode.

(b) Asymmetrical Bridge with Diodes (HFAS-2D)

The Fig. 2.10 shows the asymmetrical bridge with two diodes. The supply neutral must be available for the asymmetrical configuration with two diodes. In this converter, the control range of firing angle is divided into three ranges. In the first range when the firing angle is less than 30°, the operation is very simialr to that of a fully-controlled converters. In this range the output voltage comprises of segments of ac line voltages. In the second range $30^{\circ} < \alpha \leq 90^{\circ}$, the output voltage

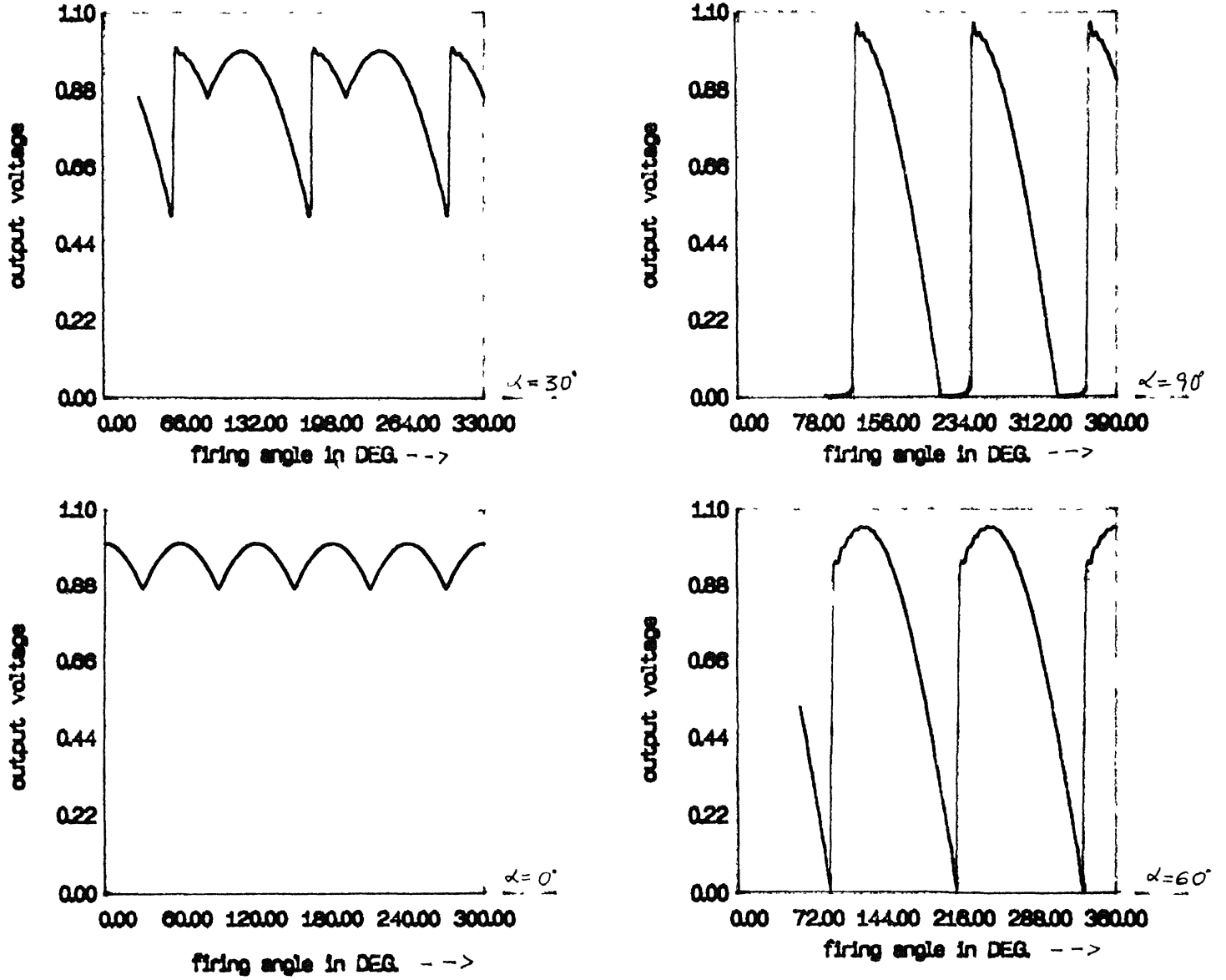

Fig. 2.7 output voltage waveforms associated with half-controlled symmetrical converter

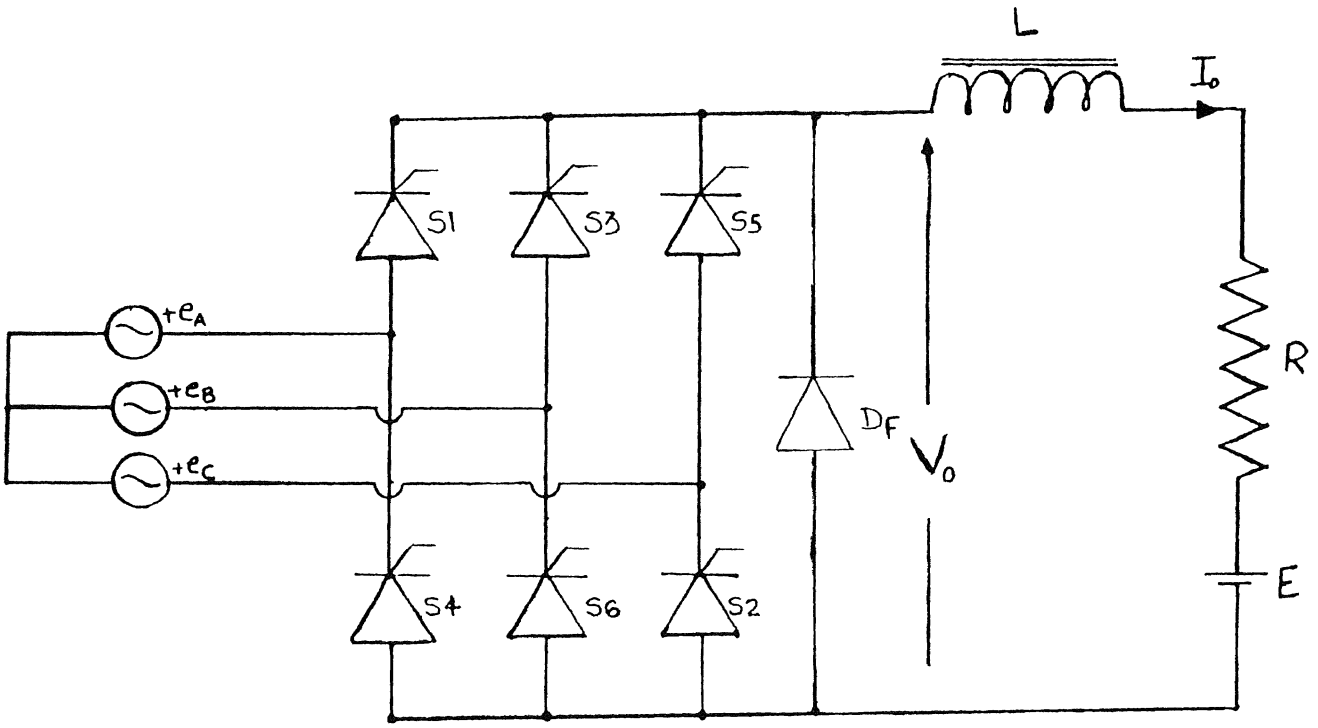

Fig. 2.8 three-phase half-controlled asymmetrical converter with one diode

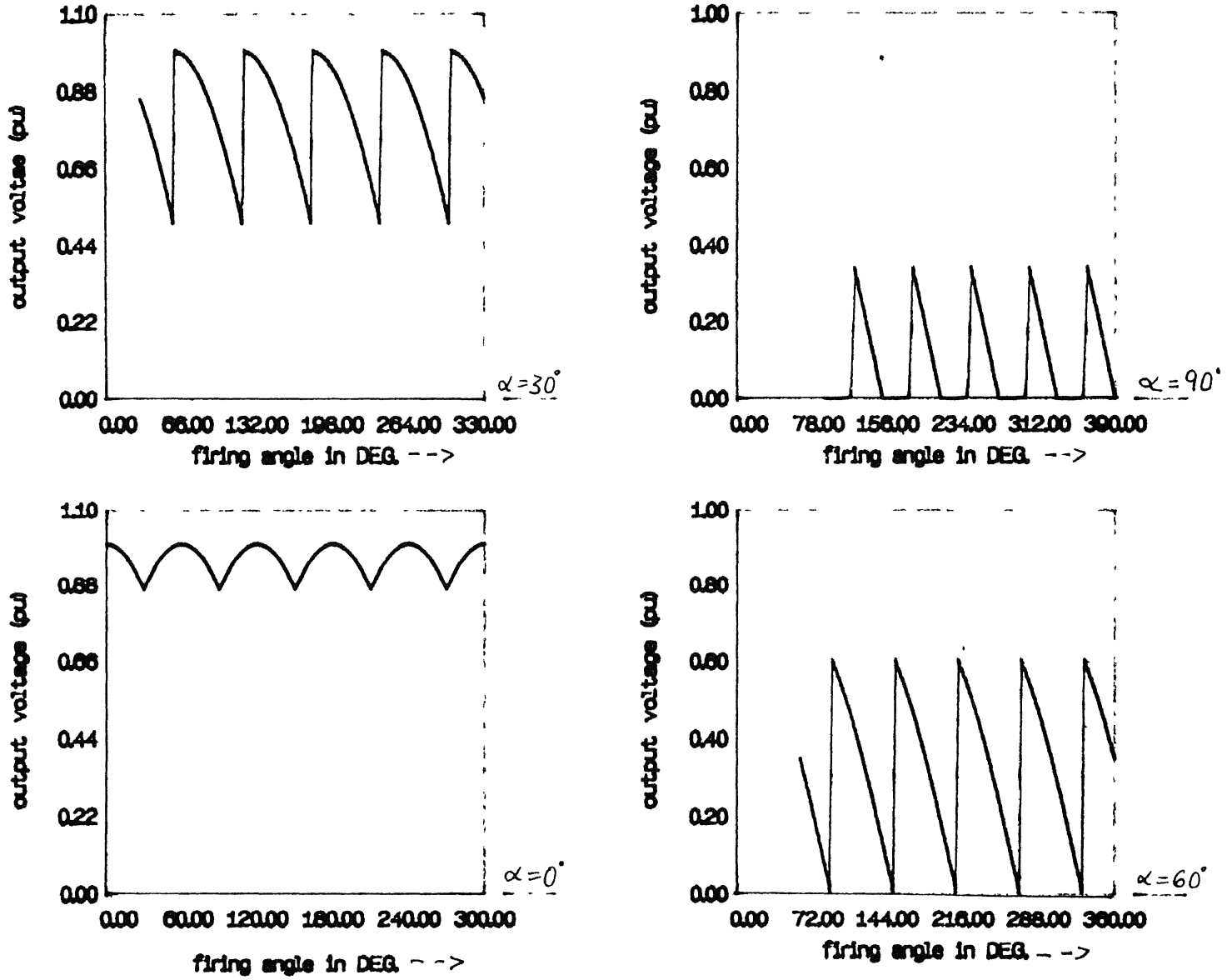

Fig. 2.9 output voltage waveforms associated with half-controlled asymmetrical converter with one diode

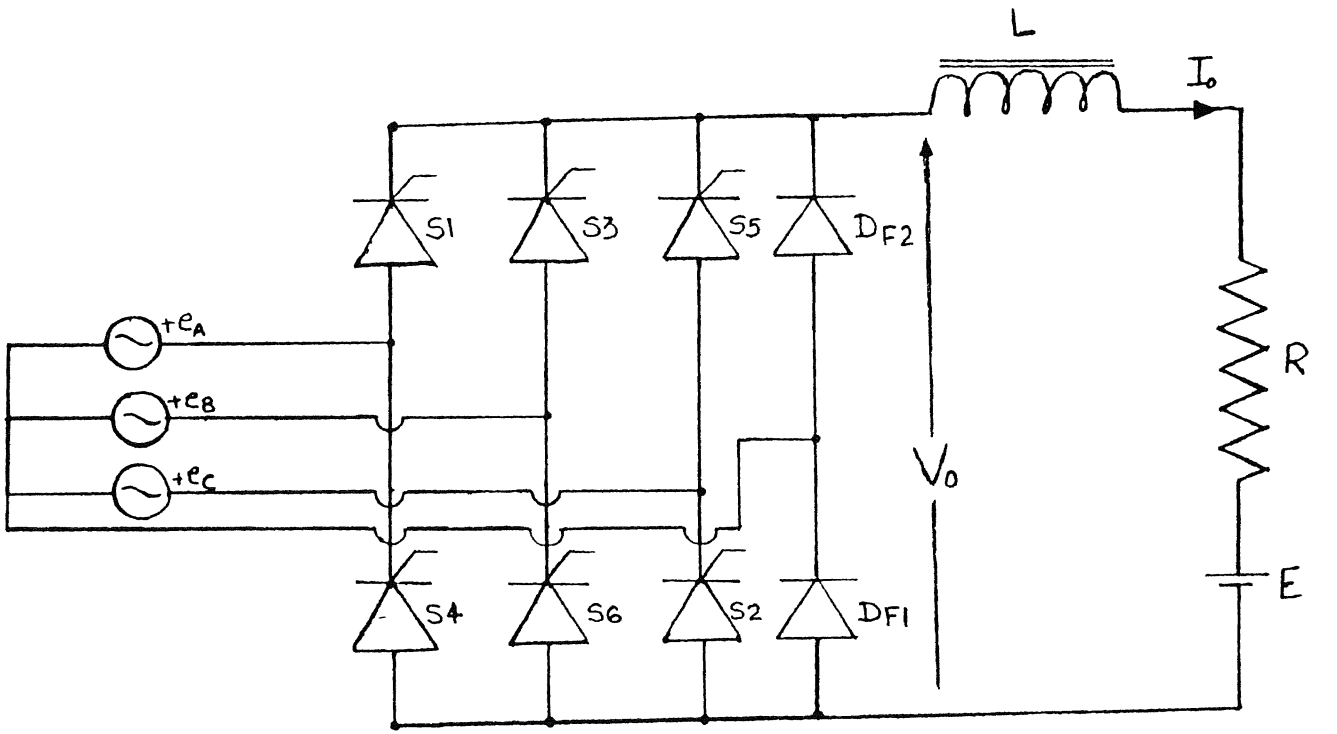

Fig. 2.10 three-phase half-controlled asymmetrical converter with two diodes

is made up of segments of line voltage and phase voltage. When the firing angle exceeds 90°, two diodes begin to conduct making the output voltage zero for $(\alpha - \frac{\pi}{2})$. Thus, it consists of segments of phase voltage and zero voltage intervals (Fig 2.11).

The output voltage waveform can be synthesized either by taking the appropriate segments of supply voltage or by summing the dc voltage and individual harmonic voltages. The output voltage waveforms shown in earlier figures are obtained by the latter method. The procedure is described in detail in the next section.

2.3 SIMULATION OF PERFORMANCE CHARACTERISTICS OF PHASE CONTROLLED CONVETER

A computer program in 'C' language is developed to calculate the performance characteristics of the three-phase phase-controlled converters. The programme is divided into four major sections :

(i) Subprogramme voltage :

The subprogramme voltage computes the harmonics present in the output voltage which are used to generate the output voltage waveform and output voltage ripple factor. The output voltage repeats after every $(2\pi/p)$ interval where p is the number of pulses present in 2π interval. Since it is periodic, it can be represented by general Fourier series, the coefficients of which are then evaluated to get the harmonic voltage present at the

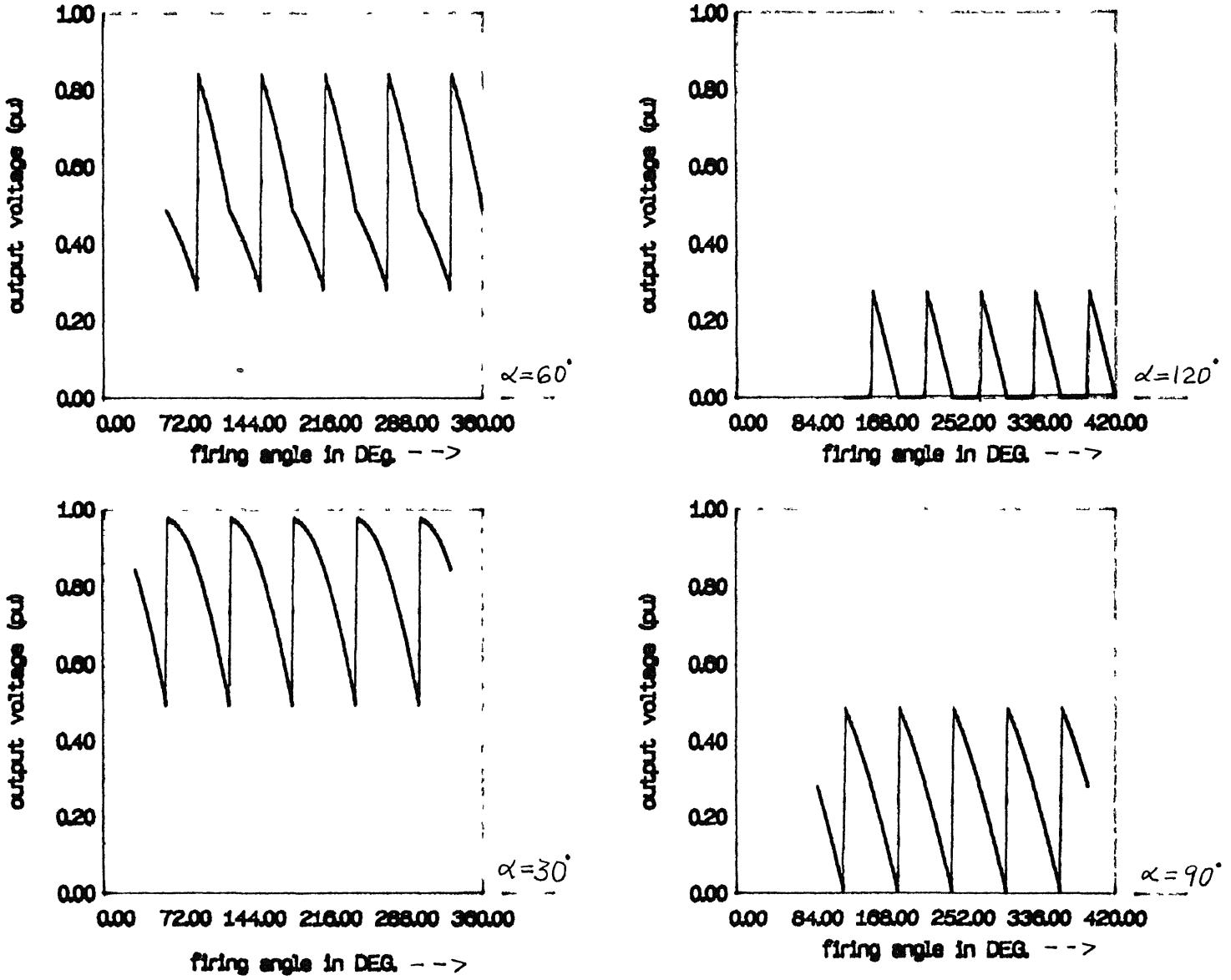

Fig. 2.11 output voltage waveforms associated with half-controlled asymmetrical converter with two diodes

output terminals. The instantaneous dc terminal voltage of a converter is synthesized from the summation of individual harmonic voltages together with the dc average voltage.

To evaluate the coefficients of the Fourier series for input voltage segment, that appears across the output terminals, ROMBERG integration method is used (Appendix A). The method of computation of output voltage waveform is shown in Fig. 2.12.

(ii) Subprogramme continuity :

The converter may operate in continuous current mode or discontinuous current mode depending on the circuit parameters. This subprogramme determines the mode of operation of converter for the given circuit data.

The equations used by this subprogramme are given in Appendix B. The flow diagram of subprogramme is shown in Fig. 2.13. This subprogramme calculates output current ripple and average output current. It also generates the output current waveform.

(iii) Subprogramme current :

This subprogramme computes the harmonics present in input current which are used to calculate input power factor, input current harmonic factor and to generate input current waveform. The line current which is equal to load current is obtained by keeping track of the turning-on and turning-off of thyristors and conduction of diodes. The normalized current equations for the four converters are given in Appendix B.

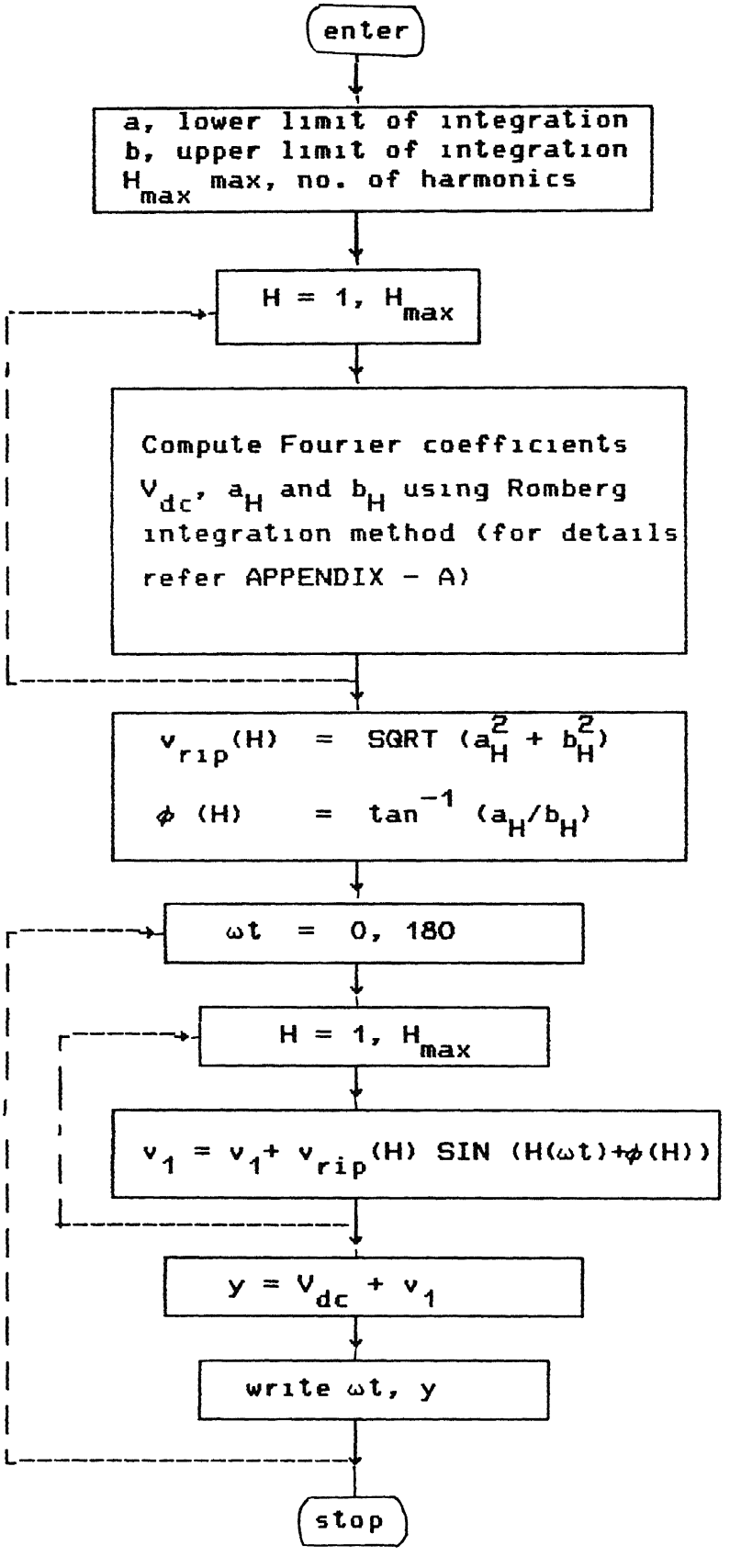

Fig. 2.12 Flow diagram for computation of output voltage

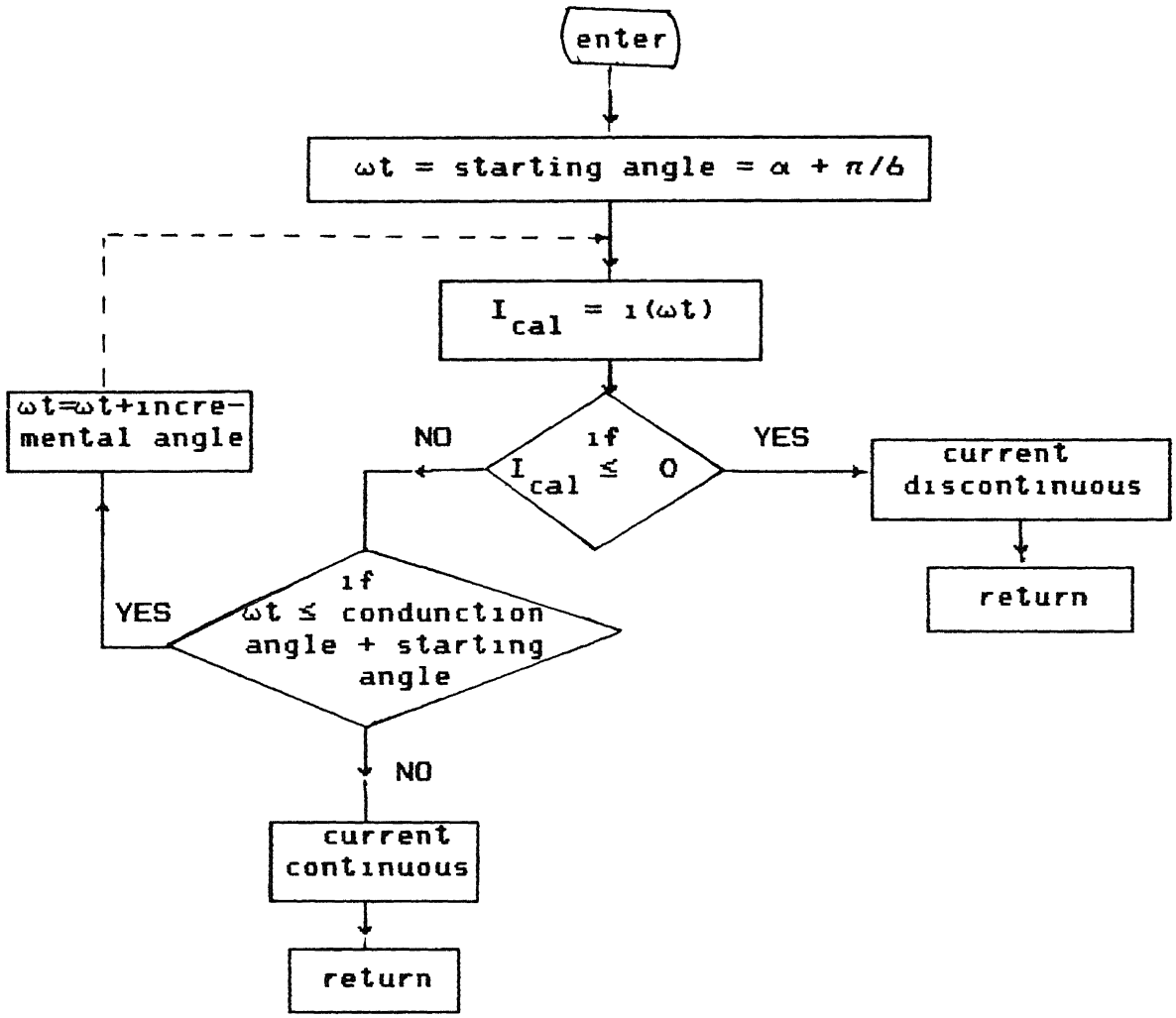

Fig. 2.13 Flow diagram for determination of continuity of load current.

(iv) Subprogramme inductance :

To operate the converter always in continuous current mode, the load circuit requires critical value of inductance which depends on the passive load, battery voltage and the firing angle. The normalized current equations given in Appendix B are used to obtain the value of inductance which is just sufficient to maintain continuous load current. The flow diagram of subprogramme inductance is shown in Fig. 2.14.Since the programme takes care of per unit as well as real values of the circuit parameters, so there is flexibility in feeding the circuit data to the programme. The following two inputs are required by the programme :

(a) Input voltage(s)

This data can be fed in two ways (a) actual values of phase voltage (rms) and battery voltage or (b) ratio of battery voltage to ac line-to-line voltage (peak) (m).

(b) Load parameter(s)

Load parameters can be fed in two ways (a) actual values of resistance and inductance of the load circuit or (b) load angle ϕ.

2.4 PERFORMANCE EVALUATION OF PHASE-CONTROLLED CONVERTERS

The performance of phase-controlled converters is studied in view of their application for front-end converter in UPS in general and battery charging circuit in particular. In the latter

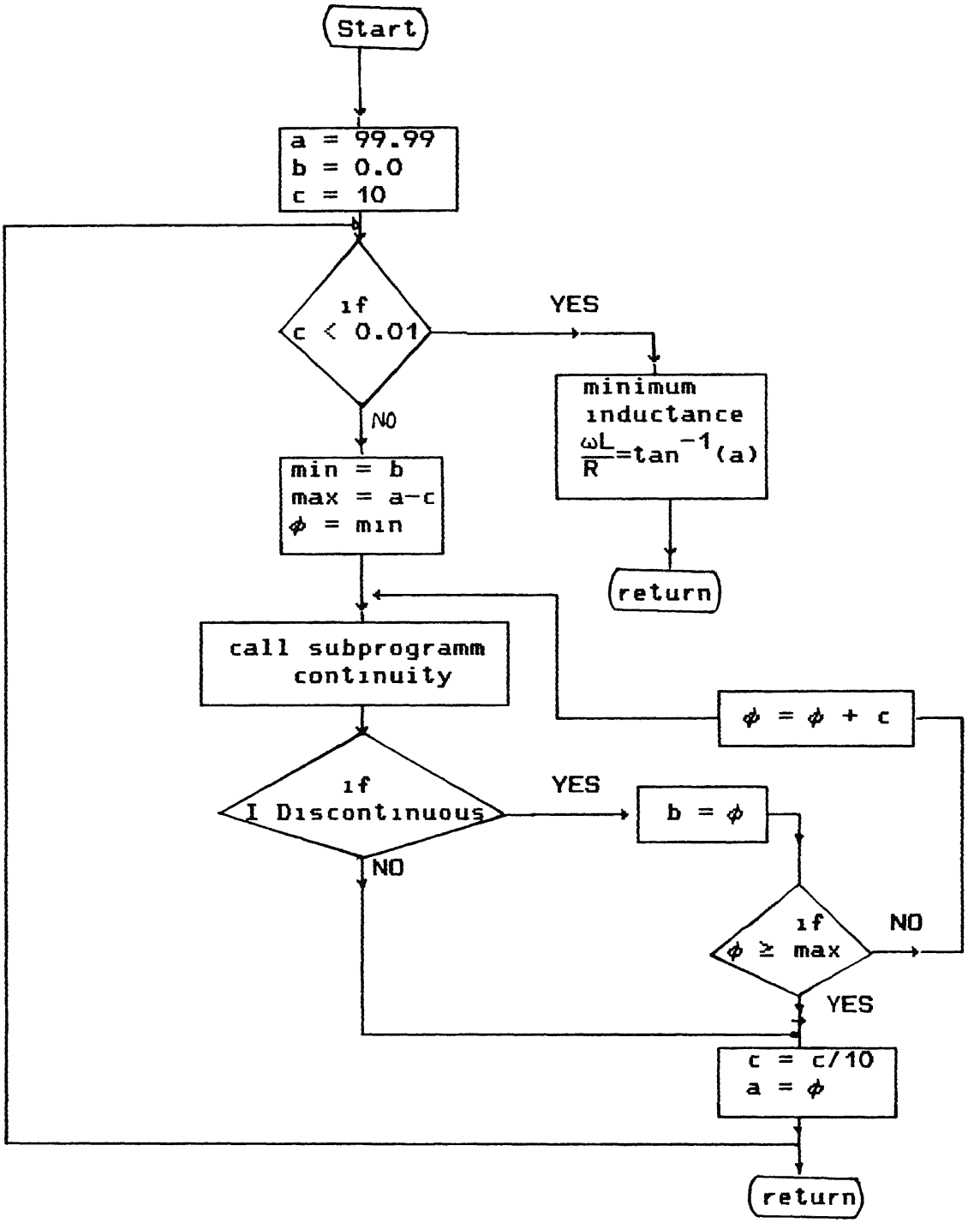

Fig. 2.14 Flow diagram for computing the minimum inductance.

application, the discharged battery is brought back to its fully charged state by initially charging the battery at a constant charging current. This causes the battery terminal voltage to increase to its trickle charge voltage level. Once the trickle charge voltage level is reached, the voltage applied is kept constant as shown in Fig. 2.15. The charging current finaly decreases to the trickle charge current and stays at that level. Therefore, the converter required for battery charging circuit must be capable of supplying fairly continuous current with controlled output dc voltage.

In phase-controlled converter with continuous current operation, the mean value of dc terminal voltage depends only upon the converter firing angle. With discontinuous current operation, on the other hand, the mean value of the dc terminal voltage depends upon both the firing angle and the load. The ac ripple current in the dc circuit is controlled by Q factor of the load circuit.

2.4.1 Performance Parameters

The parameters which evaluate the performance of the converters used for battery charging circuit are described below :

(i) Output voltage variation :

This factor indicates the controllability of the dc voltage which is important factor for the charger since the output voltage is increased with the increase in voltage of the charging battery.

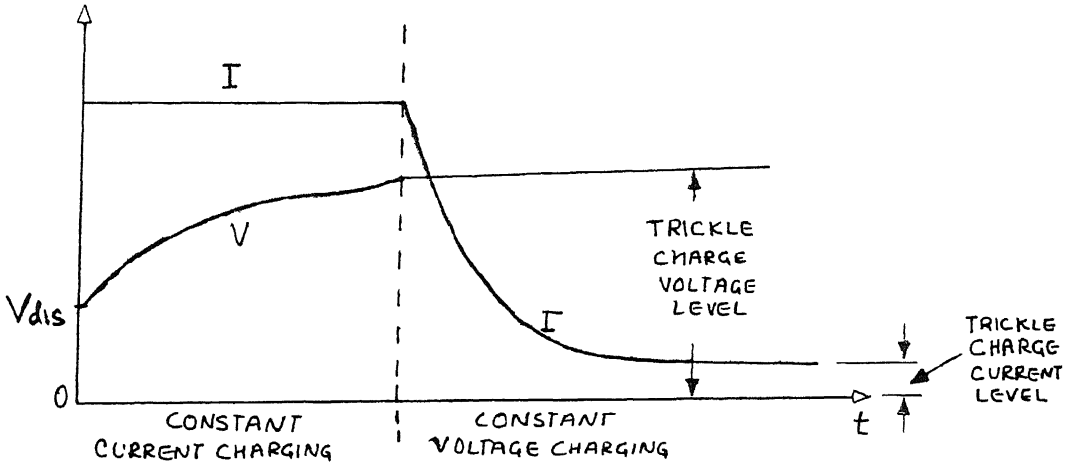

Fig. 2.15 Charging of batteryt after a line-outage causes battery discharge.

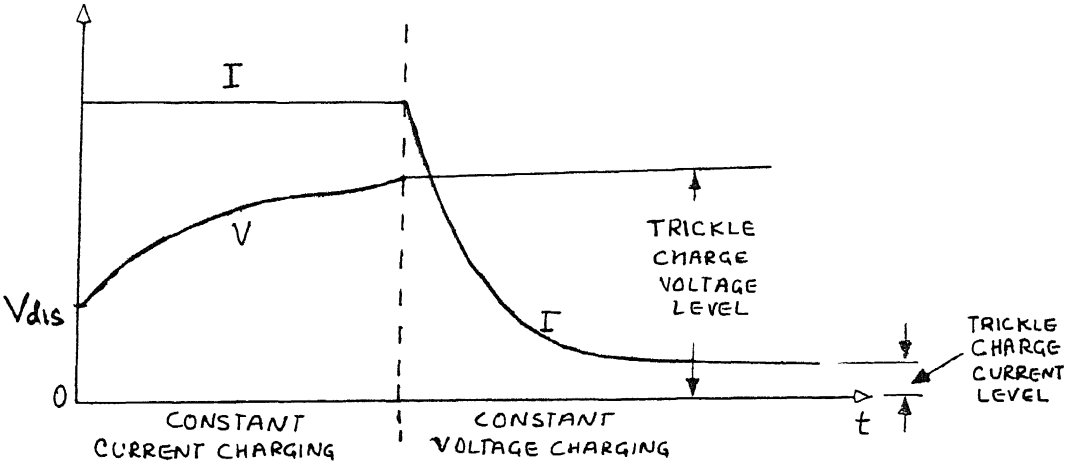

Fig. 2.15 Charging of batteryt after a line-outage causes battery discharge.

(ii) Output voltage ripple factor :

It is a measure of waviness of output voltage. It is also important from the point that the large ripple voltage may result in discontinuous load current which is undesirable in battery charging operation.

(iii) Output current ripple :

The need to study output current ripple arises when the load current is not constant. The low current ripple is desired in charging a battery. Large ripple may result in undesirable discontinuous load current.

(iv) Critical inductance :

This is the minimum inductance that will make the load current just continuous. The selection of the critical inductance depends on the trickle charge voltage of battery, firing angle and the minimum trickle current.

The converters used for battery charging are connected to the ac supply source. These converters affect the performance of the supply source. The performance parameters in the supply source are :

(i) Input displacement factor :

This is defined as the cosine of the input displacement angle ϕ which is the angular displacement between the fundamental component of the ac supply current and the phase voltage. The

input displacement factor is also known as the fundamental power factor. The displacement angle depends upon the firing angle α.

$$DF = \cos \phi$$

(ii) Input power factor :

It is the ratio of the total mean input power to the total rms apparent power input to the converter

$$PF = \frac{V I_1 \cos\phi}{V_{rms} I_{rms}}$$

Since $V = V_{rms}$, $PF = \left(\frac{I_1}{I_{rms}}\right) \cos \phi$

(iii) Input current harmonics :

The harmonic spectra in the ac line current depends on the type of the converter and the firing angle. As the amplitudes of harmonics increase, the size of the input transformer and other apparatus increases. Losses in the input apparatus to the converter also increase.

(iv) Input current harmonic factor :

It is the ratio of the total harmonics content to the fundamental component

$$HF = \frac{\left[I_{rms}^2 - I_1^2\right]^{1/2}}{I_1}$$

The harmonic factor indicates the harmonics content in the input supply current.

In what follows the performance parameters of fully and half controlled converters are obtained as a function of the firing angle for both constant continuous dc current and pulsating continuous dc current.

2.4.2 Performance under Constant Load Current :--

It is assumed that the sufficient large inductance is present in the load circuit which is capable to maintain load current constant for all values of battery voltage and firing angle.

(i) Output voltage variation :

Figure 2.16 indicates that a continuous reduction of the dc output voltage from maximum to zero is brought about by a continuous phase retardation of firing angle from 0° to α_{max}. The control range (α_{max}) is 90°, 180°, 120° and 150° for FCC, HFC, HFAS-1D and HFAS-2D respectively. Within the control range, the half controlled converter provides the highest output voltage among the four converters for a given firing angle. The output voltage of the FCC follows a cosine law.

(ii) Output voltage ripple factor :

The half controlled converters provide low output voltage ripple compared to fully controlled converter. This is mainly

OUTPUT VOLTAGE

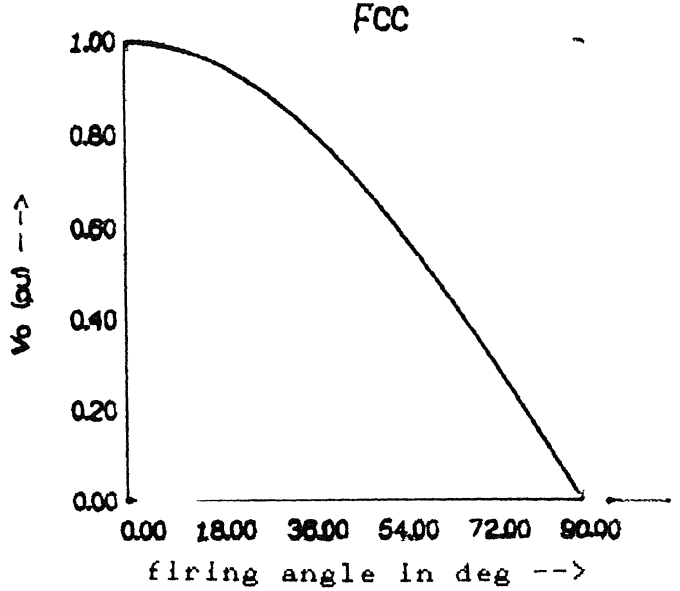

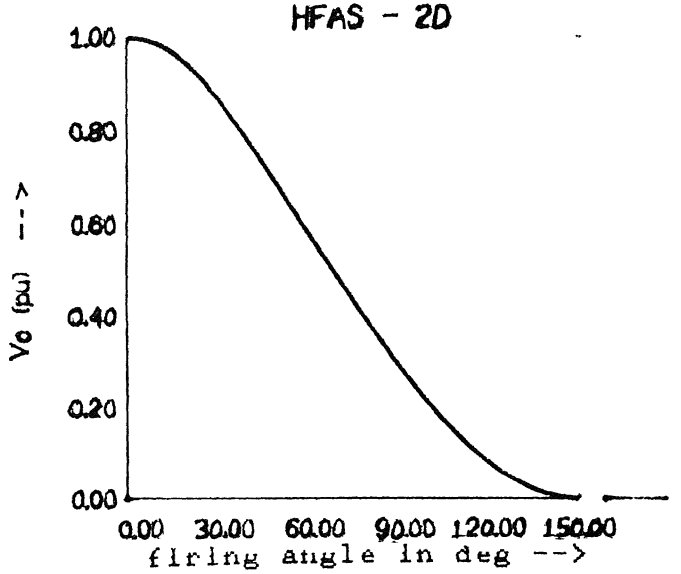

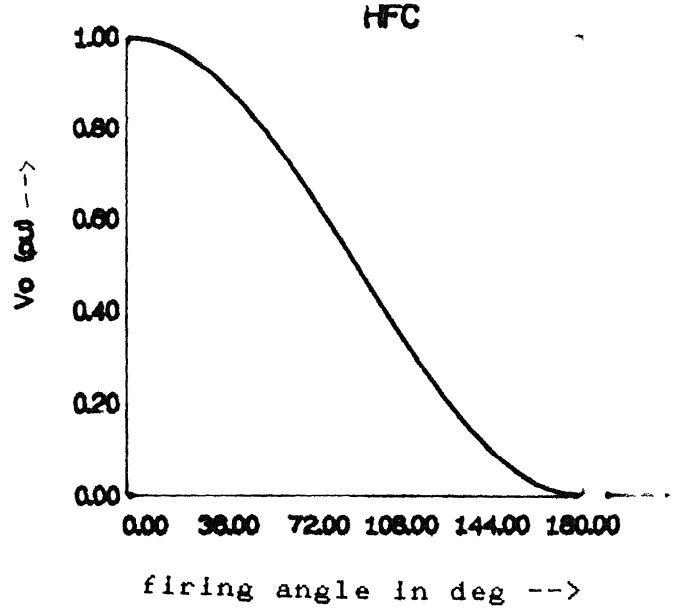

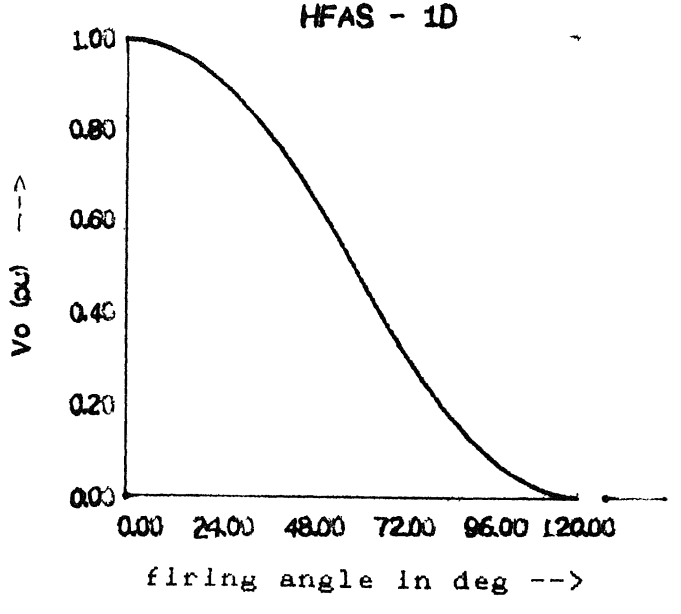

because of freewheeling action in the half controlled converter as shown in Fig. 2.17. Among the half controlled converters, th ripple factor improves with the asymmetrical converters. Betwee the converters HFAS -1D and HFAS - 2D the latter provide considerably low ripple over a wide range of firing angl variation. In the case of HFAS - 2D, there is a sharp variatio in the output voltage around the firing angle $\alpha = 90^{\circ}$. This i expected because the output voltage comprises of phase voltag segments and zero values for $\alpha > 90^{\circ}$.

(iii) Input current displacement factor :

Fig. 2.18 shows that the half controlled converters give low displacement angle compared to fully controlled converter for a given firing angle. This causes high PF in these converters. As the firing angle increases the input current displacement factor decreases and therefore the demand of fundamental reactive power from converter side increases. The half controlled symmetrical converter demands less fundamental reactive power over a wide range of firing angle than the HFAS-1D and HFAS-2D.

(iv) Input power factor :

The input power factor of four converters is shown in Fig. 2.19. The high input power factor in half controlled converters arises due to freewheeling action by the conduction of diode. The energy stored in the inductor is recovered to supply the necessary power to the load and no power is drawn from the supply source during the freewheeling interval. As a result, the power factor

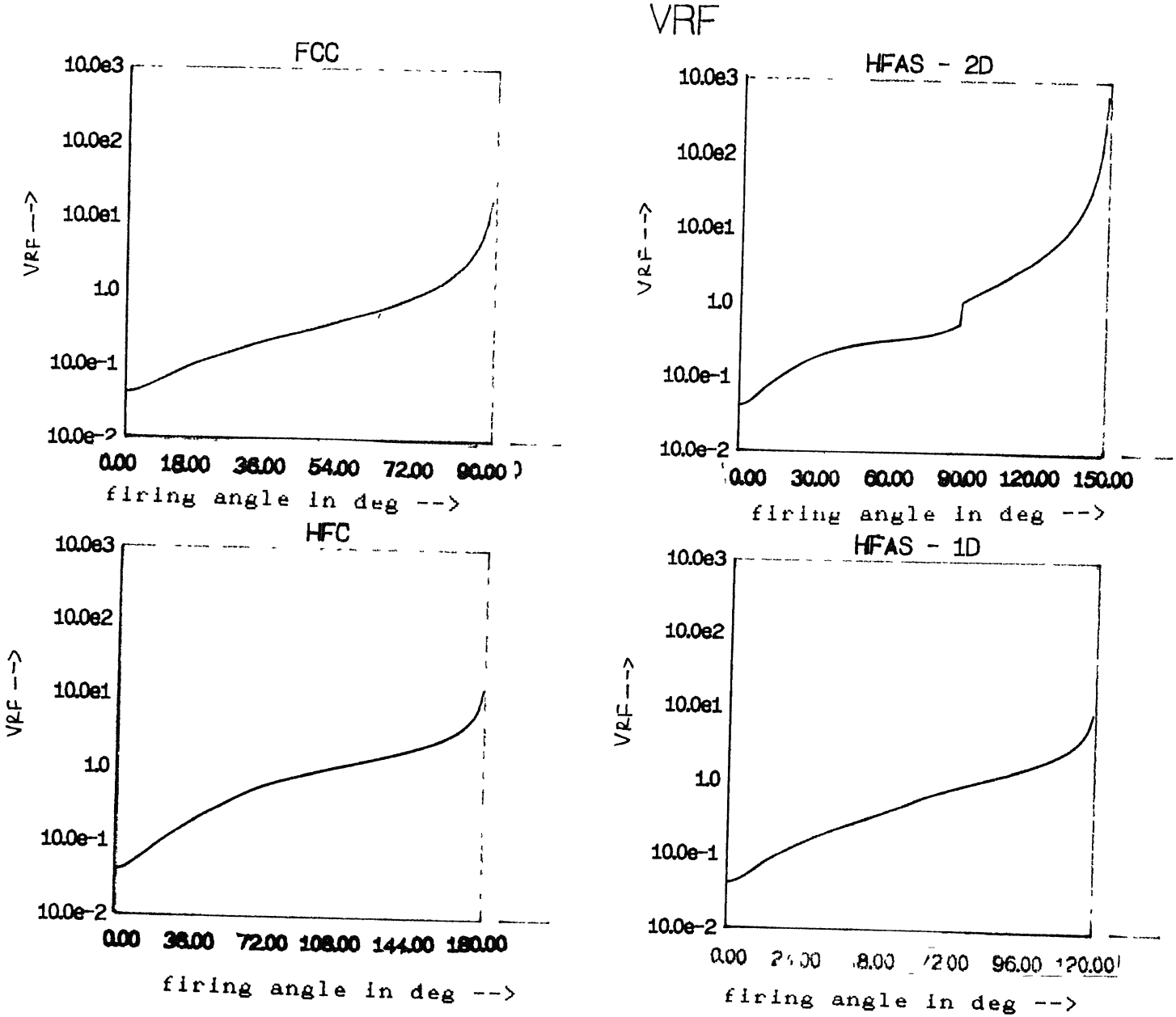

Fig. 2.17 Relationship between output voltage ripple factor and firing angle.

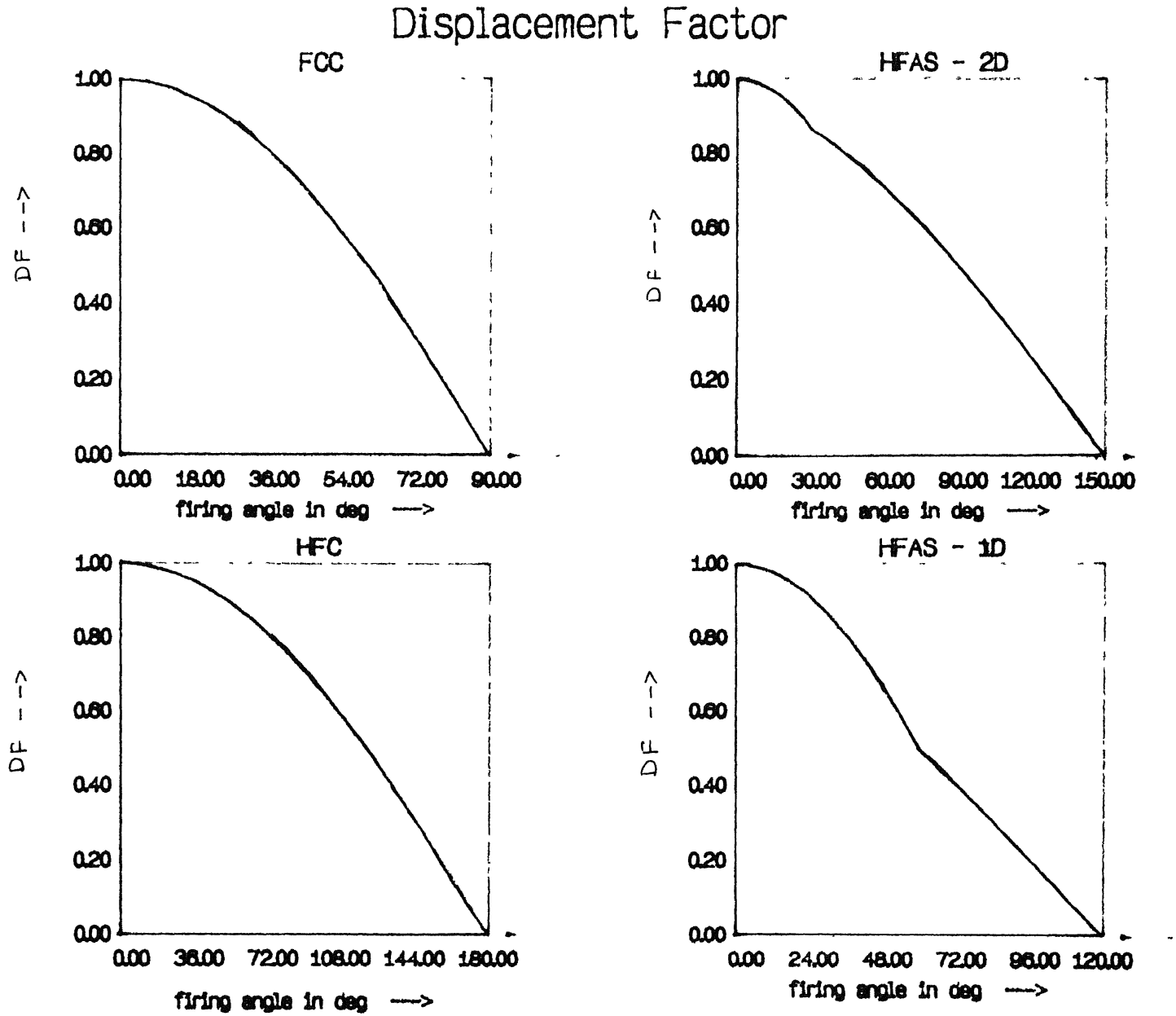

Fig. 2.18 Relationship between input current displacement factor and firing angle.

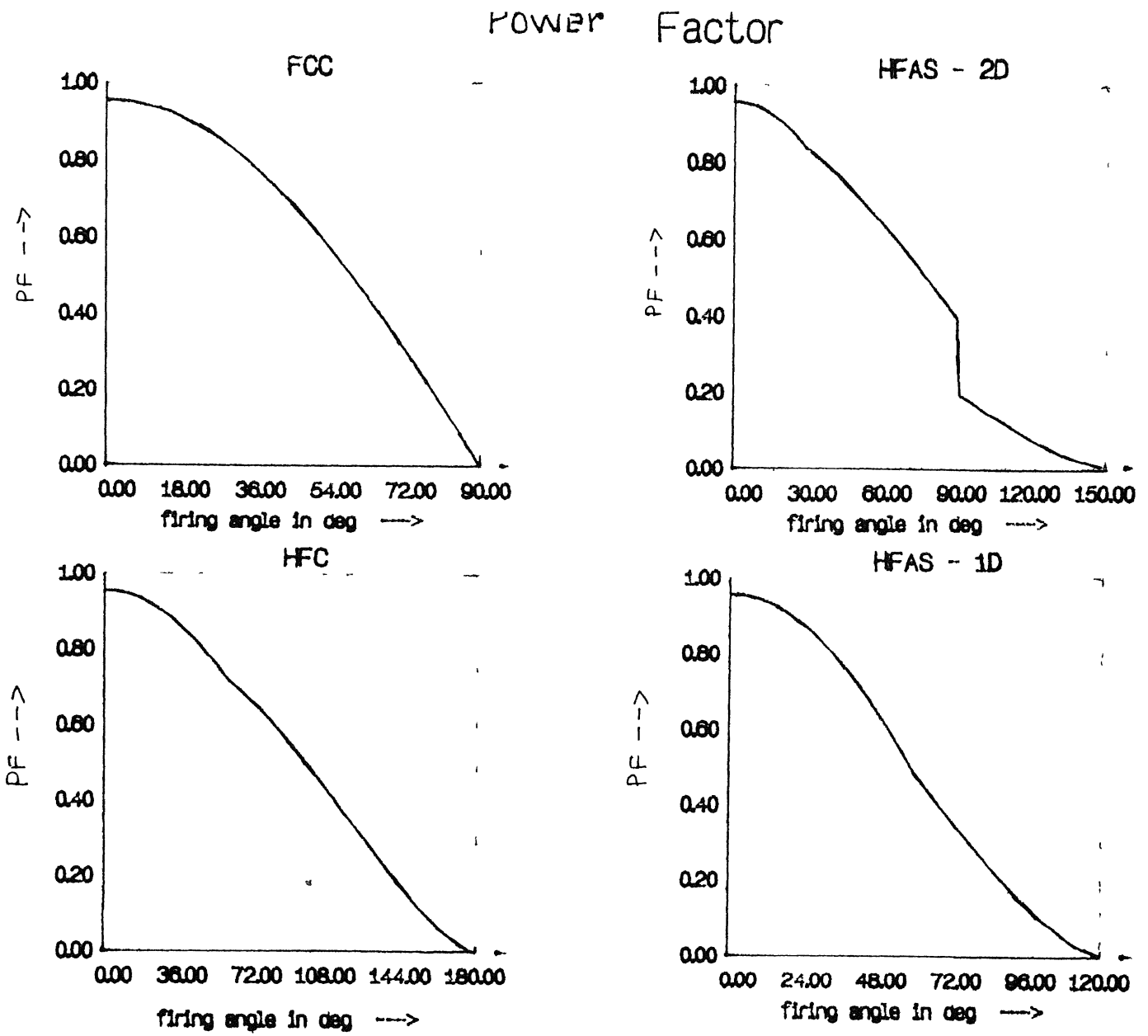

Fig. 2.19 Relationship between input power factor and firing angle.

is generally high in all half controlled converters. Among the half controlled converters the half controlled symmetrical converter has high input power factor compared to other two half controlled asymmetric converters for any given firing angle.

(v) Input current harmonics :

Fig. 2.20 shows the variation of harmonics of order upto eleventh present in the input line current. The shape of the input current waveform depends on the conduction of thyristors and diodes in the half controlled converters while it remains the same in fully controlled converter at any given firing angle. The curves are drawn between I_n/I_1 and firing angle where I_n stands for magnitude of nth order input ac current harmonic and I_1 stands for magnitude of fundamental input line current. In the fully controlled converter, the orders of harmonics present are $6n\pm1$, where $n = 0,1,2,\ldots$. The magnitude of individual harmonic reduces as n increases but it remains independent of firing angle. In half controlled converters, the conduction periods of thyristors and diodes are not equal which causes the change in input current harmonics. In half controlled symmetrical converter, triplen harmonics are absent and the magnitudes of harmonics vary with the firing angle. The half controlled asymmetrical converter, $(6n\pm1)$th harmonics are present where $n = 0,1,2,3\ldots$. In HFAS - 1D converter, the magnitudes of harmonics remain independent of firing angle till $\alpha \leq 60^\circ$. When $\alpha > 60^\circ$ the magnitudes of harmonics vary with α. In case of HFAS - 2D converter, the limit of firing angle till the magnitudes of

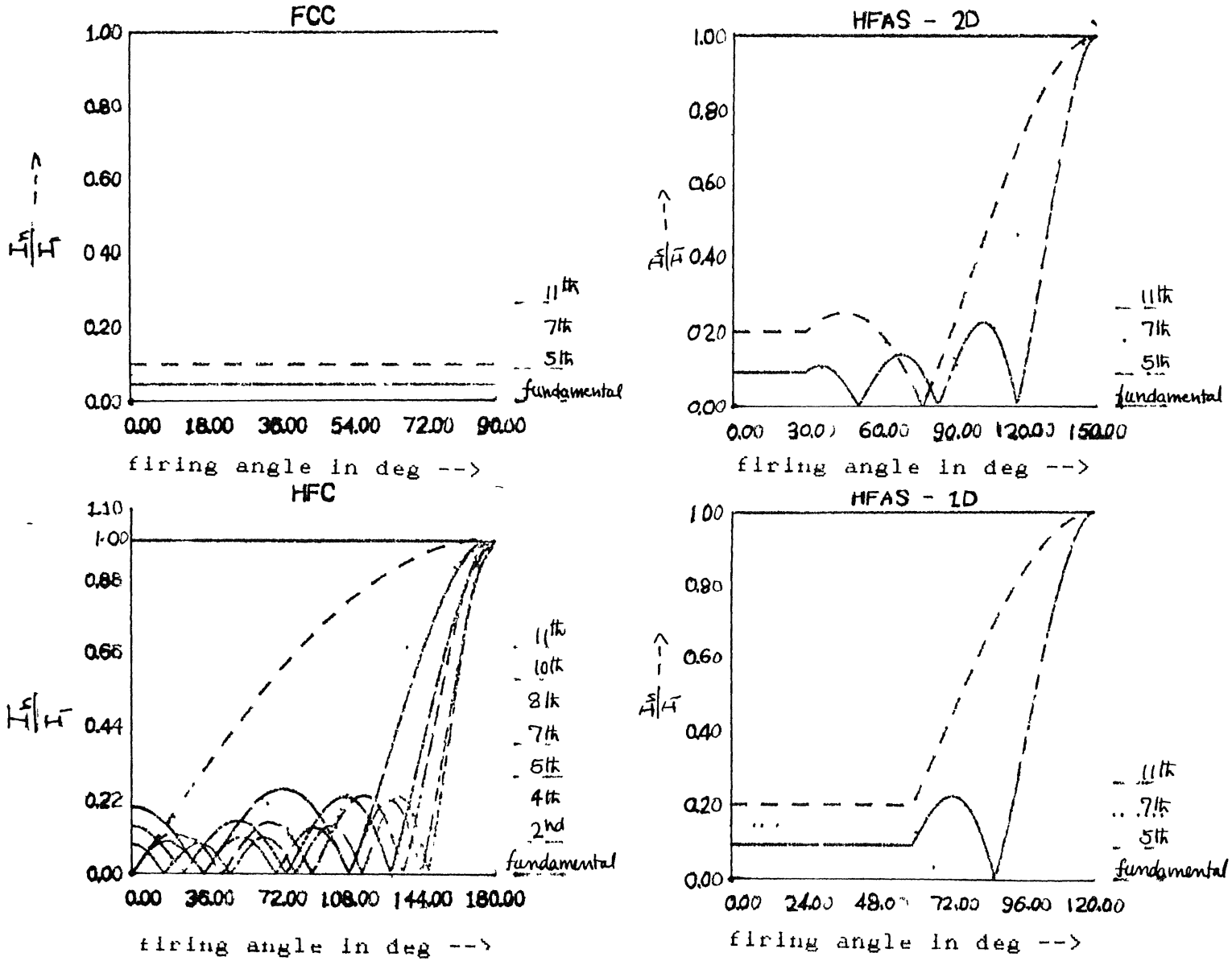

Fig. 2.20 Relationship between input current harmonic and firing angle.

harmonics are constant is $\alpha \leq 30^{\circ}$. The fully controlled converter generates considerable low order harmonics which are independent of firing angle.

(vi) Input current harmonic factor :

Fig. 2.21 shows the input current harmonic factor of the four converters. The input current harmonic factor of fully controlled converter is independent of firing angle and remains constant. In case of half controlled converters, the current harmonic factor increases with the firing angle. Unlike in fully controlled converter, the waveshape of the output current depends on value of the firing angle. There are two ranges in each of HFC and HFAS - 1D, and three ranges of firing angle in HFAS - 2D. The harmonic factor increases with increasing intervals of freewheeling. This can clearly be seen from Fig. 2.21. The input current harmonic factor is the lowest in fully controlled converter among the four converters.

2.4.3 Performance under Pulsating Load Current : --

The ac ripple currents in the dc circuit are not negligible in comparison to mean dc current in pulsating continuous current operation. The ac ripple depends upon the inductance present in the load circuit. The value of inductance just capable to keep the peak value of ac ripple current less than the mean dc current is termed as critical inductance. The critical inductance depends on both firing angle and trickle voltage of battery.

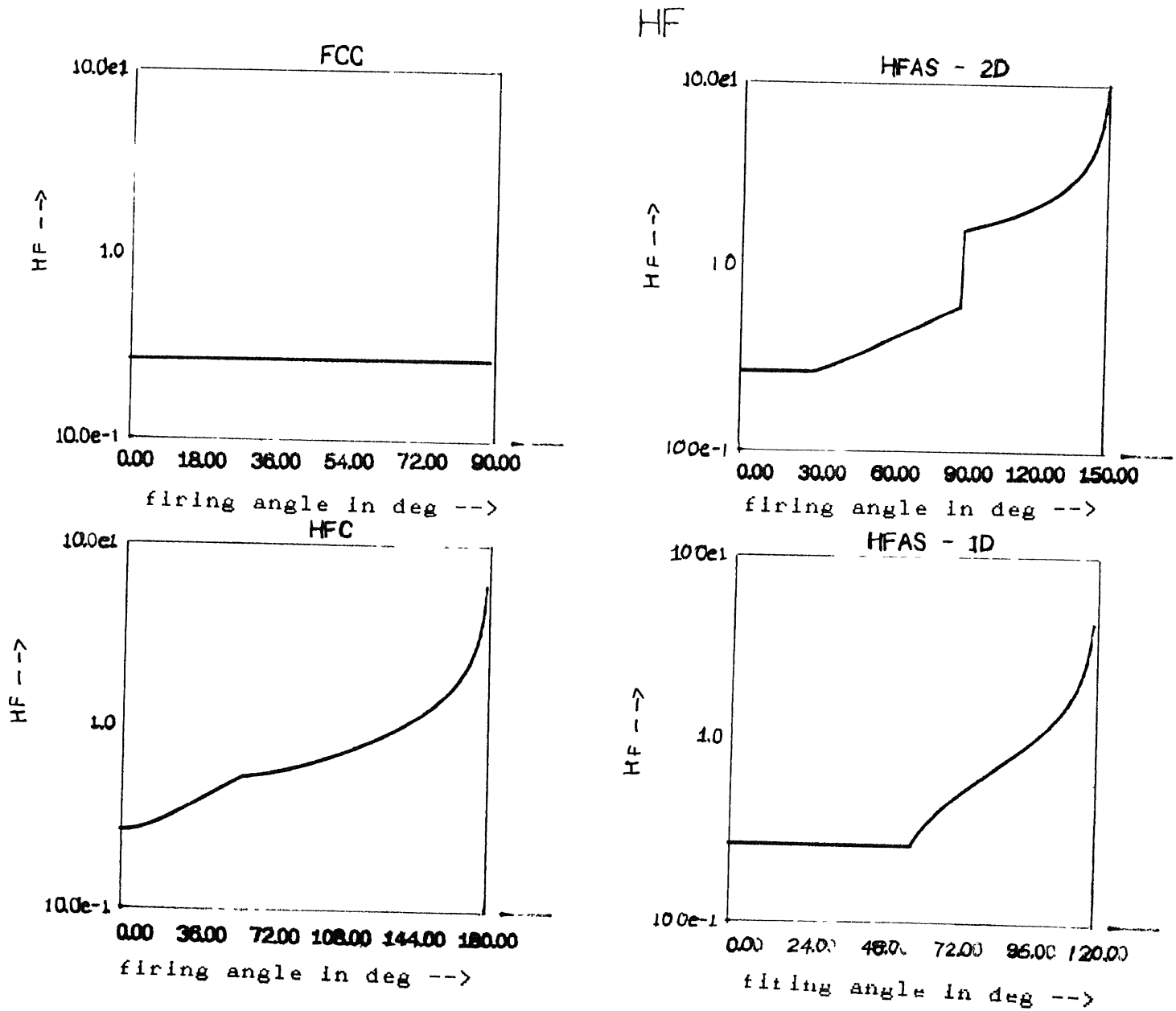

Fig. 2.21 Relationship between input current harmonic factor and firing angle.

The output voltage variation, output voltage ripple factor and input current displacement factor remain unaffected with the change in the instantaneous value of load current as long as the current remains continuous.

(i) Critical inductance :

Figs. 2.22(a) to 2.22(d) show the critical inductance for different values of m for all the four converters. The requirement of critical inductance increases with the peak dc voltage ripples. When the peak dc output voltage ripples are larger than mean dc output voltage, the large value of inductance is required to maintain the load current just continuous. The critical inductance also depends on the instantaneous battery voltage and increases with it. For the same operating condition the requirement of critical inductance depends on the type of the circuit used in the battery charger. The value $\omega L/R$ versus firing angle curve is divided into three parts. The three parts are idicated for the curve corresponding to m = 0.75 in Fig. 2.22(a). These three parts for other curves can be easily noted. In the first part A-B,the load current in the circuit is continuous or just continuous. In this part of the firing angle the need of critical inductance does not arise. The firing angle at the boundary of this part is termed as $\alpha_{critical}$. In the second part of the curve B-C the critical inductance is required to keep the current just continuous in the load circuit. This part extends to about $\omega L/R$ = 100. The requirement of critical inductance increases with the firing angle. In the last part of the curve

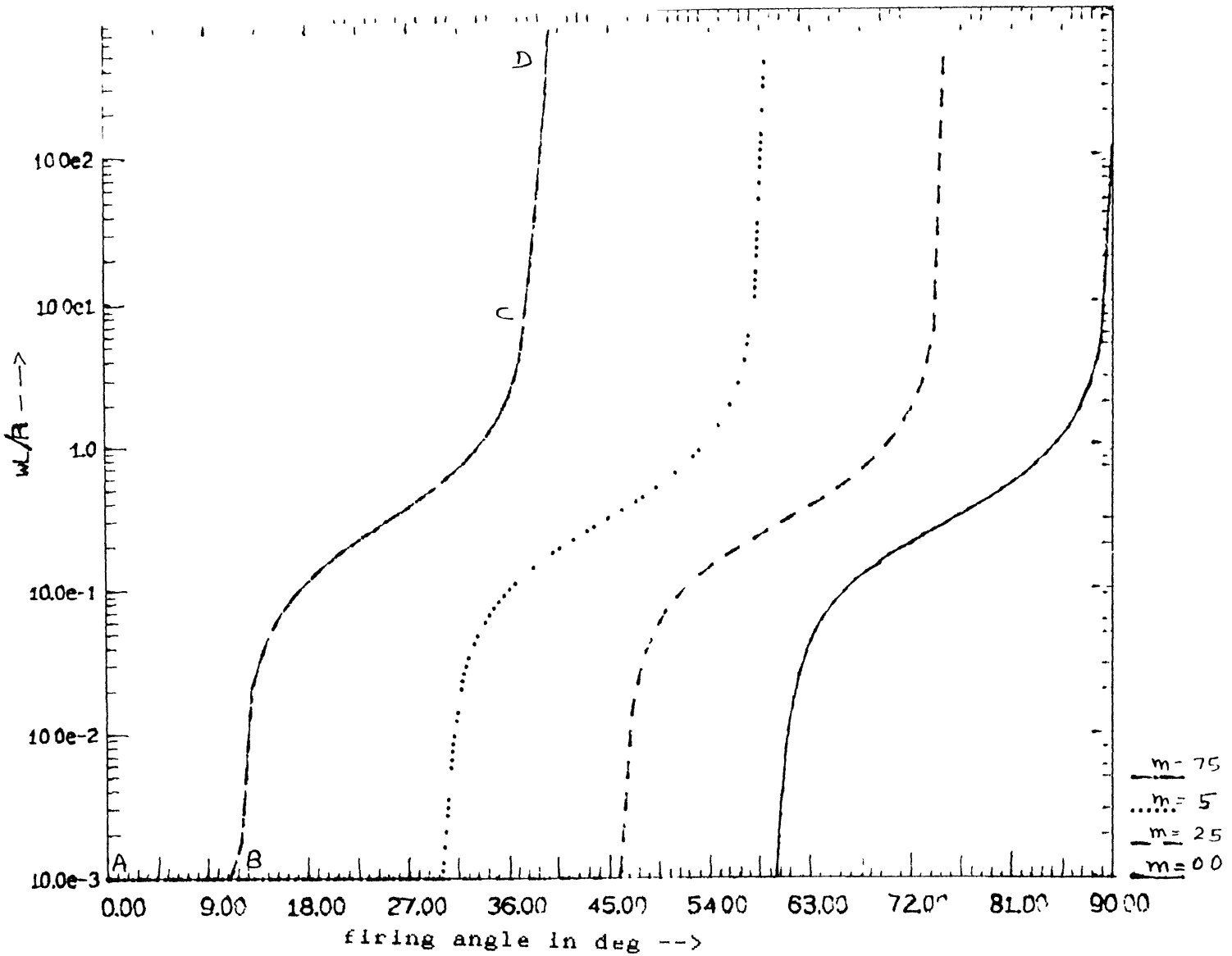

Fig 2 22(a) Relationship between ωL/R and firing angle for fully controlled converter

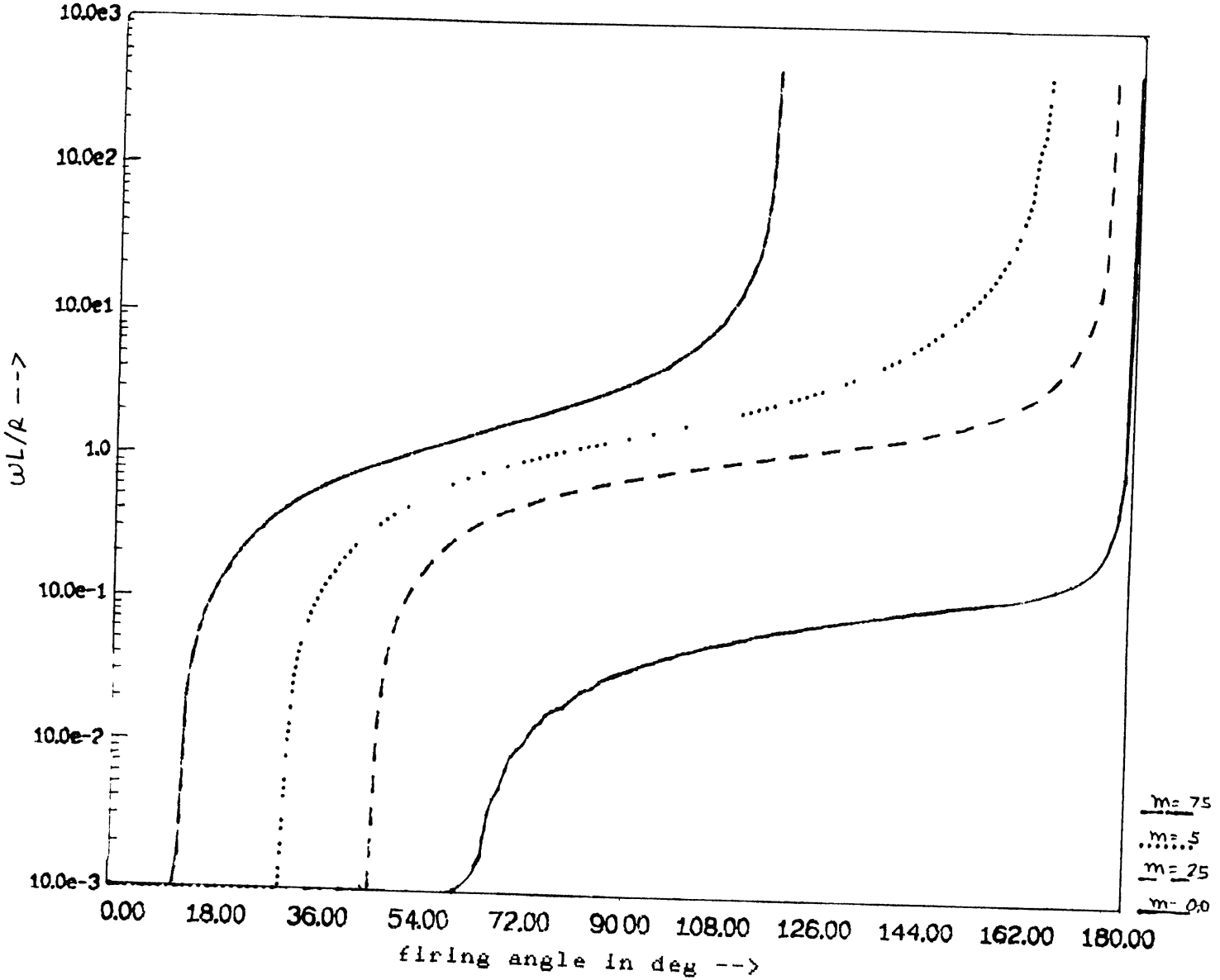

Fig. 2.22(b) Relationship between ωL/R and firing angle for half controlled symmetrical converter

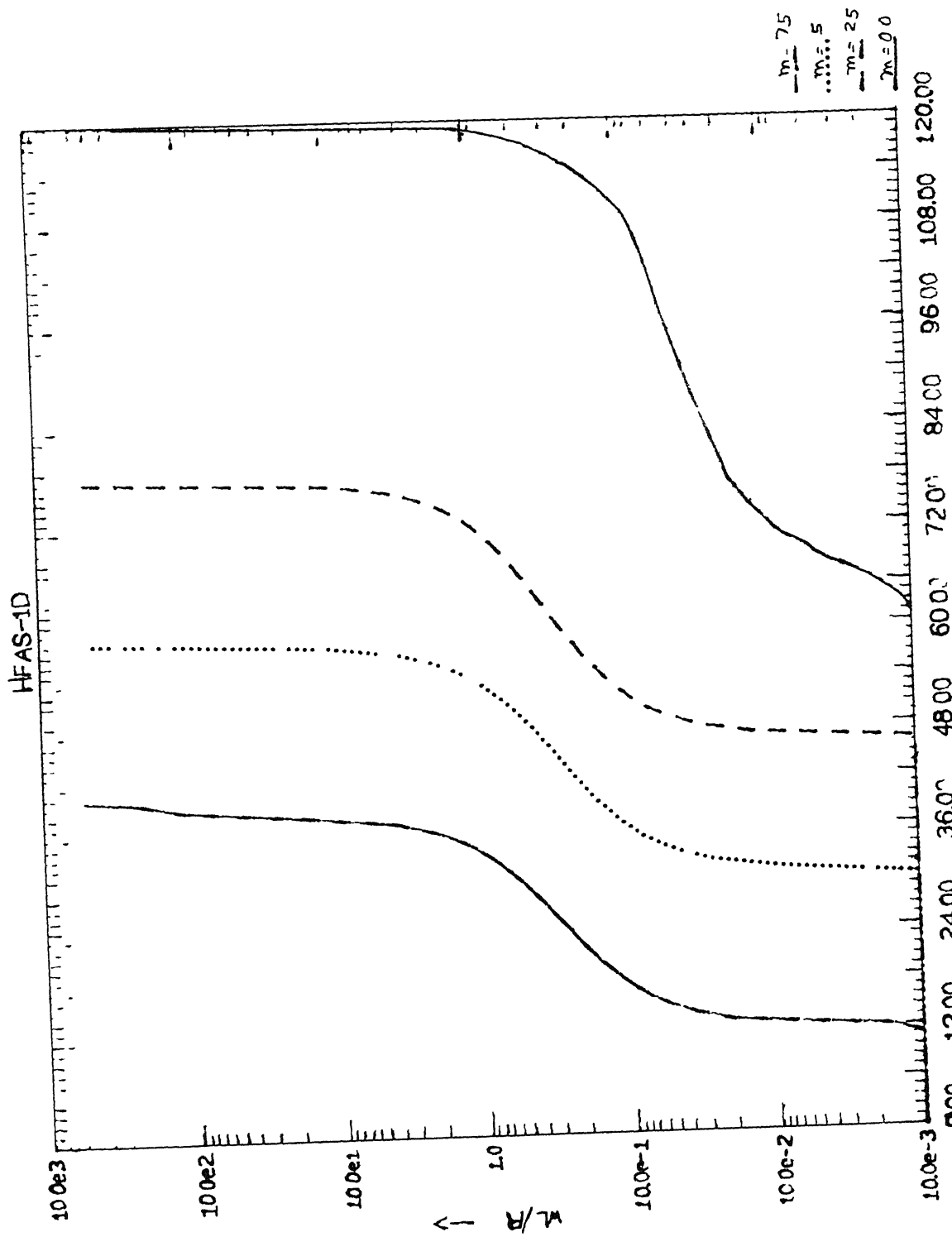

Fig. 2.22(c) Relationship between ωL/R and firing angle for half controlled asymmetrical converter.

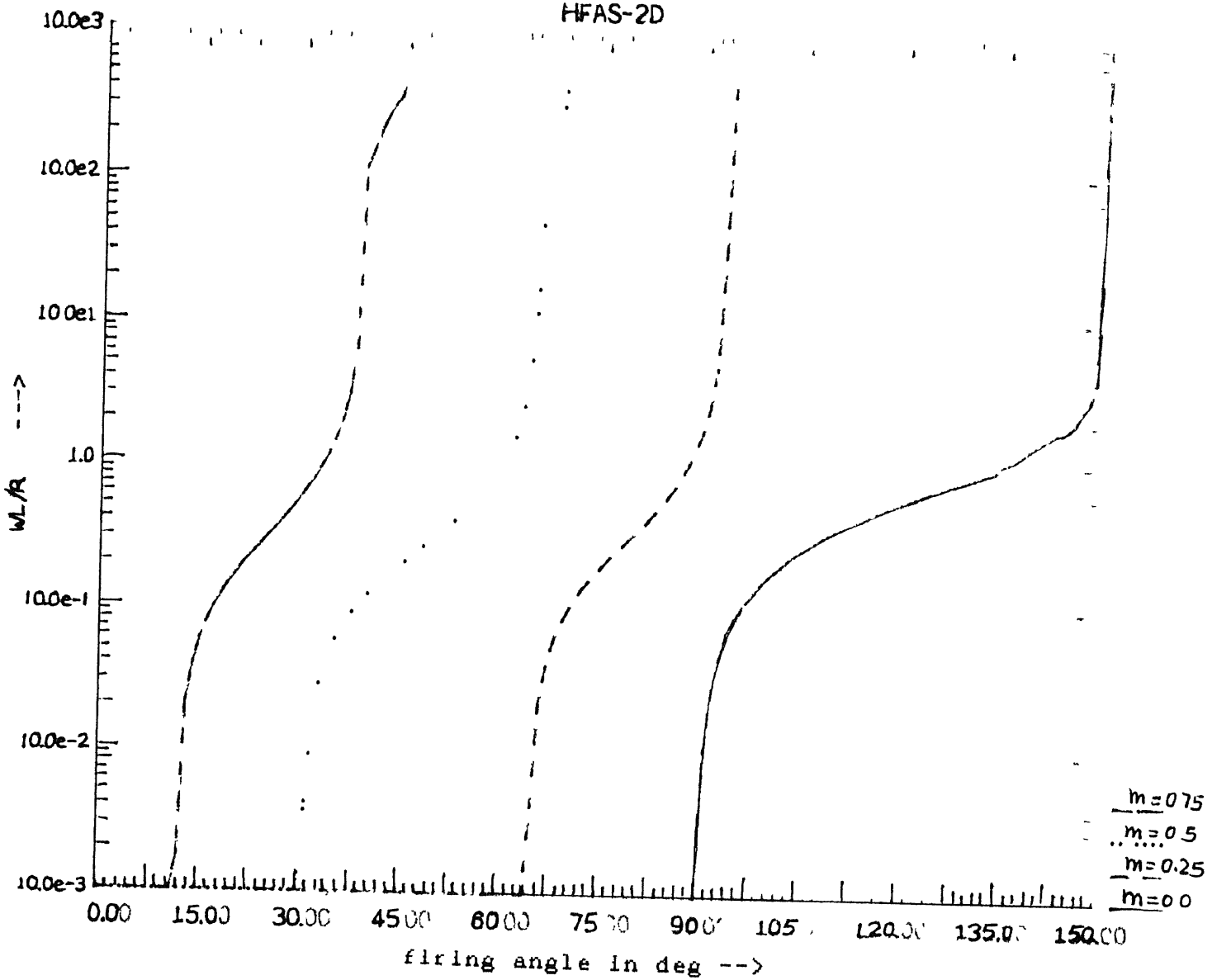

Fig. 2.22(d) Relationship between ωL/R and firing angle for half controlled as asymmetrical converter with one diodes.

C-D with the small increment in the firing angle, a large value of critical inductance is required to keep the current just continuous. After certain value of firing angle corresponding to point D, which is termed as α_{max}, the curve becomes vertical. The α_{max} is the maximum controllable range of converter. The $\alpha_{critical}$ and α_{max} depend on the type of the converter and value of m. The half controlled converters need small value of critical inductance compared to fully controlled converter. This is due to the fact that the freewheeling action takes place in case of half controlled converters. The half controlled symmetrical converter needs lowest value of critical inductance in load circuit for continuity of load current compared to other converters under the same operating conditions. The value of critical inductance to maintain current continuous as the need arises, can directly be obtained from Fig. 2.22. The determination of minimum inductance that ensures continuous conduction in battery charging is explained below. The variables which need to be specified are :

v_m : maximum value of ac phase voltage

v_{dis} : voltage of the discharge battery (Fig. 2.15)

v_{tri} : trickle charge voltage of fully charged battery (Fig. 2.15)

m : v_{tri}/v_m

α_c : firing angle at which output voltage of converter is equal to v_{dis}

R : current limiting resistance in output circuit

ω : $2\pi f$

First of all, the control range of the firing angle should be specified. Let the range of α be 0 to α_c. The value of $\omega L/R$

corresponding to α_c and m is read from Fig. 2.22(b). Let it be x. The minimum or critical inductance in Henrys is then given by

$$L_c = \frac{R}{\omega} x$$

(ii) Output current ripples :

Fig. 2.23(a) shows the variation of output current ripple in the four converters. The average load current for the same operating conditions is shown in Fig. 2.23(b). The current ripple is calculated with load current either continuous of just continuous with the critical inductance in the load circuit. The value of critical inductance is calculated from Figs. 2.22(a) to 2.22(d) for FCC, HFC, HFAS - 1 D and HFAS - 2D respectively. Depending upon the m, upto critical firing angle ($\alpha_{critical}$) the load current remains continuous and current ripple increases with the firing angle. As the firing angle increases beyond the $\alpha_{critical}$ inductance is inserted in the load circuit to maintain the just continuous current condition. The current ripple after the insertion of critical inductance in circuit starts to decrease with the increase in firing angle. The operating range of converter under just continuous current condition gradually decreases with increasing value of m. It is clear from Fig. 2.23(a) that half controlled asymmetrical converter with two diodes gives the lowest current ripple among the four converters. Additional inductance, however, is required to be inserted in to load circuit if the output current ripple is to be restricted within certain limit.

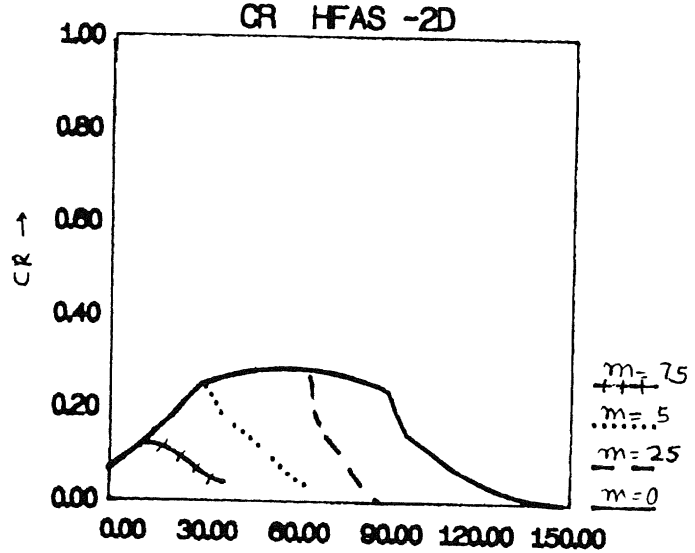

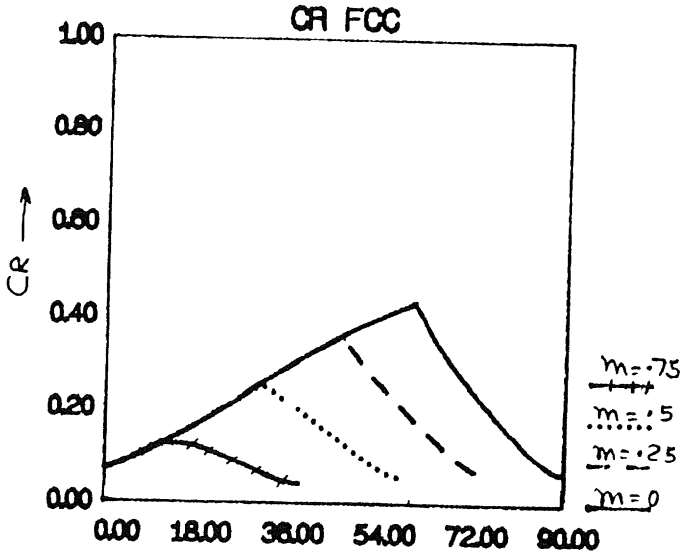

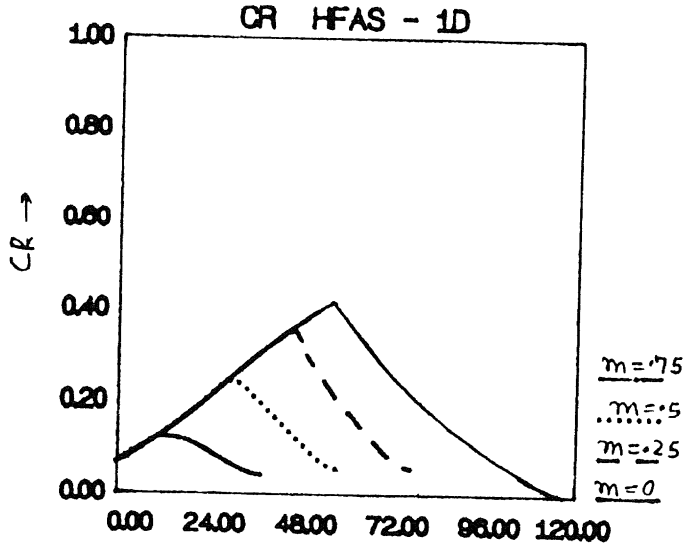

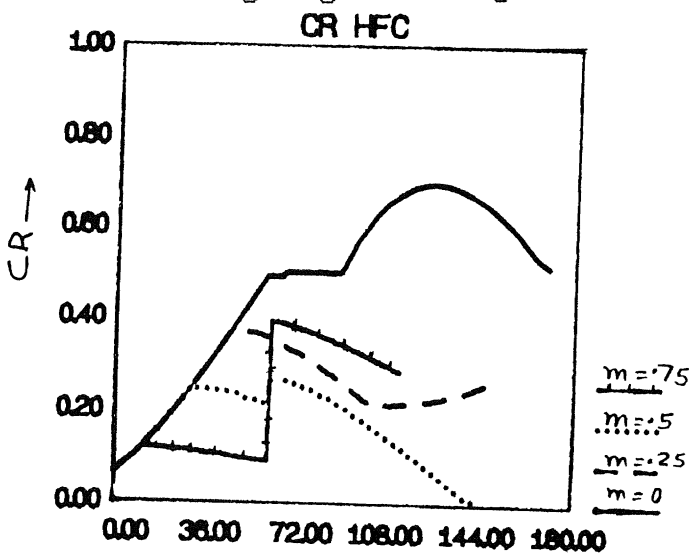

Fig 2 23(a) Relationship between load current ripple and firing angle

shb *

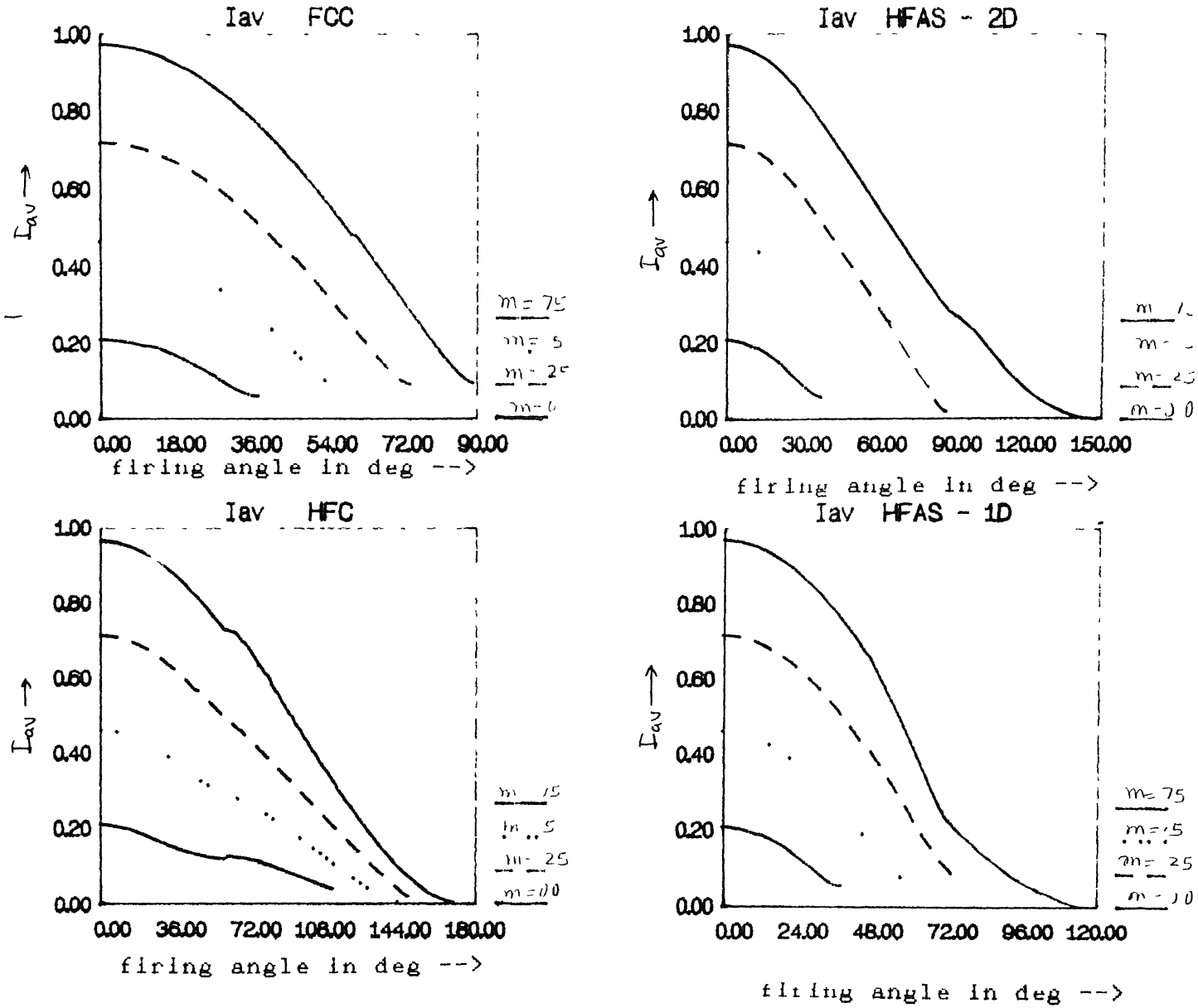

Fig 2.23(b) Relationship between average load current and firing angle

(iii) Input power factor :

The input power factor for four converters is shown in Fig. 2.24. The input power factor in case of pulsating continuous load current does not show any significant change from that of constant load current for any given circuit. This is due to the fact that the displacement factor remains almost the same in both cases whether the current constant or continuous with ripple. The half controlled symmetrical converter has high input power factor compared to the other circuits.

(iv) Input current harmonics :

Figs. 2.25(a) to 2.25(d) show that the orders of the harmonics present in the input current in case of pulsating continuous load current remains the same as that of constant dc current, but the magnitude of the nth harmonic depends on the pulsating dc current, the firing angle and m.In case of fully controlled converter, the magnitudes of input current harmonics increase gradually with firing angle till $\alpha_{critical}$. Beyond $\alpha_{critical}$ the magnitudes of line current harmonics become independent of firing angle and remain constant. With the increase in m, the duration for which magnitudes of harmonics vary decreases. In case of half controlled symmetrical converter, the magnitudes of input current harmonics increase with firing angle. The second order harmonic rises much faster than the other higher order harmonics with the firing angle. In the upper range of control angle, that is beyond $\alpha_{critical}$, the lower as well as

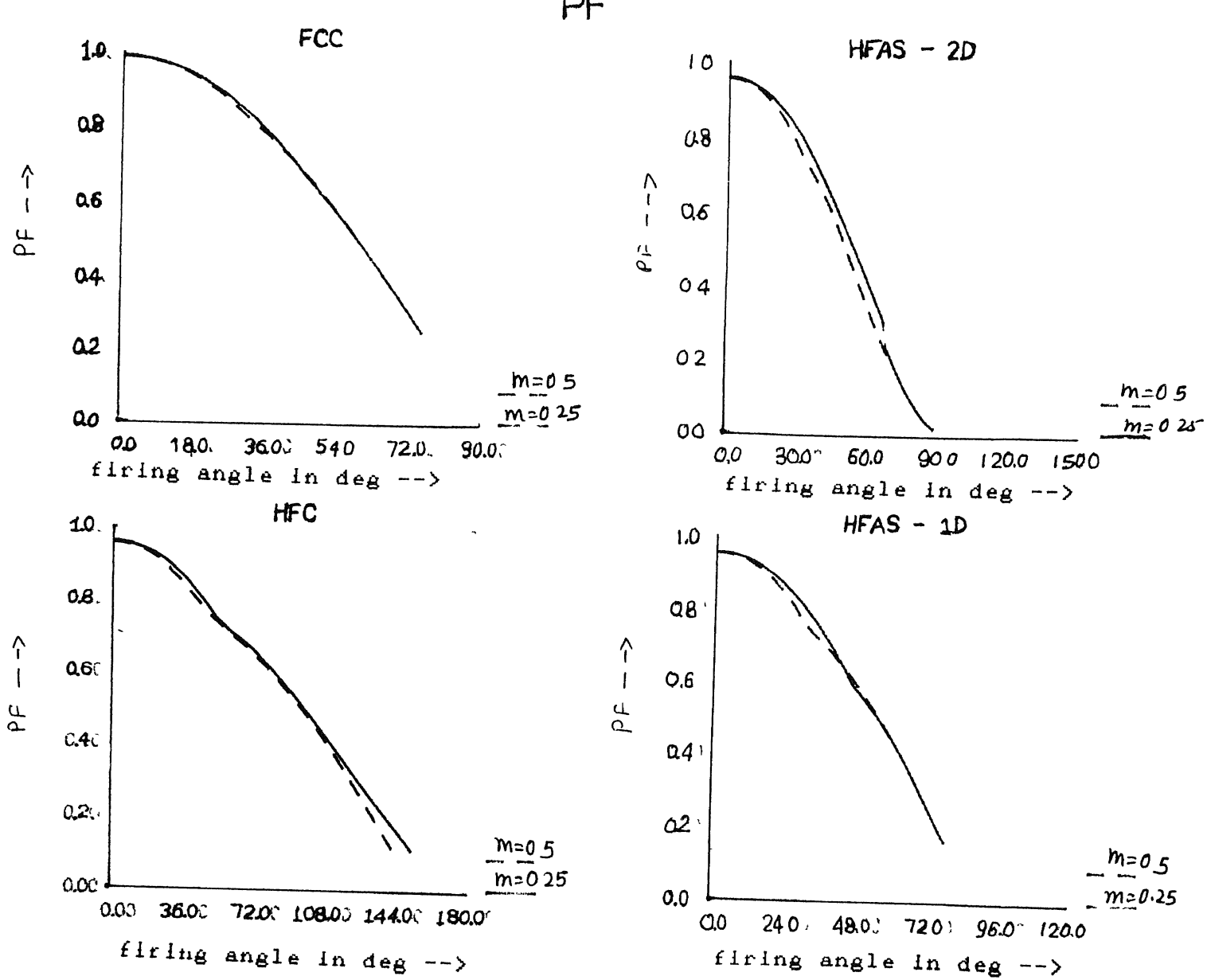

Fig 2.24 Relationship between input power factor and firing angle.

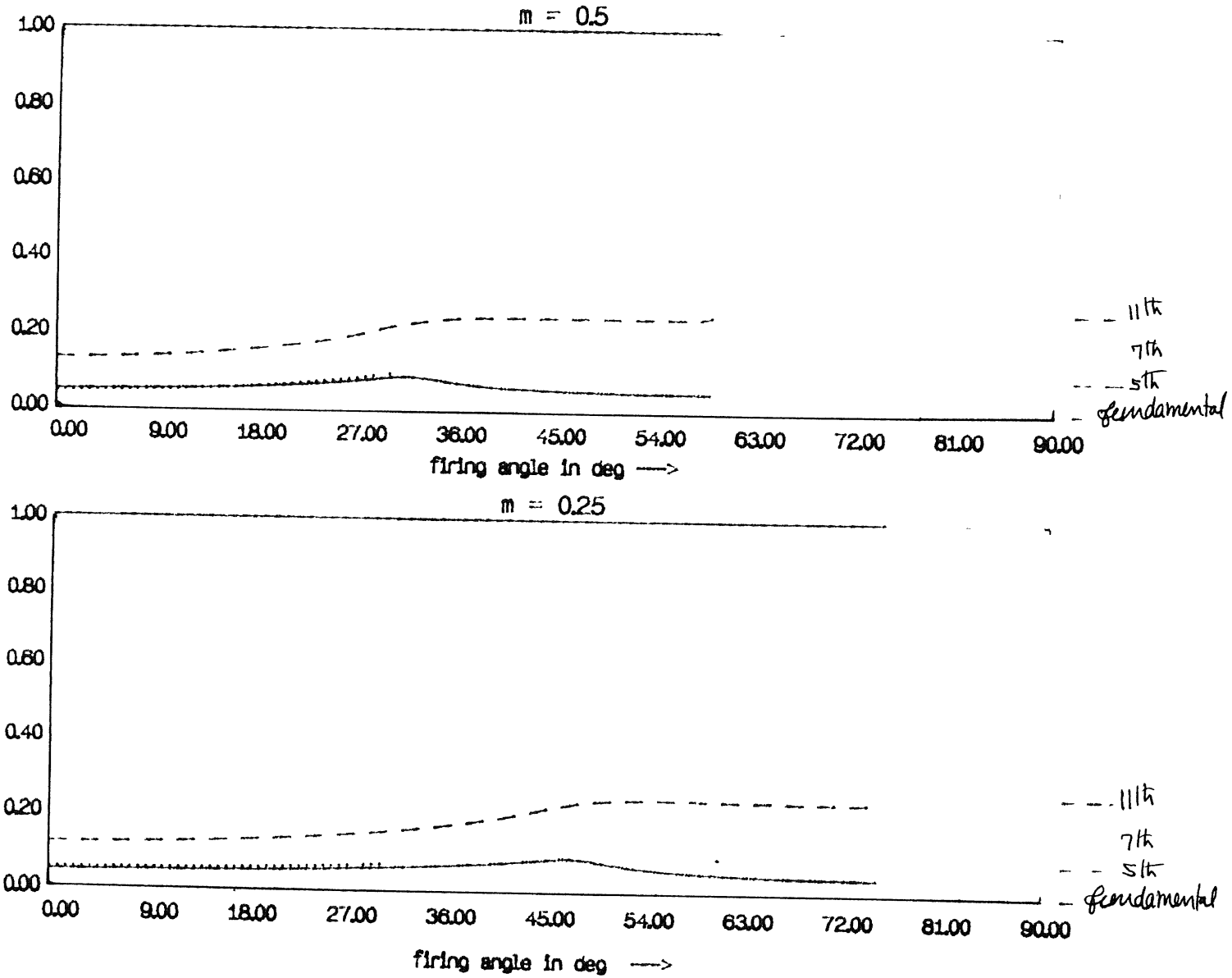

Fig. 2 25(a) Relationship between input current harmonics and firing angle for fully controlled converter.

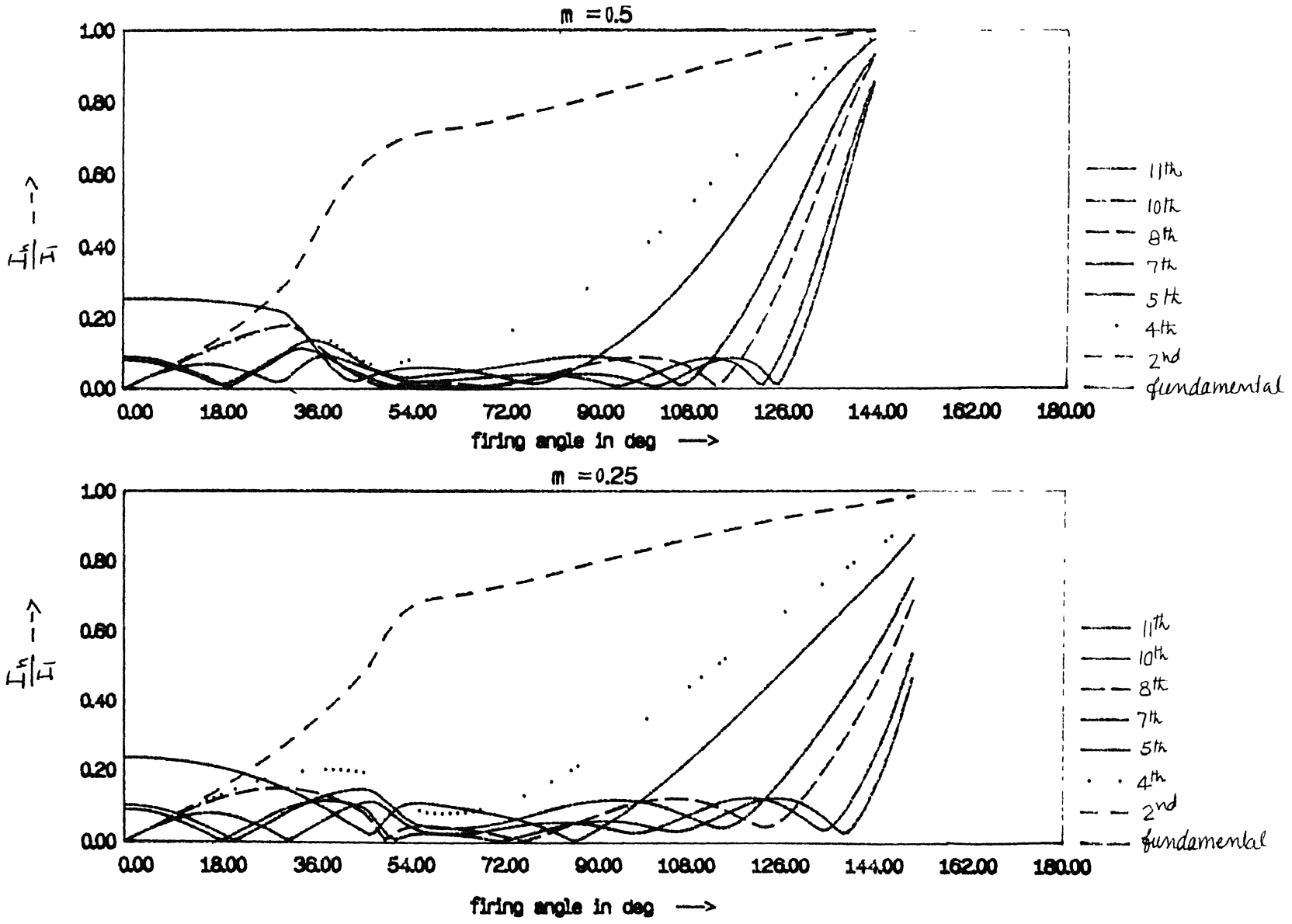

Fig 2.25(b) Relationship between input current harmonics and firing angle for half controlled symmetrical converter.

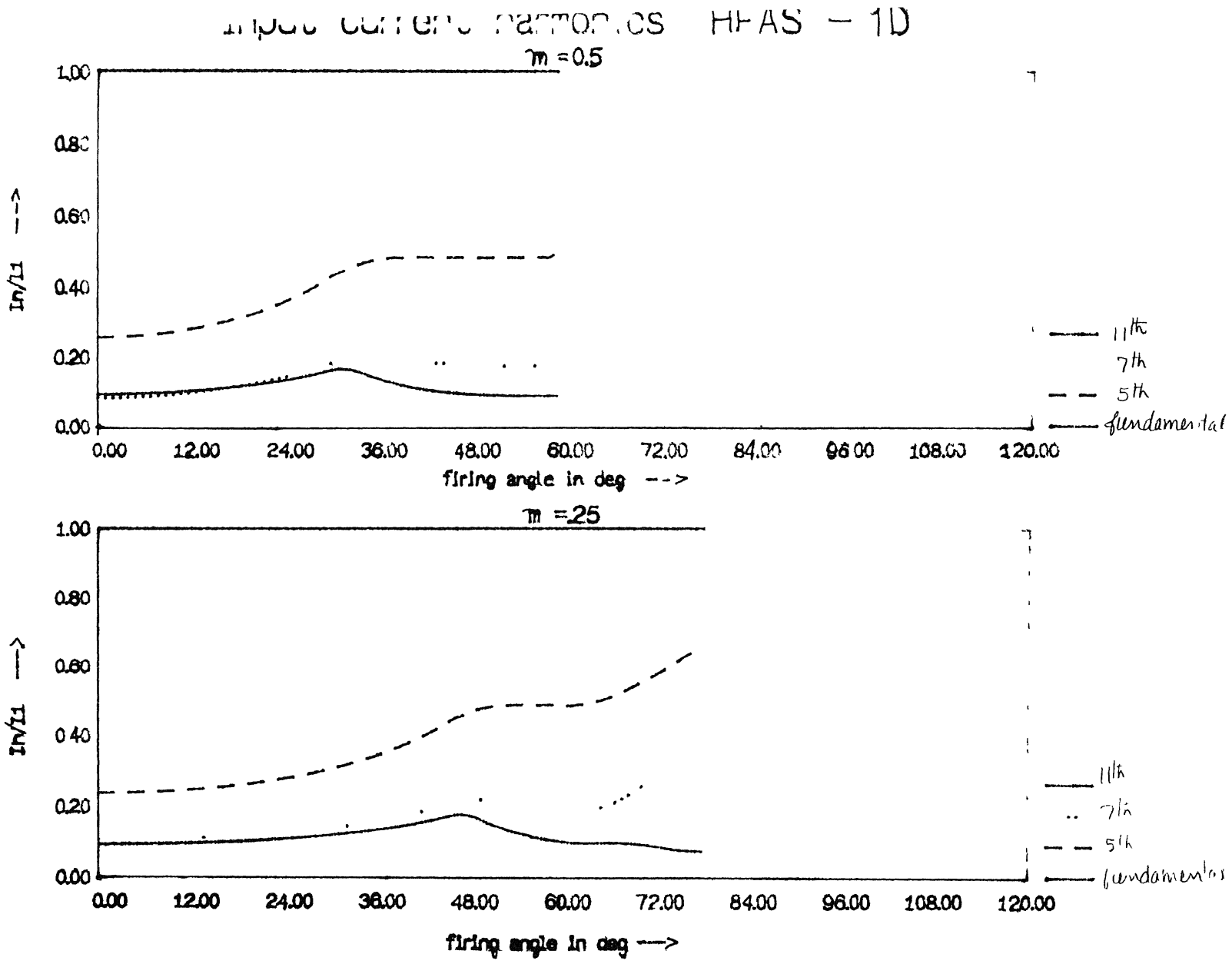

Fig. 2.25(c) Relationship between input current harmonics and firing angle for half controlled asymmetrical converter with one diode

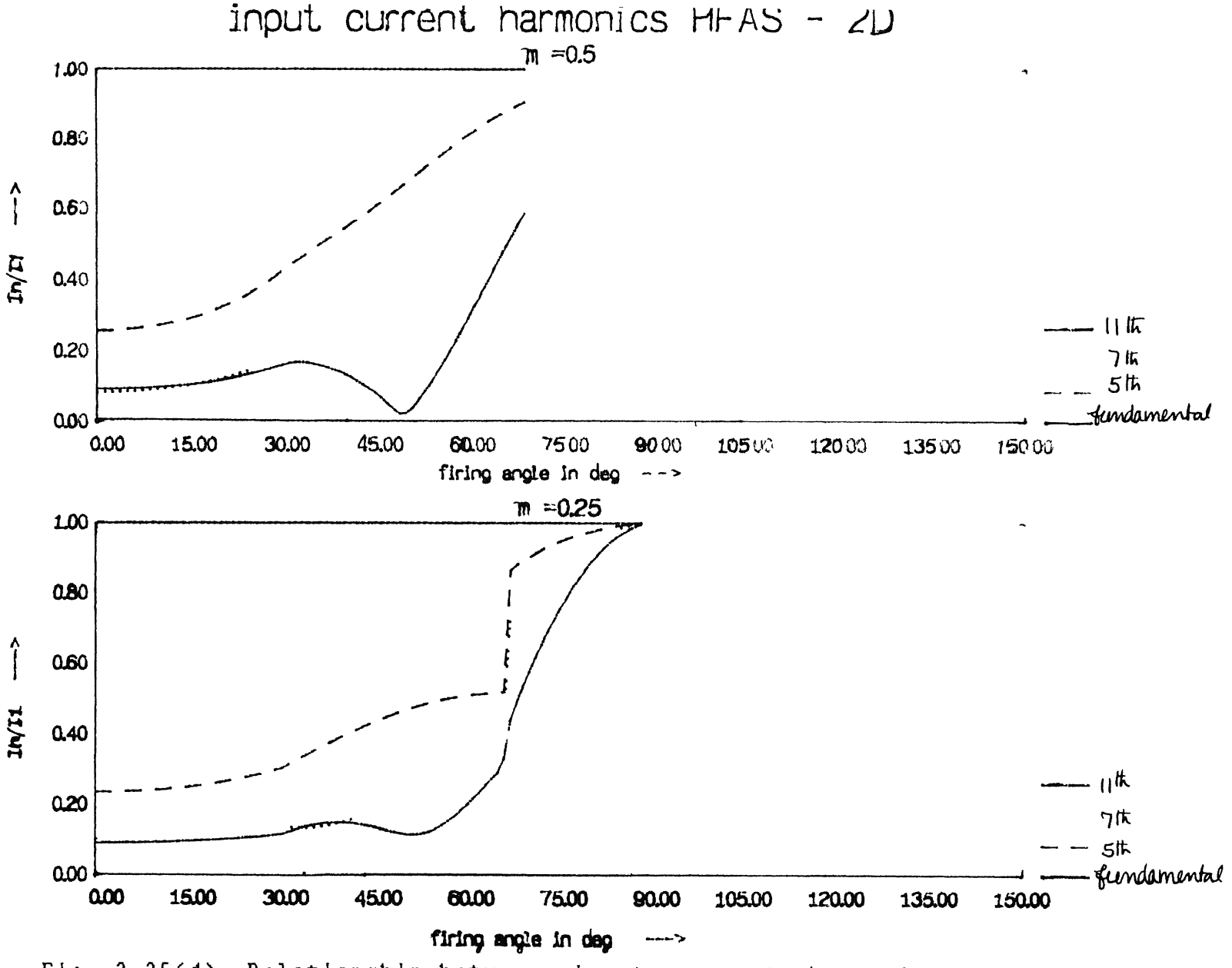

Fig 2 25(d) Relationship between input current harmonics and firing angle for half controlled asymmetrical converter with two diodes

* cc-iit/k :

higher order harmonics become the comparable to fundamental harmonic. In asymmetrical converters the trend of variation of magnitudes of harmonics in the lower range of firing angle are similar to that of fully controlled converter. In the upper range of firing angle the magnitudes of harmonics increase with α in asymmetrical converter with two diodes. Whereas in asymmetrical converter with one diode the nature of variation of magnitude of harmonics depends on m as shown in Fig. 2.25(c).

(v) Input current harmonic factor :

Fig. 2.26 shows that the input current harmonics factor is significantly low in case of pulsating continuous load current compared to constant load current. The fully controlled converter has lowest input current harmonics factor among the four circuits.

2.5 EXPERIMENTAL RESULTS

With the help of three-phase thyristor-diode module, half controlled converter circuits were assembled in the laboratory to obtain the experimental results under pulsating current operation. Fig. 2.27 shows the spectra of the output dc voltage while Fig. 2.28 shows the frequency spectra of output load current of HFC, HFAS - 1D and HFAS - 2D. The experiments were carried out under the following conditions.

AC source : 120 V (line-to-line voltage), 50 Hz

Circuit components : L = 42.5 mH

R = 50 Ω

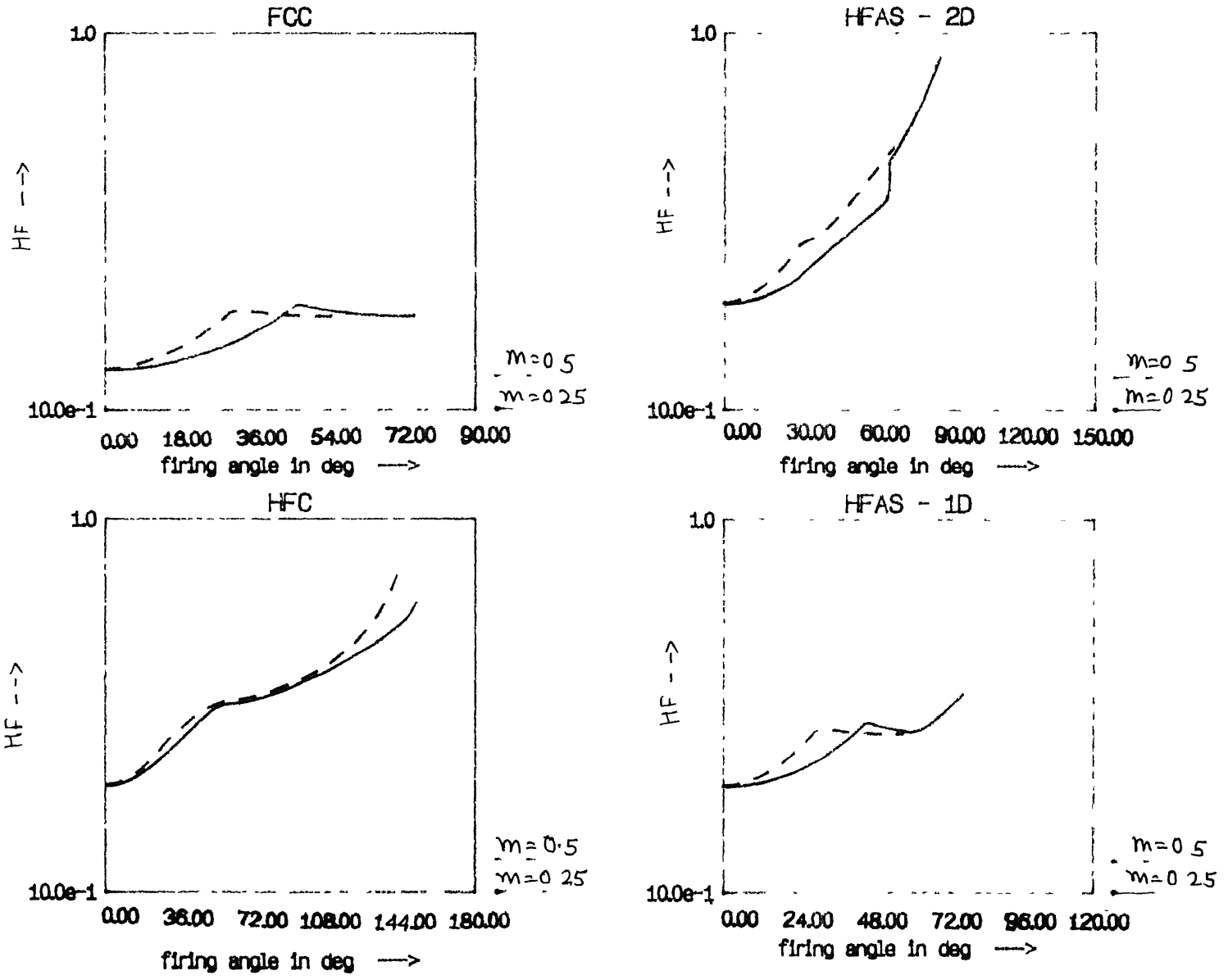

Fig 2.26 Relationship between input current harmonic factor and firing angle

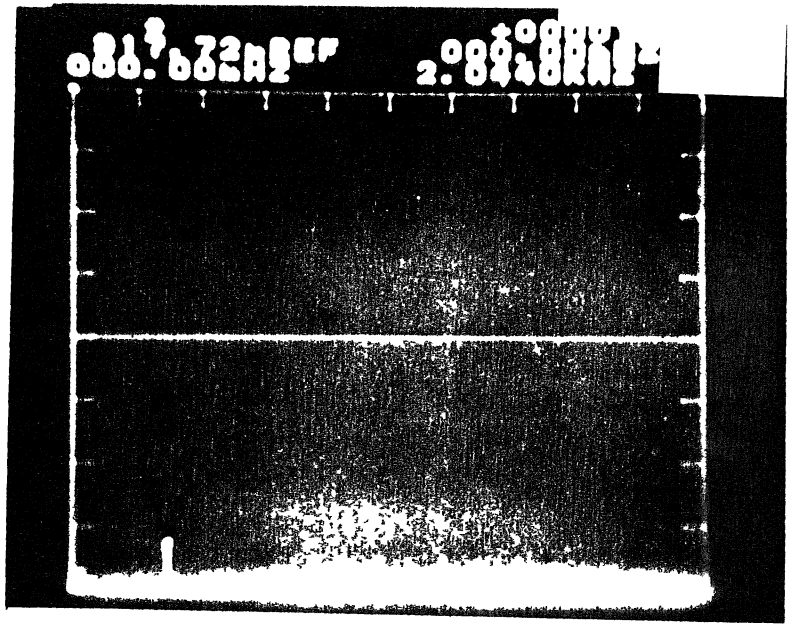

(b)

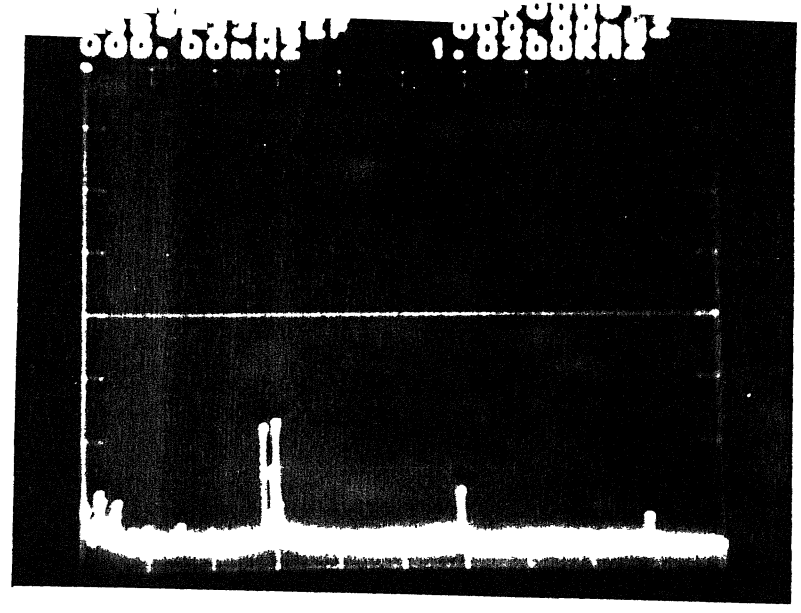

(c)

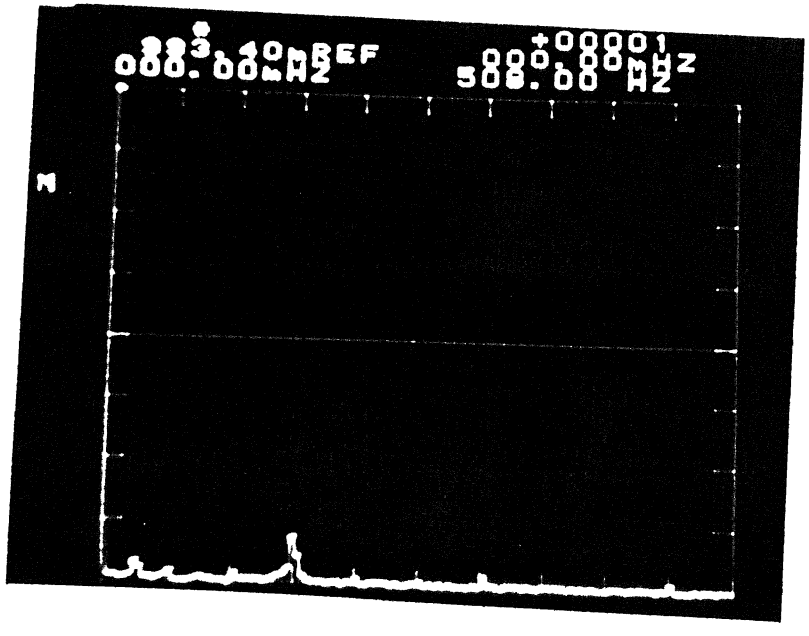

Fig. 2.28 Frequency spectra of output load current

(a) HFC

(b) HFAS – 2D

(c) HFAS – 1D

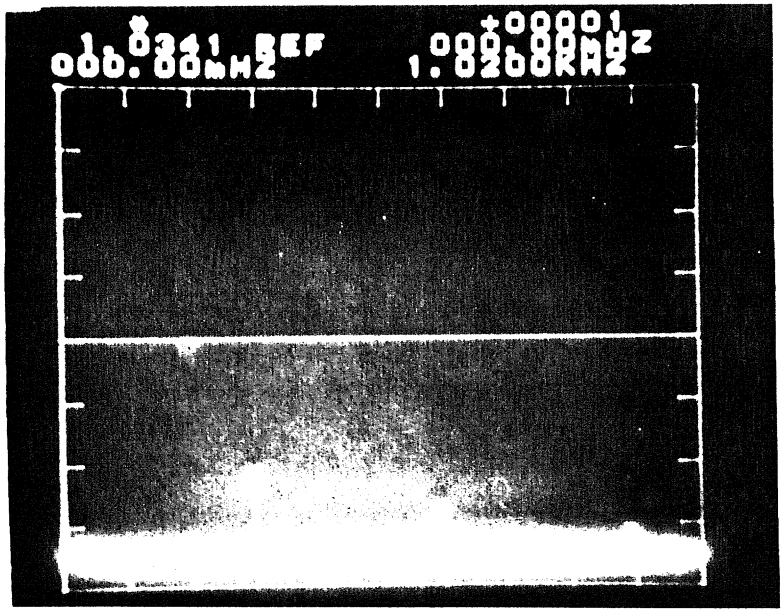

(b)

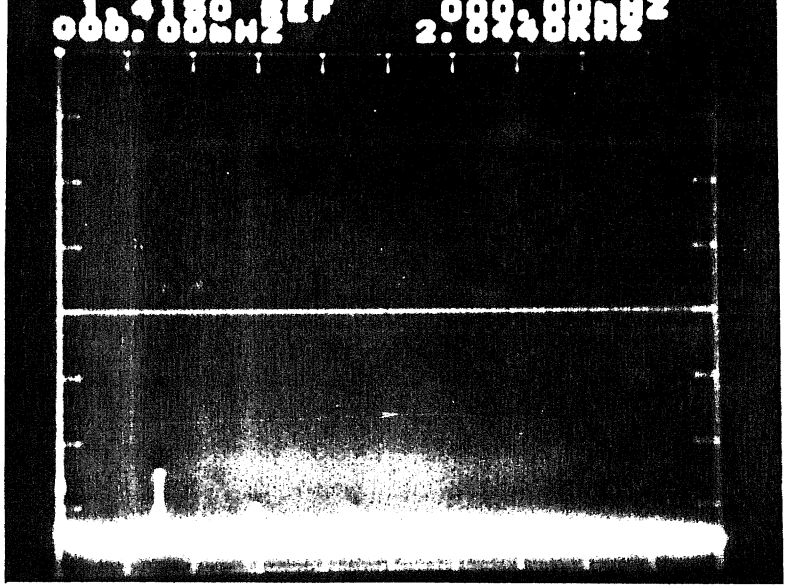

(C)

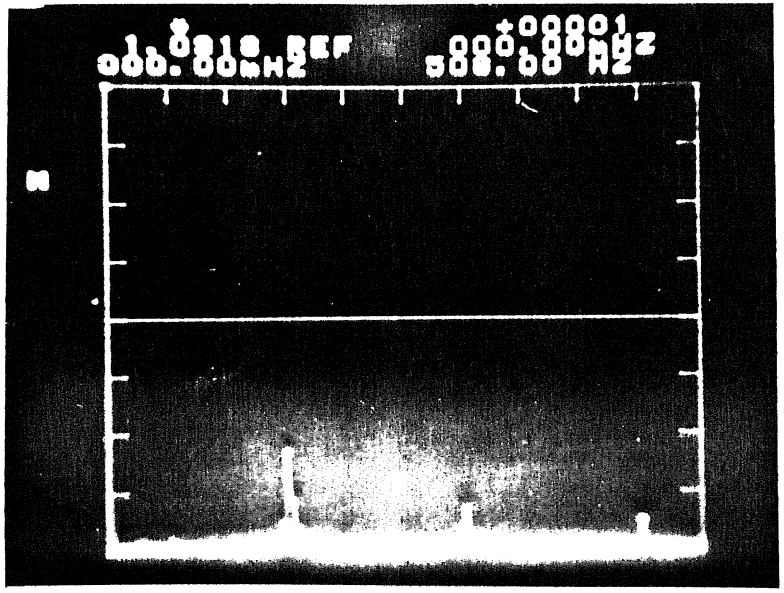

Fig. 2.27 Frequency spectra of output dc voltage

(a) HFC

(b) HFAS - 2D

(c) HFAS - 1D

E = 30 V (back emf of separately excited dc shunt motor)

From Fig. 2.27, it is clear that the fundamental alongwith 6nth harmonics are present in the output voltage of HFAS - 1D and HFAS-2D whereas the output dc voltage of HFC contains fundamental and 3nth harmonics, where n = 1,2,3,.... . As the order of harmonic increases the magnitude of a harmonic voltage reduces rapidly. Fig. 2.28 shows the frequency spectra of output load current. Since the current is continuous the orders of harmonics present in the load current are the same as those present in the ourput dc voltage. Fig. 2.29 shows the frequency spectra of input line current of HFAS - 2D. It is evident from the Fig. 2.29 that (6n±1)th harmonics are present in the input line current of half controlled asymmetrical converter with two diodes, where n = 0,1,2,3, ... The experimental results are in close agreement with the general theory of phase-controlled converters.

2.6 CONCLUSION

The comparative performance study of various phase controlled converters is carried out in this chapter. From the performance-wise the half controlled symmetrical converter is in general better than the other three converters. It uses three thyristors and three diodes which makes it less costly than the other converter where 6 thyristors and diodes (in case of asymmetrical converters) are the minimum requirement. For a given battery voltage, it requires less critical inductance to keep

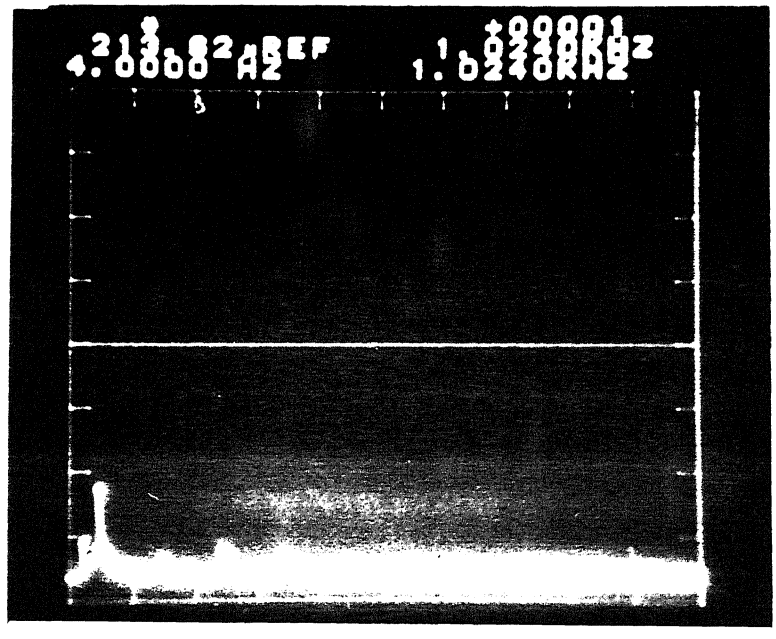

Fig. 2.29 Frequency spectra of input line current for HFAS - 2D

current continuous. It has the greater control over output voltage due to the wider range of control angle. In half controlled symmetrical convrerter the high displacement factor and power factor causes the reduction in the requirement of reactive power from ac supply. The main disadvantage of half controlled symmetrical converter is that it generates low order harmonics in the input line current. This drawback can be overcome by the use of proper filter circuit. Therefore, it can be concluded that for the medium and high power battery charging circuits, the three phase half controlled symmetrical converter provides better performance than the other converters.

CHAPTER - 3

PERFORMANCE STUDY OF SINGLE-PHASE AC-DC CONVERTER WITH EPWM, SPWM AND SEPWM SCHEMES

3.1 INTRODUCTION

Phase controlled converters are widely used as they are simple and need no special means for commutation. However, these converters deteriorate the power factor at the source side especially at large phase-angle delays. They also introduce lower order harmonics of substantial magnitude in the source current, which can be filtered only by a large size filter at the source terminals. The source current harmonics reduce the over-all power factor, adversally affect other loads connected to the same line and cause radio frequency interference. If the inductance present in the load circuit is small, discontinuous current conduction may result at low average value of current. This badly affects the performance of UPS in general and life of battery in particular.

The aim of this chapter is to find the techniques which are better than the phase-controlled techniques in terms of both load side and source side performance foe low power UPS.

There are techniques employing forced commutation which make the fundamental power factor unity in the entire control range of output voltage. The ripple in the output current and lower order

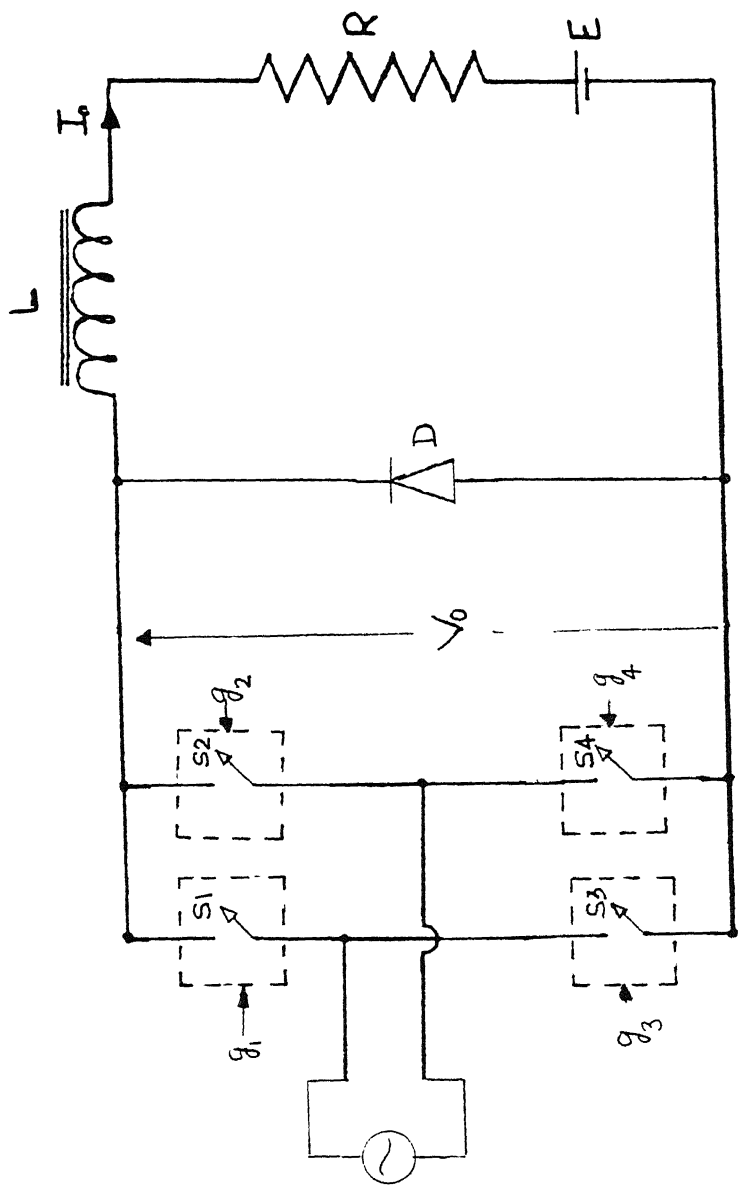

Fig 3 1 Ideal single-phase PWM ac-dc converter.

greater than the modulating voltage. The frequency of carrier signal depends on the number of pulses required in one cycle of ac source. The control of output voltage is obtained by varying the peak value, V_{mp} of modulating signal with respect to peak value, V_{rp} of carrier signal. The ratio V_{mp}/V_{rp} is termed as amplitude modulation ratio m_a. The ratio of the frequency of carrier signal to fundamental frequency of synchronizing signal is termed as frequency modulation ratio m_f. The instants of turn-on (α's) and turn-off (β's) of control switch in converter depend on m_a, m_f and the PWM technique.

3.2.1 Carrier Signal

The carrier signal is a triangular wave. The frequency of the carrier signal is always greater than the synchronising signal. The carrier signal for any kth pulse is mathematically expressed as

$$v_r = \pm V_{rp} \left[\frac{p}{\pi}\omega t - 2(k-1)\right]$$

where V_{rp} is the peak value of carrier signal

v_r is the instantaneous value of carrier signal

p is number of pulses per half cycle

ω is frequency of synchronizing signal

+ sign stands for a positive slope of triangular wave

- sign stands for a negative slope of triangular wave.

3.2.2 Equal Pulsewidth Modulation (EPWM)

A constant dc signal is compared with the carrier signal. The output of comparator gives the on pulse for the duration when dc signal remains greater than the carrier signal and the off pulse for the duration when dc signal remains less than carrier signal. The output voltage follows the input ac signal during the on pulse.

modulation signal v_m : V_{mp}

number of pulses per half cycle : p

amplitude modulation ratio : m_a

turn-on instant of kth pulse α_k : $\frac{\pi}{p}\,[\,2k - 1 - m_a\,]$

turn-off instant of kth pulse β_k : $\frac{\pi}{p}\,[\,2k - 1 - m_a\,]$

The Fig. 3.2 shows waveforms of carrier signal and modulating signal in case of EPWM. The waveforms of output voltage and input current are also shown in Fig. 3.2 under ideal condition of constant load current.

3.2.3 Sinusoidal Pulsewidth Modulation (SPWM)

A rectified sinusoidal ac signal is compared with the carrier signal. The comparator gives the on pulse for the duration when the sinusoidal signal is greater than the carrier signal. The off pulse is obtained when the carrier signal is greater than the sinusoidal modulating signal. The output voltage follows the input voltage during the on pulse. Fig. 3.3 shows the gating pulses to the switches, output voltage and input current waveforms under constant load condition.

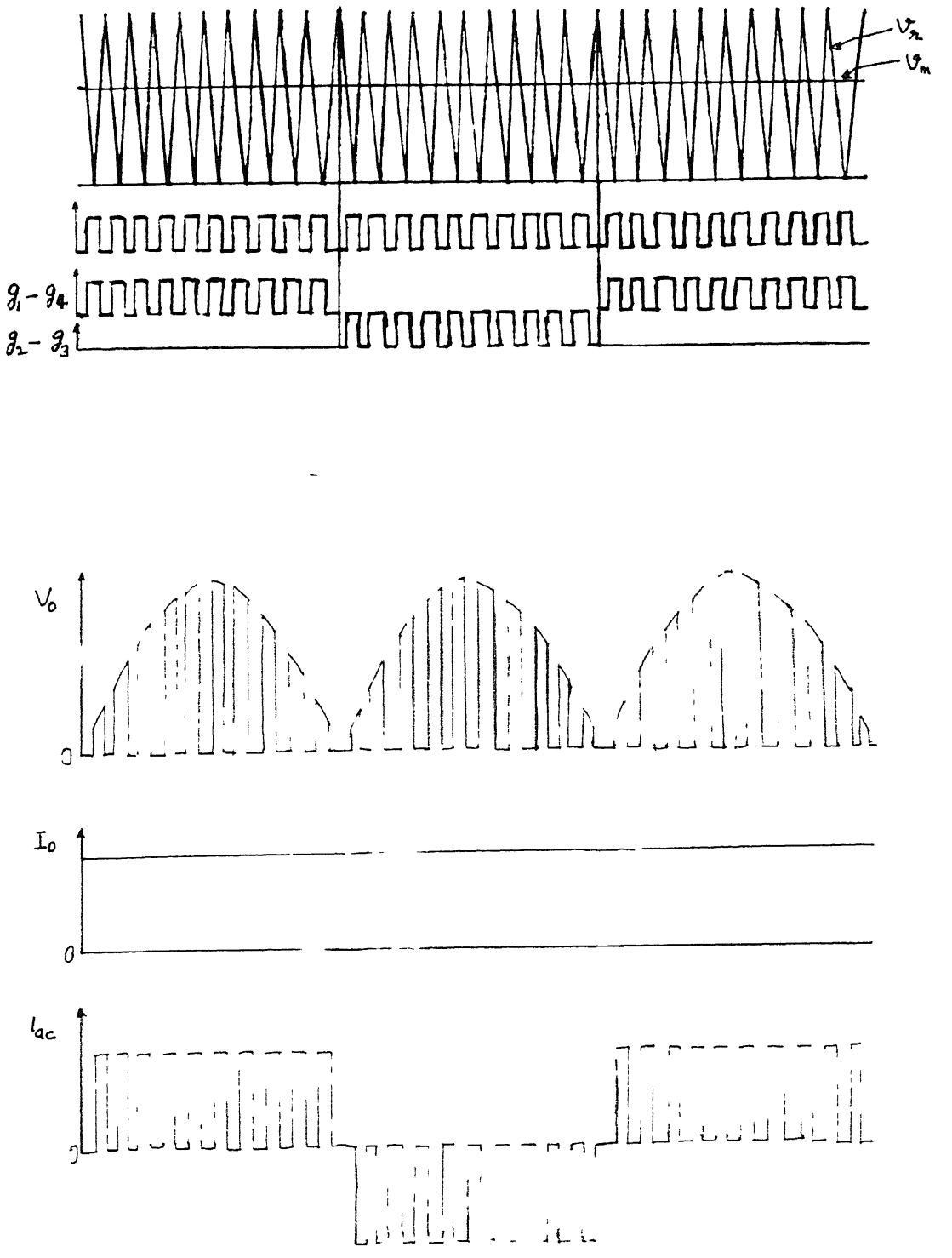

g. 3.2 Waveforms of single-phase bridge converter with EPWM.

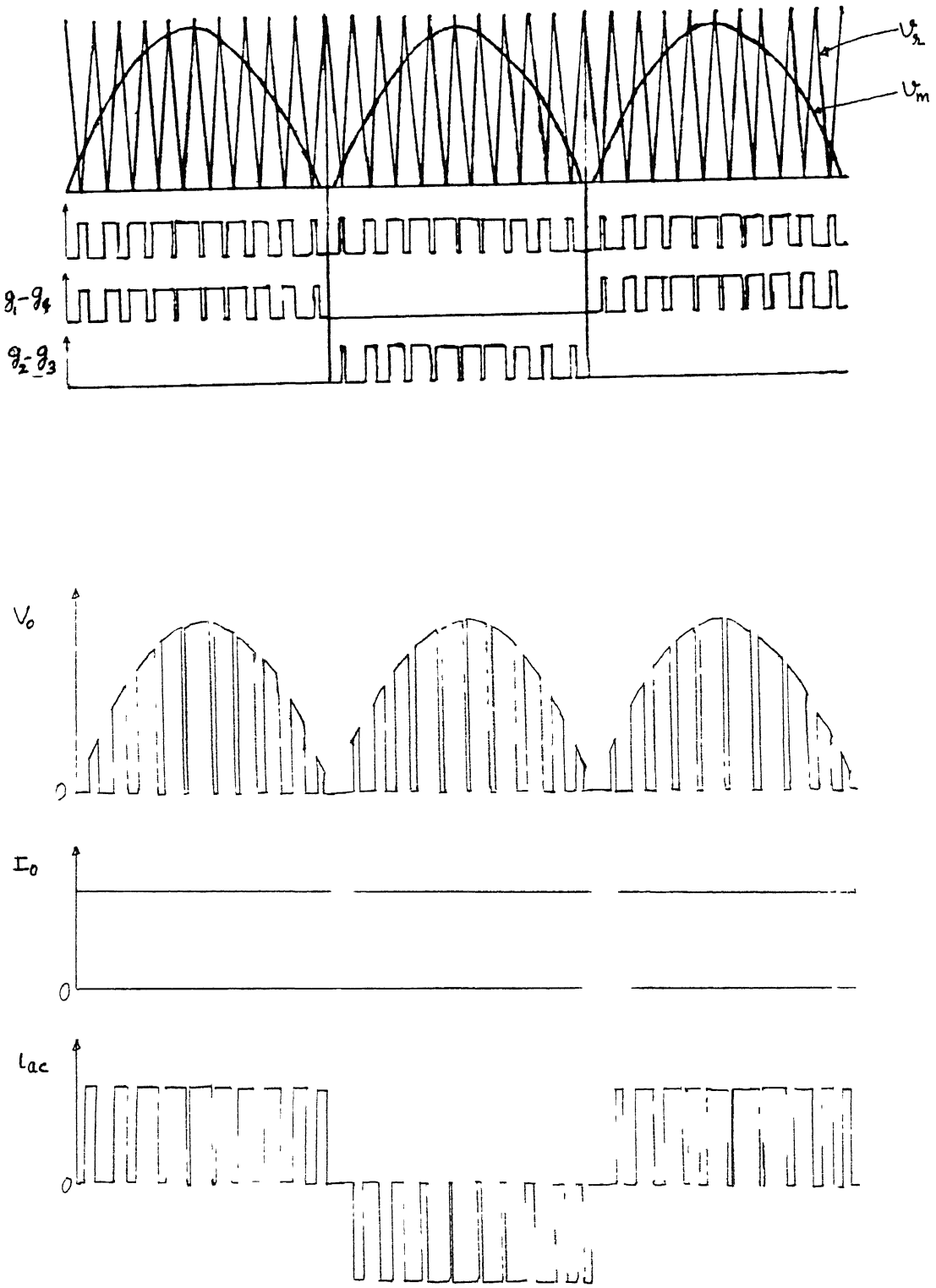

Fig 3.3 Waveforms of single-phase bridge converter with SPWM.

modulation signal v_m : $V_{mp} \sin \theta_i$

number of pulses per half cycle : p

amplitude modulation ratio : m_a

turn on instant of kth pulse α_k : $\frac{\pi}{p}\left[2k - 1 - m_a \sin\left\{\frac{2\pi}{p}(k-1)\right\}\right]$

turn off instant of kth pulse β_k : $\frac{\pi}{p}\left[2k + 1 + m_a \sin\left\{\frac{2\pi}{p}k\right\}\right]$

3.2.4 Sine-Equal Pulsewidth Modulation (SEPWM)

In the SEPWM, SPWM and EPWM are combined. These two pulsewidth modulation schemes with different amplitude modulation ratios are combined into one signal. The amplitude modulation ratio of SPWM is always greater than the modulation ratio of EPWM. Fig. 3.4 shows the gating pulses for the switches, output voltage and input current waveforms under constant load condition in this scheme.

modulation ratio of EPWM : m_E

modulation ratio of SPWM : m_S

number of pulses per half cycle : p

number of pulses generated using EPWM technique $p_E = \frac{m_E}{m_S} \times p$

Amplitude modulation ratio SEPWM : m_E (when $m_E \neq 0$ else m_S)

number of pulses generated using SPWM technique, $p_S = p - p_E$

The pulses p_S are located at the centre of the half cycle of the synchronising signal where as the pulses p_E are located on either side of p_S pulses.

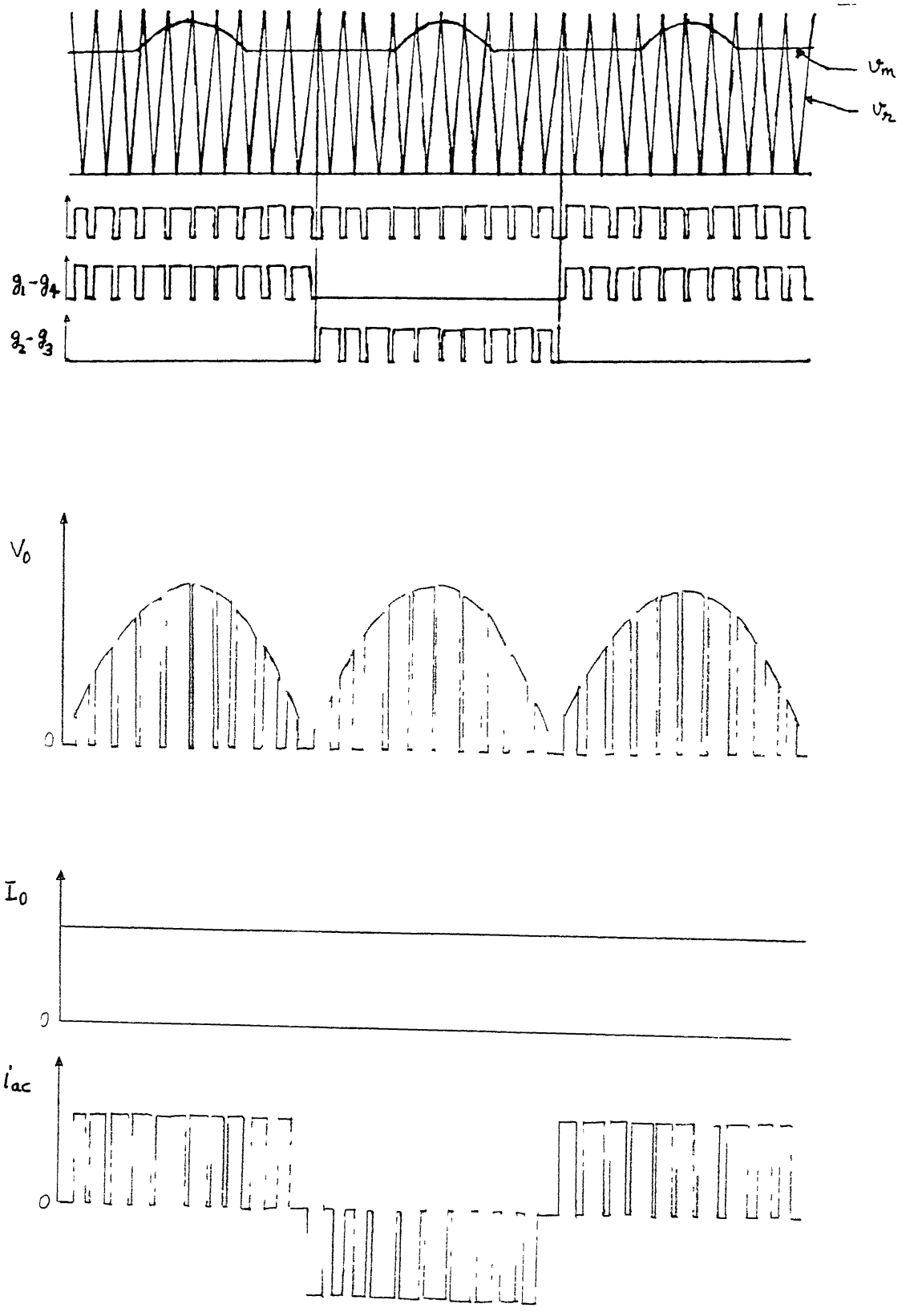

Fig 3 4 Waveforms of single-phase bridge converter with SEPWM.

3.3 STUDY OF PERFORMANCE CHARACTERISTICS OF PWM CONVERTER

The following performance curves are obtained theoretically for the above mentioned three modulation schemes. These characteristics are shown in Figs. 3.5 to 3.14 as a function of amplitude ratio m_a and frequency modulation ratio m_f.

(i) Output voltage :

The output voltage v_o follows the input ac voltage when the controlling switches are closed, zero otherwise. The average output oltage v_{dc} is calculated by averaging v_o for a period of π

$$v_{dc} = \sum_{i=1}^{p} \left[\frac{2}{2\pi} \int_{\alpha_i}^{\beta_i} V_m \sin \omega t \, d(\omega t) \right]$$

The maximum output dc voltage

$$v_{dm} = \frac{2V_m}{\pi}$$

and the normalized output dc voltage is given as

$$v_n = \frac{v_{dc}}{v_{dm}} = \frac{1}{2} \sum_{i=1}^{p} \left(\cos \alpha_i - \cos \beta_i \right)$$

Fig. 3.5 shows the variation of v_n in EPWM, SPWM, and SEPWM control strategies with m_a respectively for three values of m_f. The output voltage varies linearly with m_a in EPWM and SPWM. In case of the SEPWM the output voltage is almost constant for lower value of m_a. It then increases gradually in upper range of m_a. In case of SPWM, in the lower range of m_a, v_o increases with m_f. In

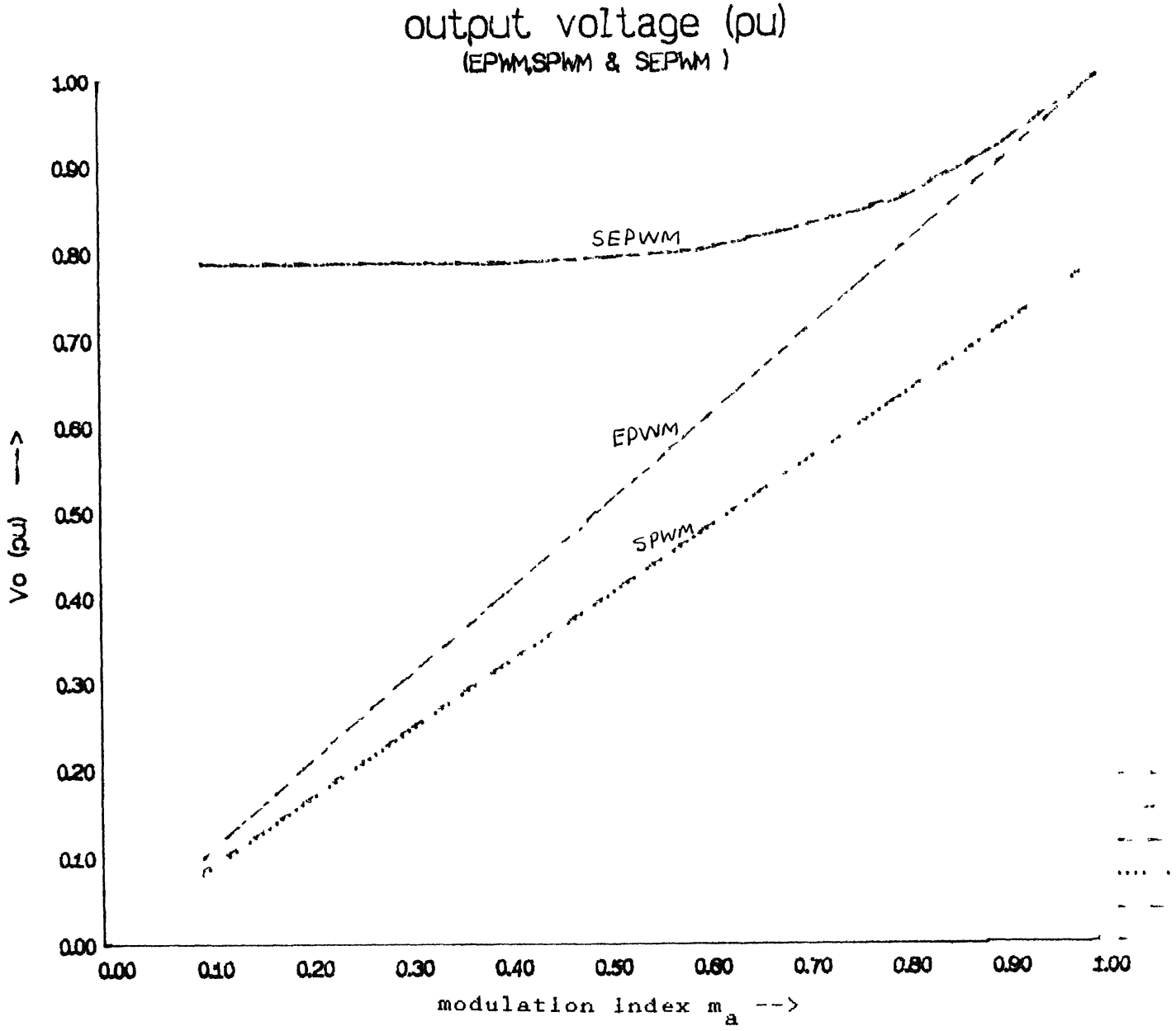

SEPWM, in the middle range of m_a, the output voltage decreases with increase in m_f. In the battery charging circuits, variable dc voltage is needed. This is fulfilled easily by both EPWM and SPWM control schemes. In case of SEPWM, the modulation ratio m_E is held at zero value and the modulation ratio m_S is varied depending upon the requirement of the battery voltage. After the battery is fully charged, the control is switched over to SEPWM to meet the required constant output voltage. Ideally, this SEPWM control is well suited for dc power supplies.

(ii) Output voltage harmonics :

The harmonic analysis of the output voltage can be carried out by expressing the output voltage expression in Fourier series

$$v_o = v_{dc} + \sum_{n=1}^{\infty} \left[a_n \cos n\omega t + b_n \sin n\omega t \right] \quad n = 1,2,3,....$$

where

$$a_n = \sum_{i=1}^{p} \frac{v_m}{\pi} \left[\left\{ \frac{\cos(n+1)\alpha_i - \cos(n+1)\beta_i}{(n+1)} \right\} + \left\{ \frac{\cos(n-1)\beta_i - \cos(n-1)\alpha_i}{(n-1)} \right\} \right]$$

$$b_n = \sum_{i=1}^{p} \frac{v_m}{\pi} \left[\left\{ \frac{\sin(n+1)\alpha_i - \sin(n+1)\beta_i}{(n+1)} \right\} + \left\{ \frac{\sin(n-1)\beta_i - \sin(n-1)\alpha_i}{(n-1)} \right\} \right]$$

Fig. 3.6 shows the output voltage harmonics for $m_f = 50$. The frequency of fundamental voltage is twice the ac supply frequency. The harmonics in the output voltage waveform appear as sidebands,

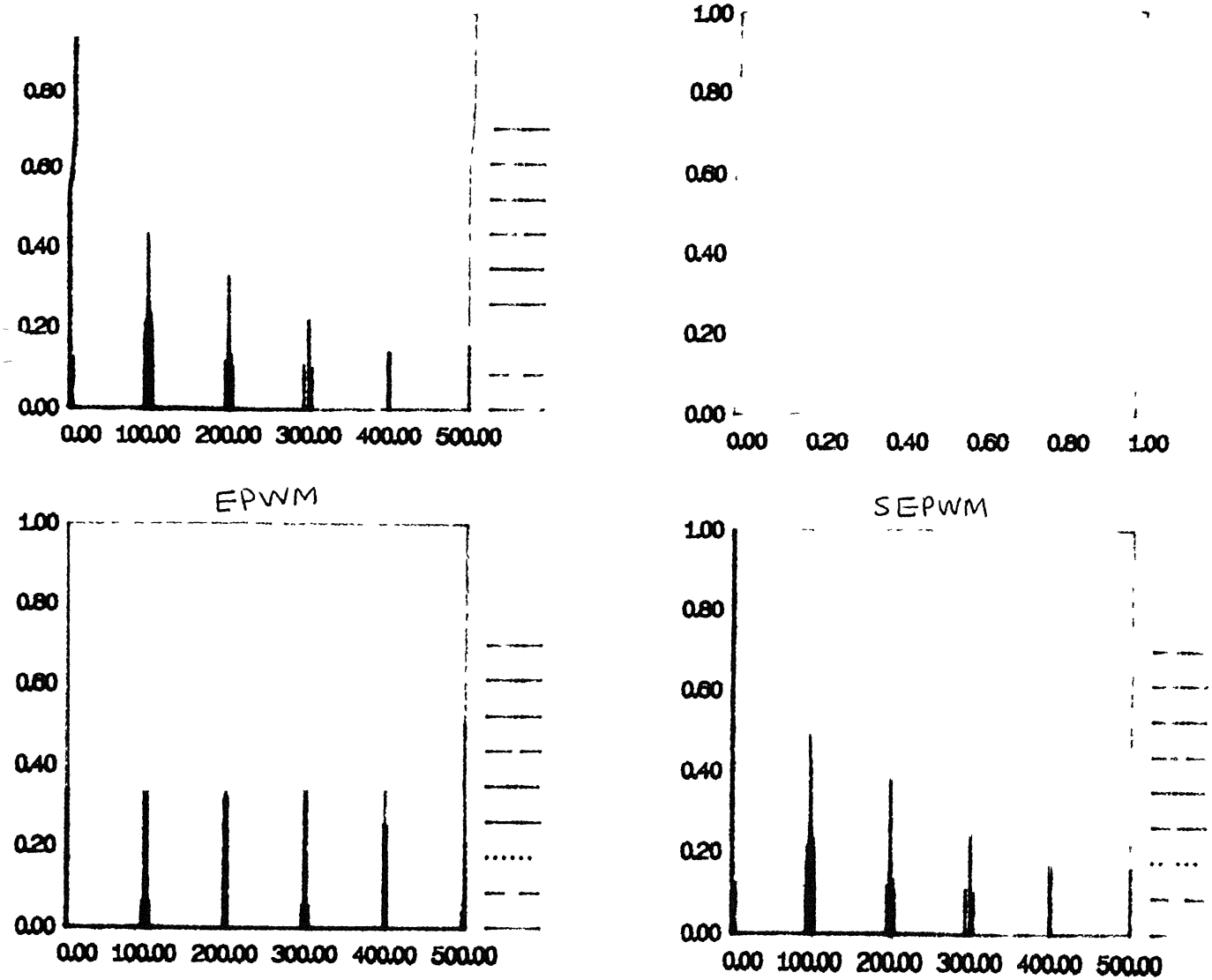

Fig 3.6 Relationship between output voltage harmonic and m_a, $m_f = 50$.

centered around the switching frequency and its multiples. The low order harmonics of small magnitudes are also present in the output voltage. The amplitudes of sidebands reduce rapidly with the increase in the order of sideband. The magnitudes of of sidebands are more prominent in SPWM and SEPWM than the EPWM.

(iii) Output current ripple :

In order to obtain the actual current waveform in the output circuit without assuming constant load current, the actual equations are solved. When a voltage is applied across an RL-battery load, the load current i, rises during $\alpha_1 < t \leq \beta_i$ and decreases exponentially during $\beta_1 < t \leq \alpha_{1+1}$. The expression for i is given as

$$i = \frac{V_m}{Z} \sin(\omega t - \phi) - \frac{V_c}{R} + \left[I_{\alpha_1} + \frac{V_c}{R} - \frac{V_m}{Z} \sin(\alpha_1 - \phi) \right] \exp\left\{ \left(\alpha_1 - \omega t \right) / \tan \phi \right\}$$

$$\alpha_1 < \omega t \leq \beta_1$$

where $i = I_{\alpha_1}$ at $\omega t = \alpha_1$

and

$$i = - \frac{V_c}{R} + \left[I_{\beta_i} + \frac{V_c}{R} \right] \exp \left\{ \left(\beta_i - \omega t \right) / \tan \phi \right\}$$

$$\beta_1 < \omega t \leq \alpha_{i+1}$$

where $i = I_{\beta_1}$ at $\omega t = \beta_1$

The expression for normalized load current can be written as,

$$i_N = \sin(\omega t-\phi) - \frac{m}{\cos\phi} + \left[I_{N\alpha_i} + \frac{E}{\cos\phi} - \sin(\alpha_1-\phi)\right] \times \exp\left\{\left[\alpha_1 - \omega t\right]/\tan\phi\right\}$$

$$\alpha_1 < \omega t \leq \beta_1$$

and

$$i_N = -\frac{E}{\cos\phi} + \left[I_{N\beta_i} + \frac{E}{\cos\phi}\right] \exp\left\{\left[\beta_1 - \omega t\right]/\tan\phi\right\}$$

$$\beta_1 < \omega t \leq \alpha_{1+1}$$

where the base voltage is V_m, and base curent is V_m/Z. The load current ripple is given as

$$CR = \frac{i_N(max) - i_N(min)}{2}$$

Fig. 3.7(a) and 3.7(b) show the output current ripple for m_f = 25 and m_f = 50 respectively. The ripple in the load current depends on battery voltage and load inductance. Since the operating range of the converter under just continuous current condition depends on the battery voltage and inductance at the dc terminal. The curves shown in Fig. 3.7 starts with the modulation ratio for which the current is just continuous. As the modulation ratio increases the ripple increases. The current ripple in SPWM and EPWM is independent of m_f. The just continuous current operation is not possible till certain value of m_a depending on the circuit parameters. But once the just continuous current conditions sets in the circuit current ripple increases with m_a. In case of SPWM,

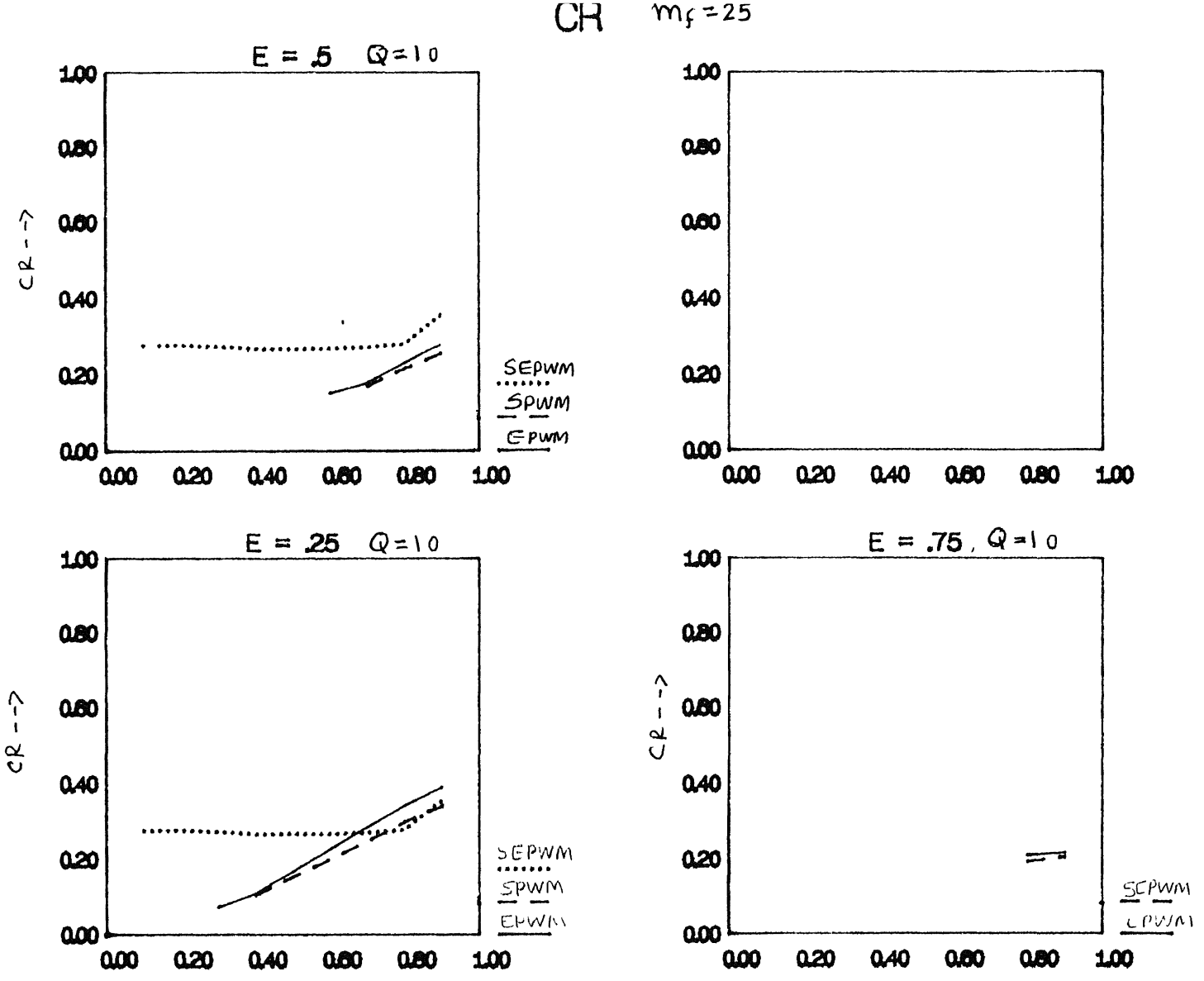

Fig. 3 7(a) Relationship between load current ripples and m_a, m_f= 25.

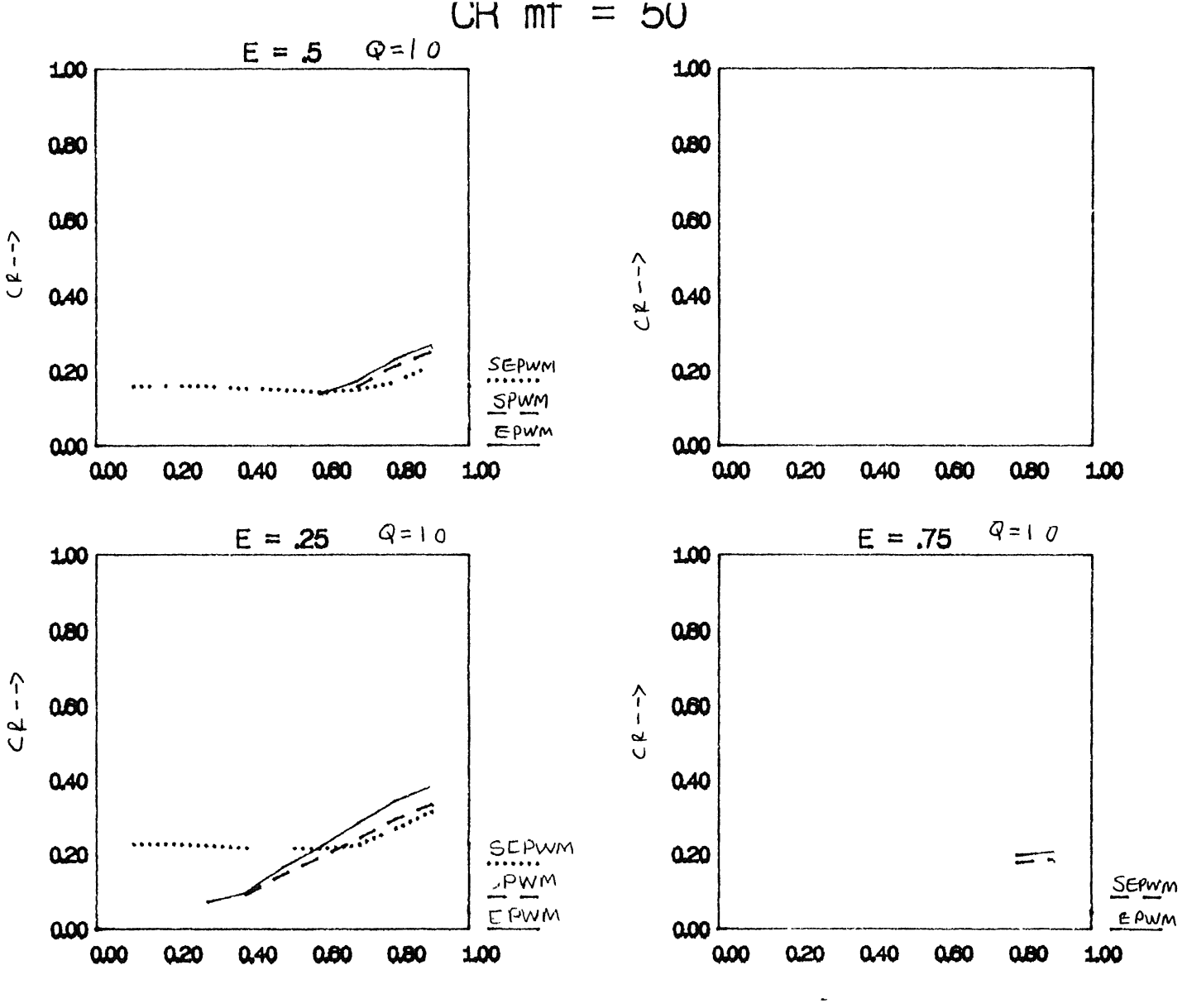

Fig 3 7(b) Relationship between load current ripples and m_a, m_f= 50

with E = 0.75 and Q = 1. The just continuous current operation is not possible in the valid range of m_a. In SEPWM controlled circuits the load current ripple remains constant for greater part of m_a. This span depends on the circuit parameters and m_f. With the increase in m_f the load current ripple reduces.

(iv) Input current harmonics :

The input current harmonics spectrum for all the three schemes are given in Figs. 3.8(a) to 3.8(c). In case of SPWM, the harmonics in the input current waveform appear as sidebands, centred around the switching frequency and its multiples. In general, the harmonic order h corresponds to the kth sideband of j times the m_f is given as

$$h = j(m_f) \pm k \qquad k = 0,1,2,....$$
$$j = 0,1,2,....$$

h = 1 corresponds to fundamental frequency. For odd values of j, the harmonics exist only for even values of k. For even values of j, the harmonics exist only for odd values of k.In EPWM and SEPWM, other lower order odd harmonics are also present besides, these sidebands. The lower order harmonics are of considerable magnitude which decreases as the harmonic order increases.It is much easier to filter out the higher order harmonics with low value of filter components in SPWM. Thus SPWM control technique is better than the other two PWM techniques in terms of input current harmonics.

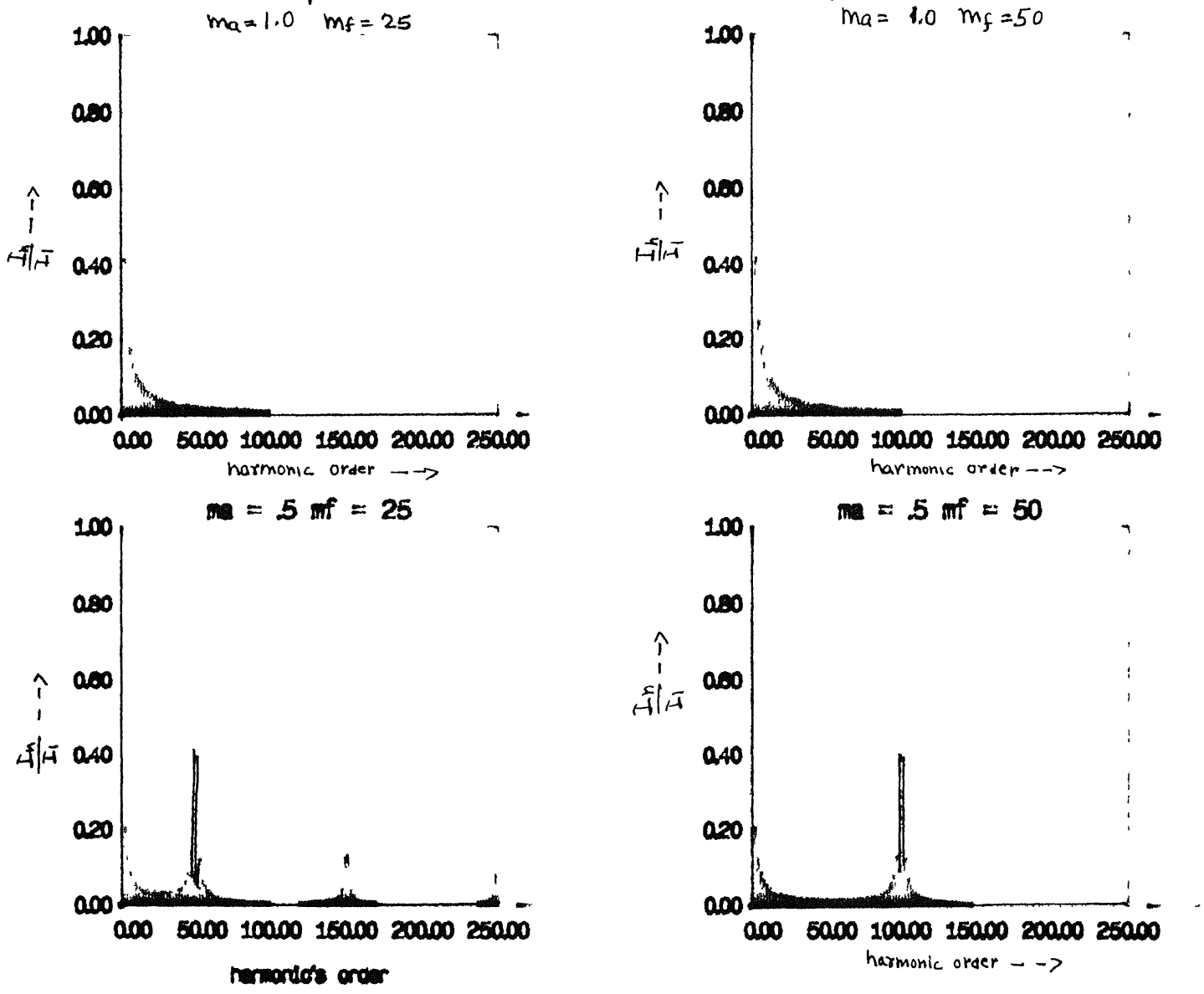

Fig 3.8(a) Relationship betwen input current harmonics and harmonic order for EPWM.

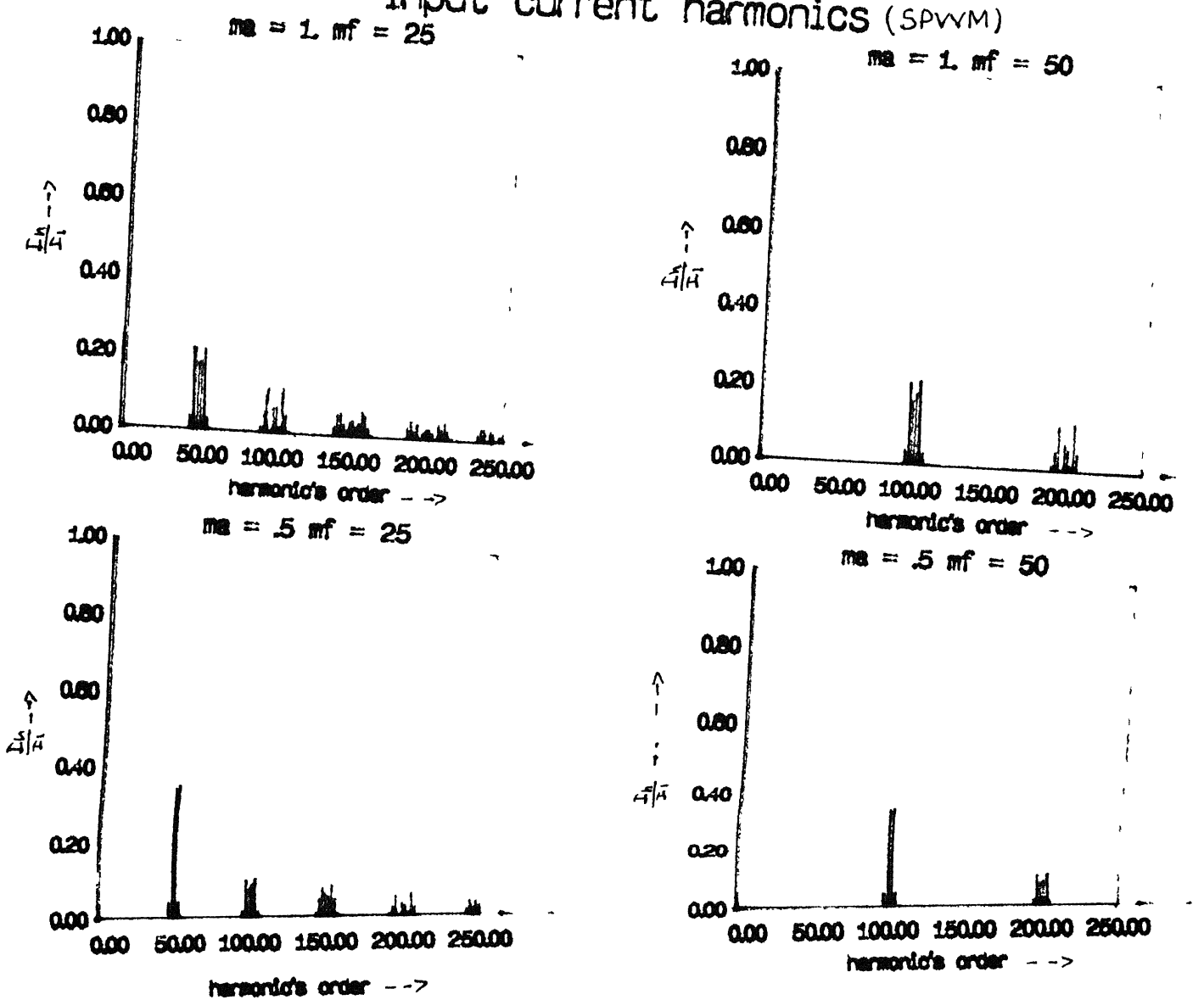

Fig. 3 8(b) Relationship between input current harmonics and harmonic order for SPWM.

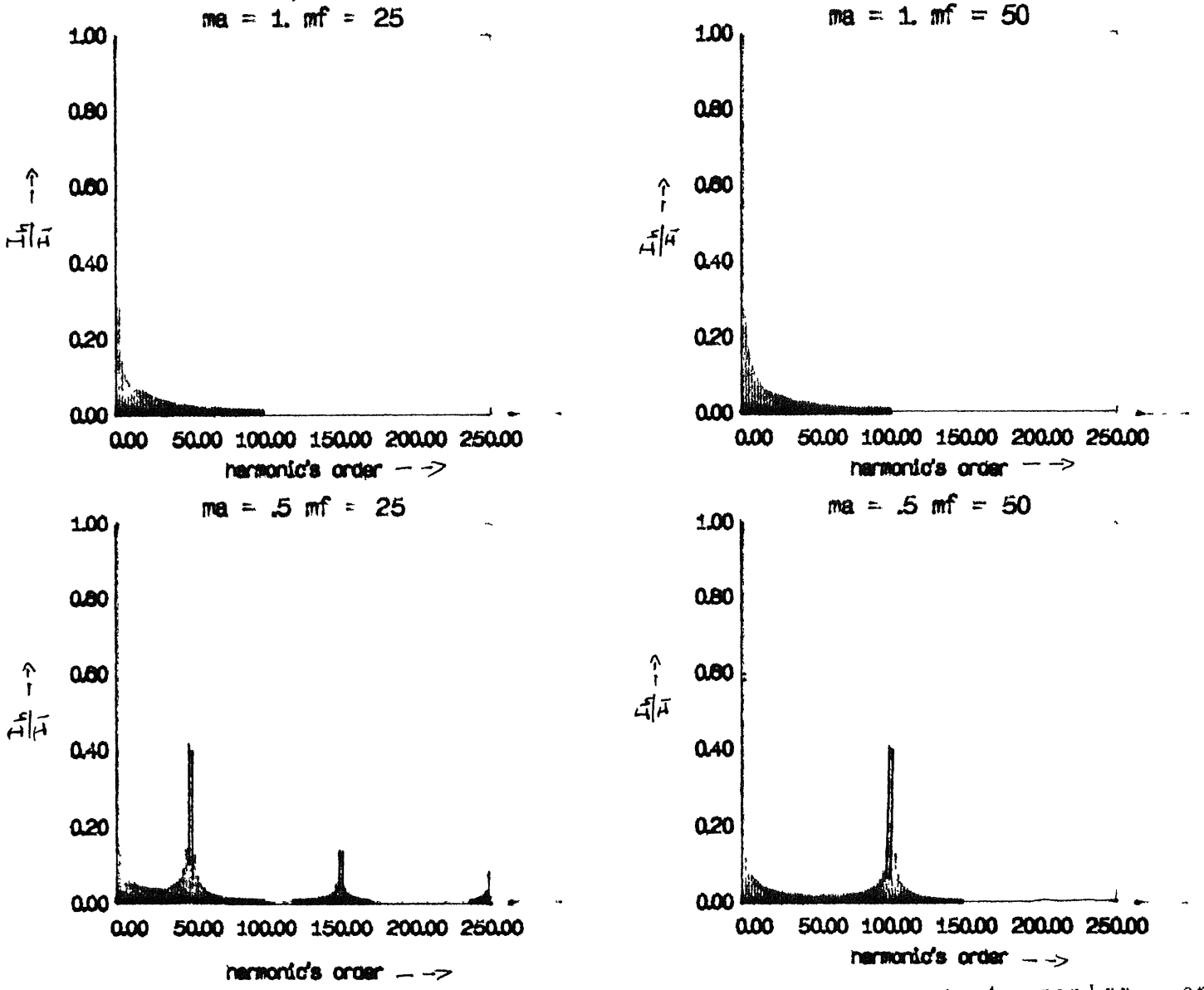

Fig 3.8(c) Relationship between input current harmonics and harmonic order for SEPWM

(v) Input current harmonic factor :

Fig. 3.9 shows the variation of input harmonic factor. The input current harmonic factor in case of EPWM and SPWM is large in lower range of m_a and reduces gradually as m_a increases. With the increase of m_f, the current harmonic factor decreases with m_a. As the m_f increases, the characteristics of two schemes almost coincide with each other throughout the full range of m_a. The shape of harmonic factor curves are independent of m_f. In the upper middle range of m_a, the current harmonic factor in SEPWM increases very minutely and thereafter it reduces slightly to coincide with the characteristics of EPWM and SPWM.

(vi) Input power factor :

Since all the PWM schemes work on the principle of symmetrical control, they have unity fundamental power factor. The power factor is given as

$$PF = \frac{I_1}{I_{rms}}$$

where I_1 is the rms fundamental input current and I_{rms} is the rms input current.

The power factor variation in EPWM, SPWM and SEPWM is shown in Fig. 3.10. In SPWM and EPWM with an increase in m_a and m_f, the power factor gets improved. In SEPWM, the power factor remains high and almost constant in the full range of m_a.

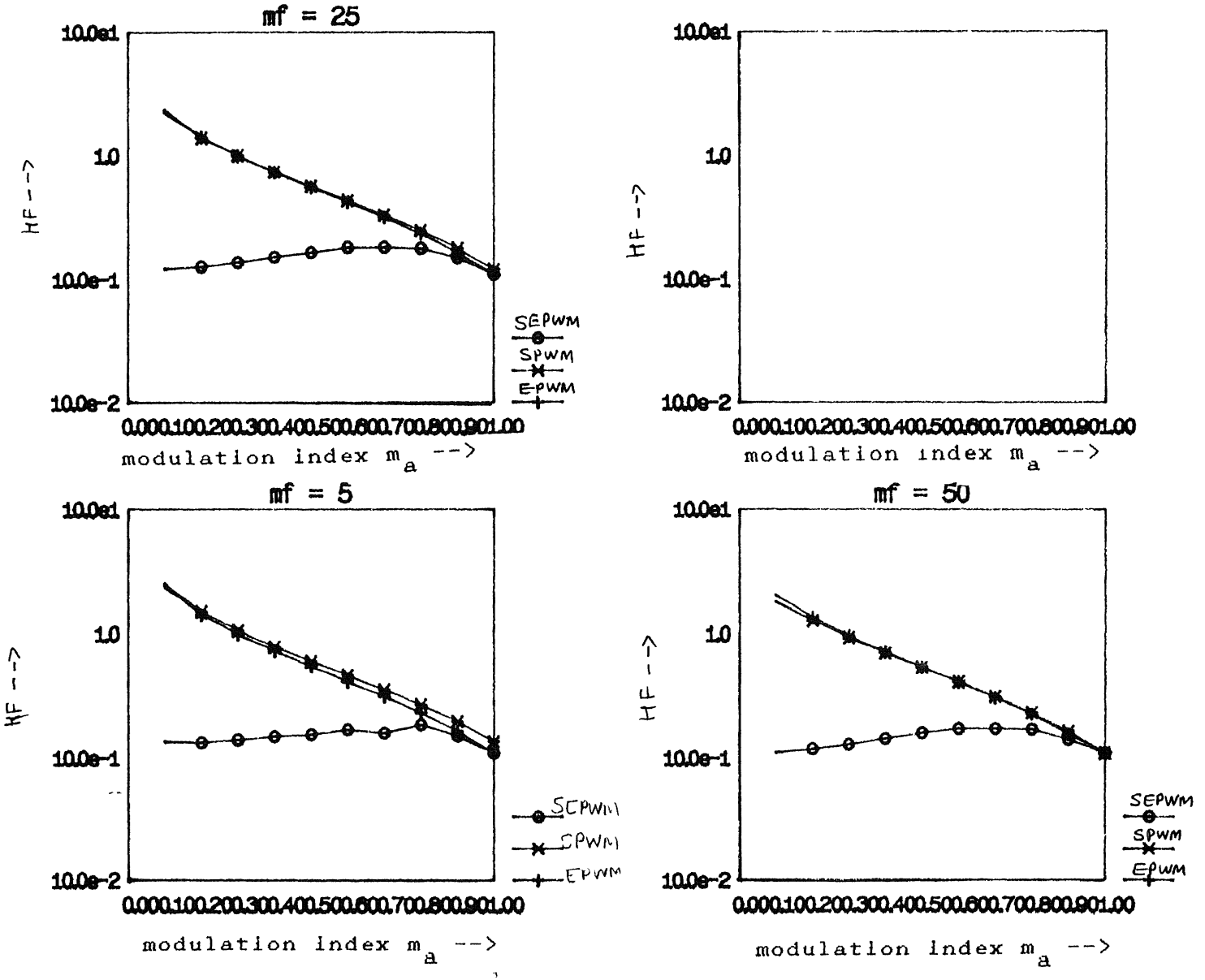

Fig 3.9 Relationship between input current harmonic factor and m_a

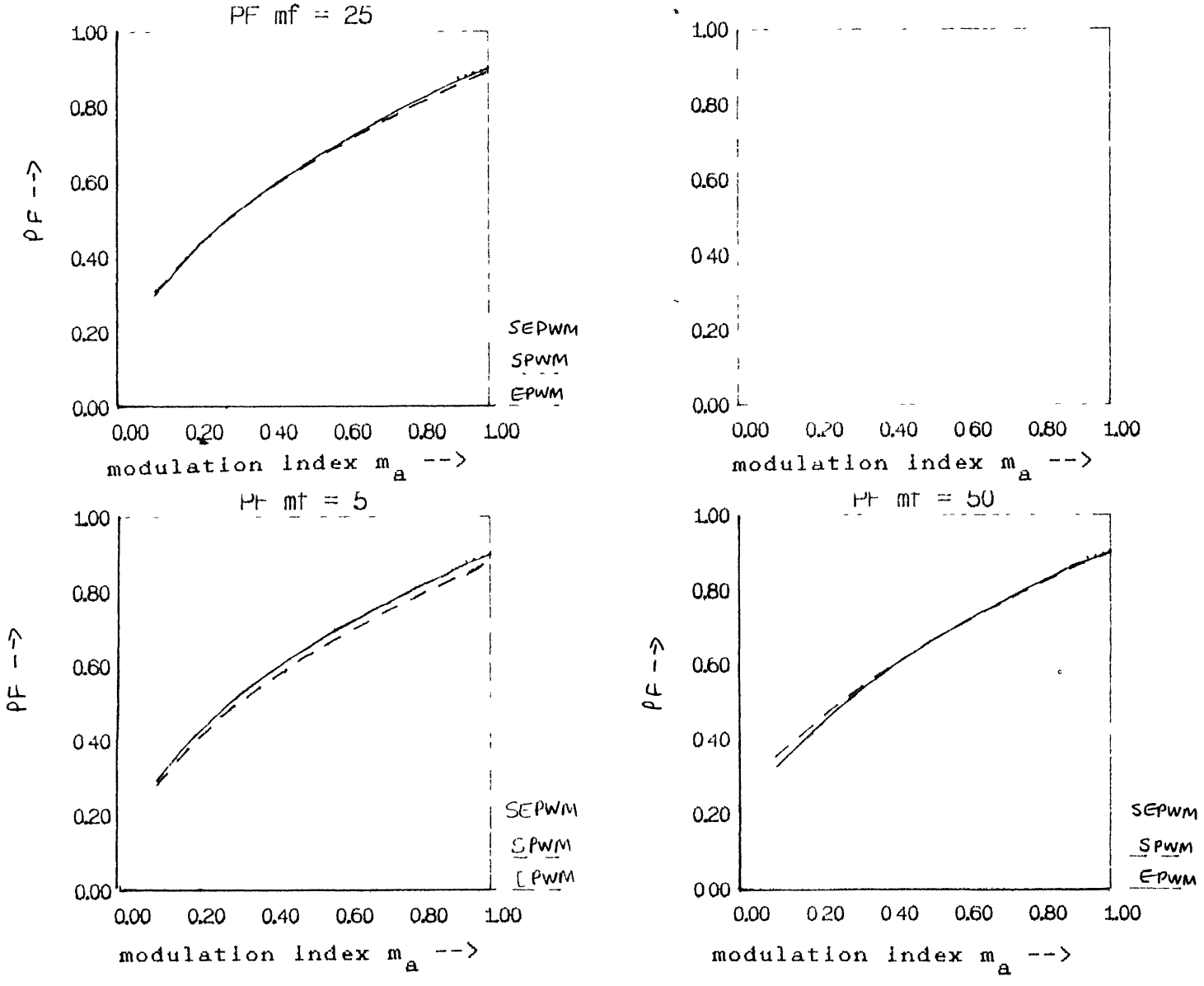

* cc-lit/k vayu * Fig 3.10 Relationship between input power factor and m_a.

3.4 SPICE SIMULATION OF SINGLE-PHASE PWM CONVERTER

Before the assembly of single-phase PWM converter in laboratory the converter's circuit is simulated using SPICE simulation package. This simulation package provdes the facility to simulate the electronic circuit very closed to physical circuit. Current monitoring is done by inserting zero voltage sources in series with the branchs. Resistances of low values are included in series with all inductors and resistances of high values are connected in parallel with capacitors to make the simultion network more realistic and also to avoid possible reactance loops. If there is any reactance loop, then the SPICE simulation is aborted due to non-convergence. Fast recovery diodes are simulated by changing the transit time (TT) parameter of standard diode model. MOSFET model mos 1 is used for simulating the active switch. The transconductance (K_p) and mobility (V_o) of the standard model is changed to get the required MOSFET characteristics close to the manufacturer's specifications.

The analysis is carried out over a period of 200 ms. Thus, stable initial conditions are established.The transient analysis is carried out for different modulation ratios in all PWM strategies.

3.5 LABORATORY SETUP AND EXPERIMENTAL RESULTS

3.5.1 Laboratory Setup

The configuration of converter tested with the help of SPICE simulation is used for facrication in the laboratory. The block

diagram of the experimental setup of PWM single phase converter is given in Fig. 3.11. The ac line voltage is fed to a step down transformer. A capacitor filter is used to filter the harmonics of the ac current. The output voltage of step-down transformer is applied to a bridge converter formed with power MOSFETs. The diagonal pair of power MOSFETs in the single phase full bridge converter are switched on and off in alternate half cycle using PWM control strategy. At the output of the converter, inductor and capacitor are used to reduce the ripple in the voltage and current. The diode provides the path for the load current when the MOSFETs are off whereby continuity for the load current is maintained. The power MOSFETs are selected as switching devices for the converter because they are extremely fast compared to other devices. At high switching speed minimal snubber is required. Easy paralleling of large number of devices is possible. Since the second breakdown is negligible due to equal distribution of current, it allows increase in peak current of device on duty cycle basis. Power MOSFETs one generally used in high frequency switching applications within the ratings of a few watts to a few KWs. However, the device has a reverse body diode which is slow due to large storage charge, therefore, at high speed applications the external fast recovery diodes are required to bypass this diode. Fig. 3.11 shows the connection of MOSFETs IRFPE 50 and fast recovery diodes (D) BYT 301000 in the circuit. The inductance L and capacitors C1 are large enough to provide the ripple free current through the load.

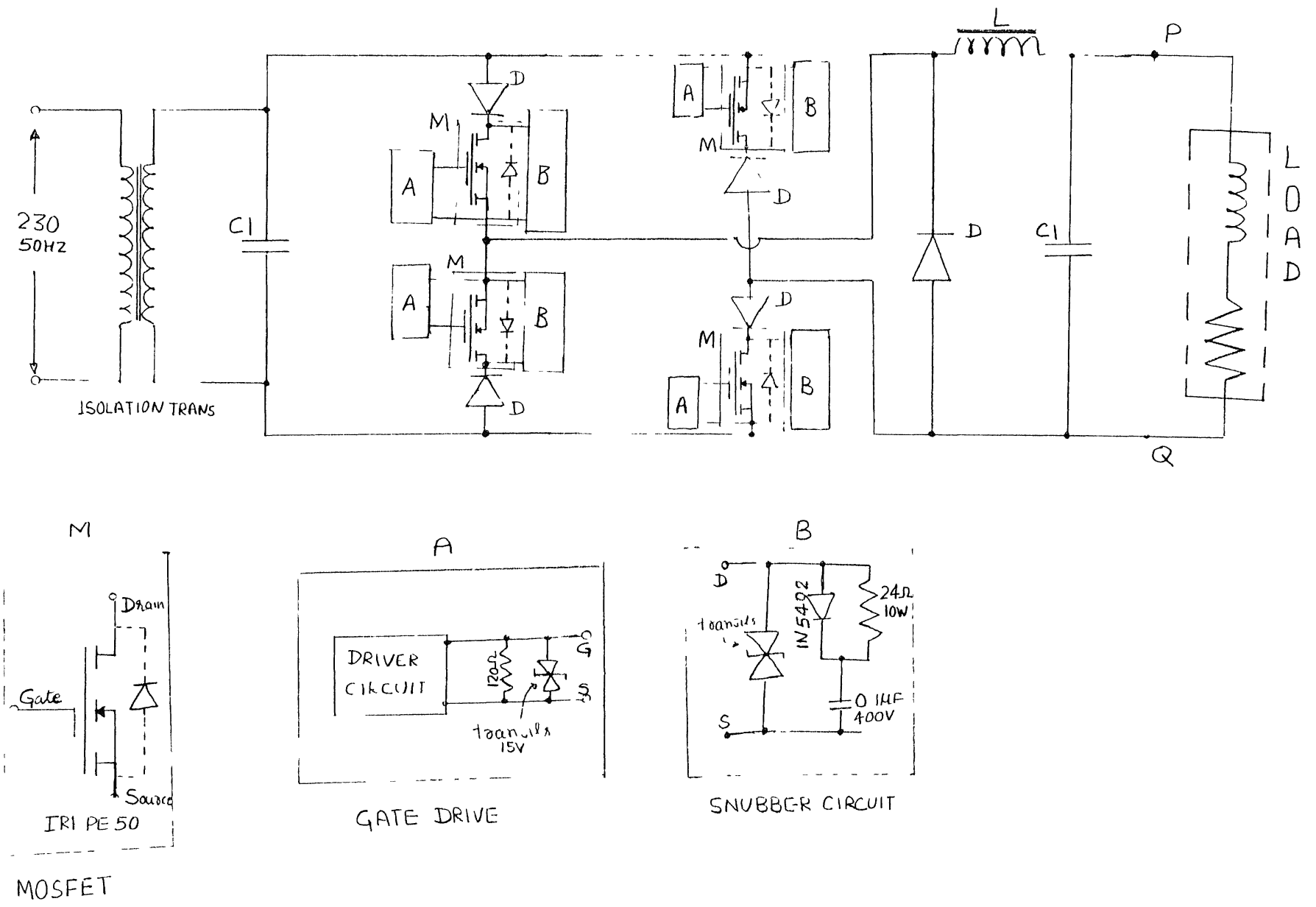

Fig. 3.11 Complete circuit diagram of single-phase PWM converter.

Figure 3.12 gives the detailed control circuit used to generate the trigger pulses. NE566 is used to generate the triangular waves. The frequency of carrier wave is kept at 10 KHz. The diagonal MOSFETs are switched on and off for 100 times in each half cycle of synchronous signal. Figure 3.13 gives the waveforms at various points of the control circuit.

Figure 3.14 gives the detailed circuit diagram of the driver card used to drive each MOSFET and floating at MOSFET's source potential. Opto isolator 6N135 is used to get the required isolation. The isolated power suplies of 5V and 12V are derived using on-card regulators 7805 and 7812 and small isolation transformer. Figure 3.15 shows the waveforms at various points.

3.5.2 Experimental Results

The experiment was carried out under the following conditions :

AC source	:	230 V (phase voltage), 50 Hz
Circuit components	:	L = 42.5 mH
		R = 50 Ω
		E = 0
Number of pulses per half cycle	:	100

Fig. 3.16 shows the oscillograms of input line voltage, input line current, output dc voltage and output load current waveforms for EPWM, SPWM and SEPWM control schemes. The oscillograms are taken with m_a = 0.9 for EPWM and SPWM and m_S =

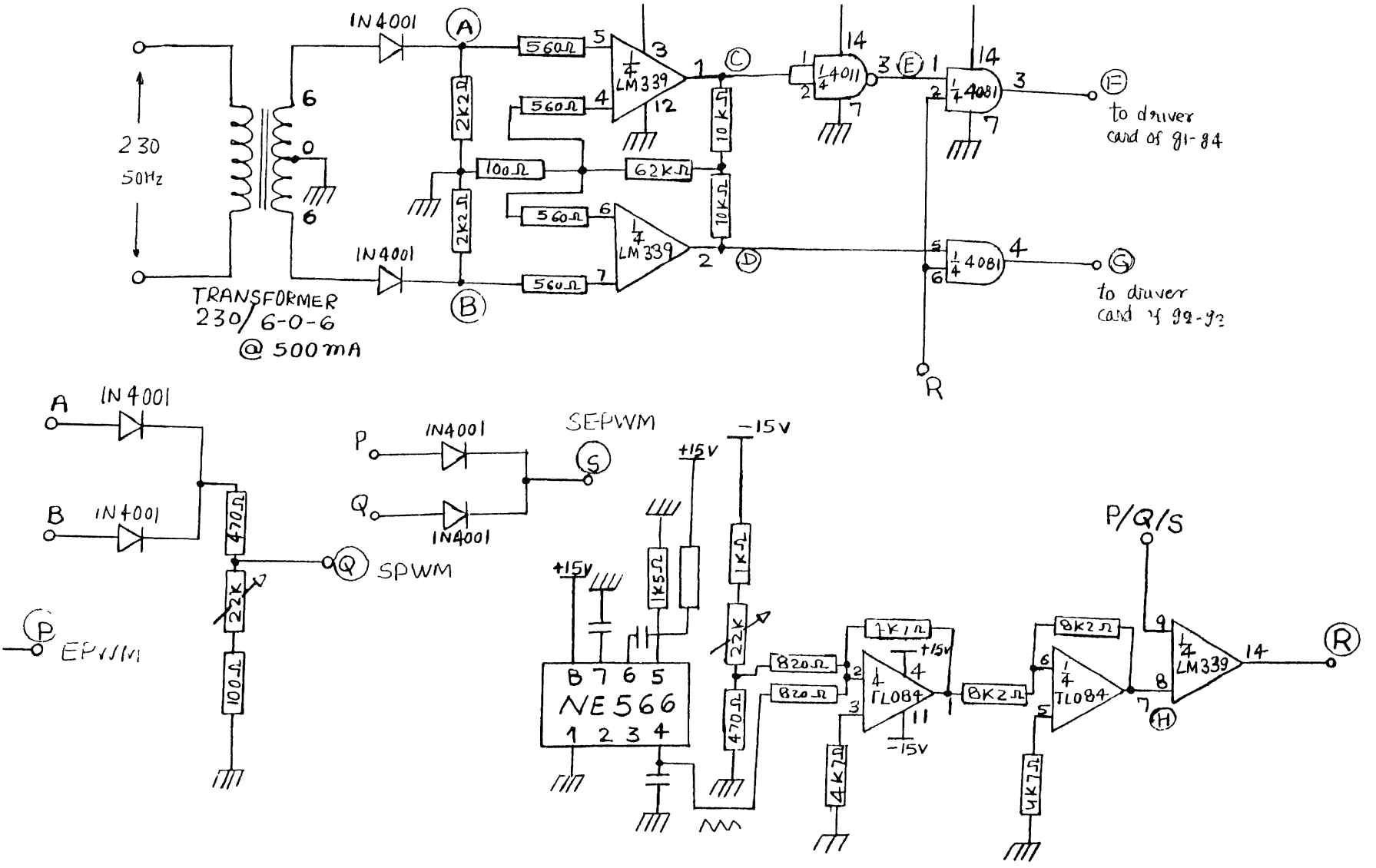

Fig 3 12 Control circuit to generate EPWM, SPWM and SEPWM control signals

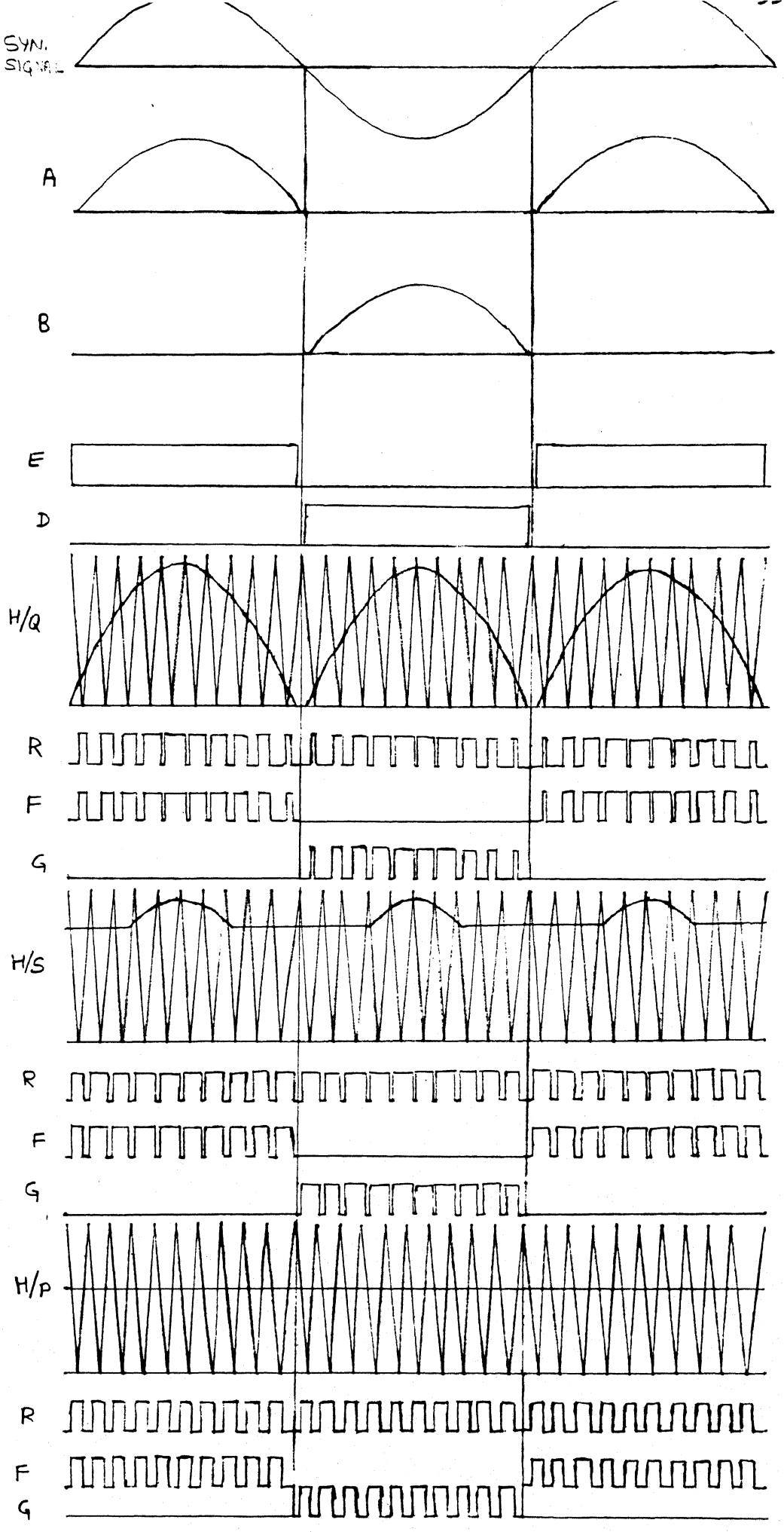

Fig. 3.13 Waveforms of control signals at different points

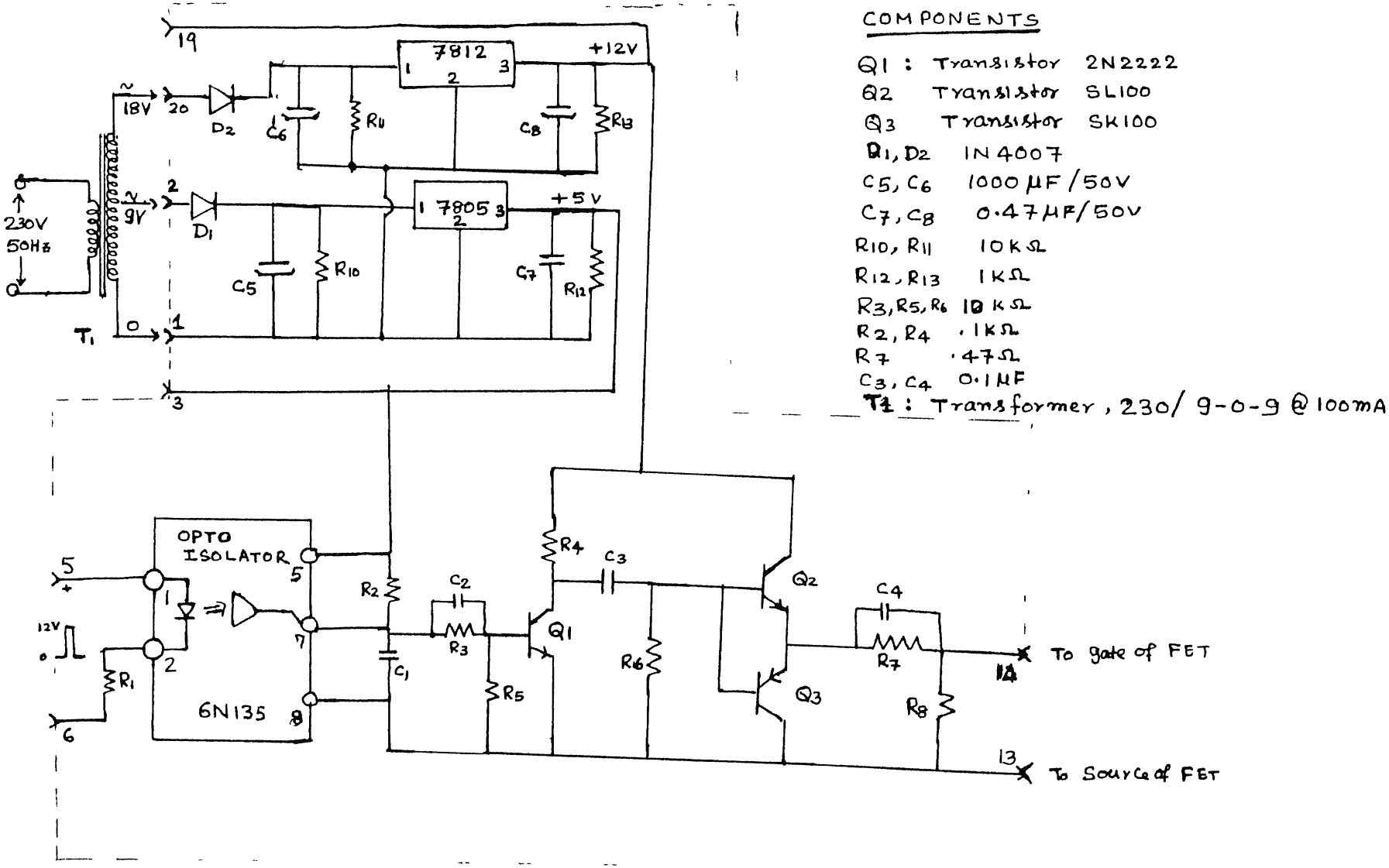

COMPONENTS

Q1 :	Transistor 2N2222
Q2	Transistor SL100
Q3	Transistor SK100
D1, D2	IN4007
C5, C6	1000 µF/50V
C7, C8	0.47 µF/50V
R10, R11	10 KΩ
R12, R13	1 KΩ
R3, R5, R6	10 KΩ
R2, R4	.1 KΩ
R7	.47Ω
C3, C4	0.1 µF

T1 : Transformer, 230/ 9-0-9 @ 100mA

Fig 3 14 Detailed diagram of the driver circuit

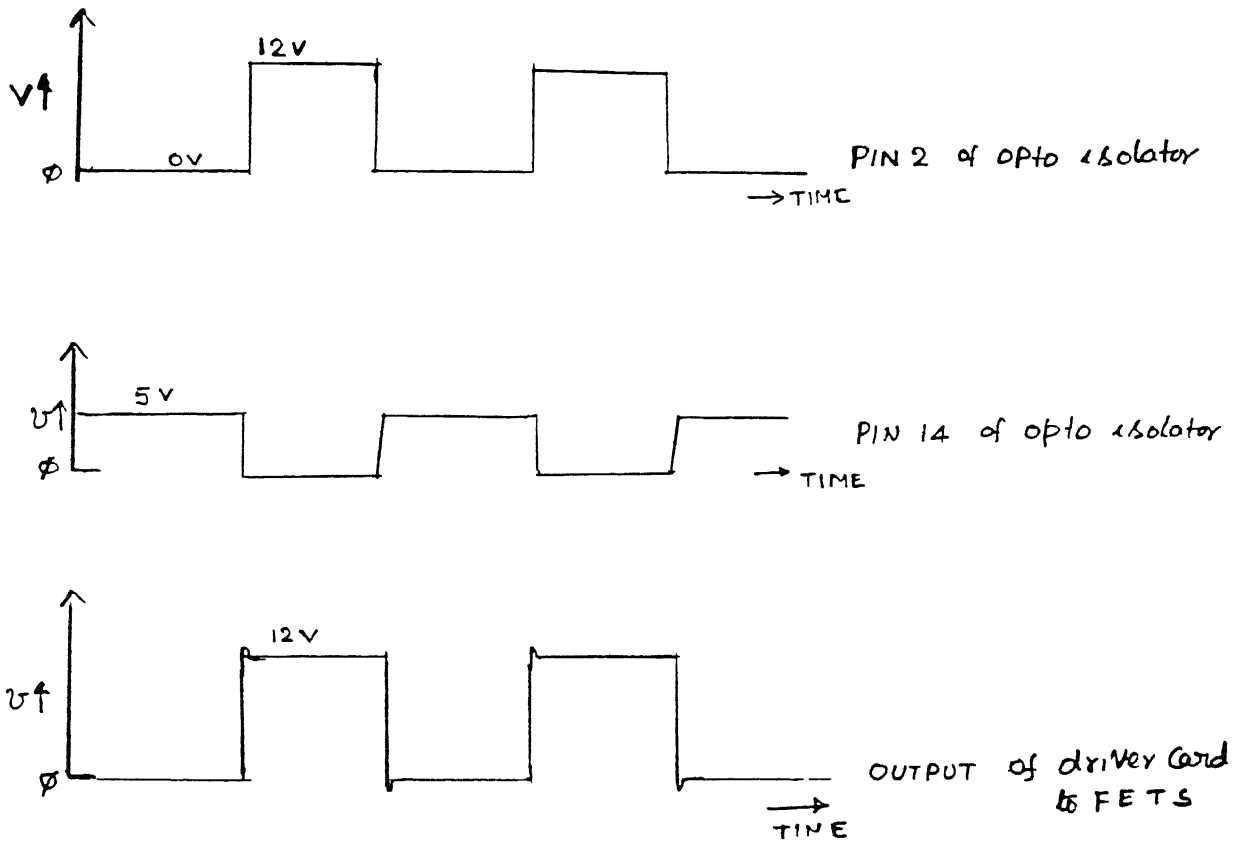

Fig 3 15 Waveforms of the driver circuit.

SPWM $m_a = 0.9$

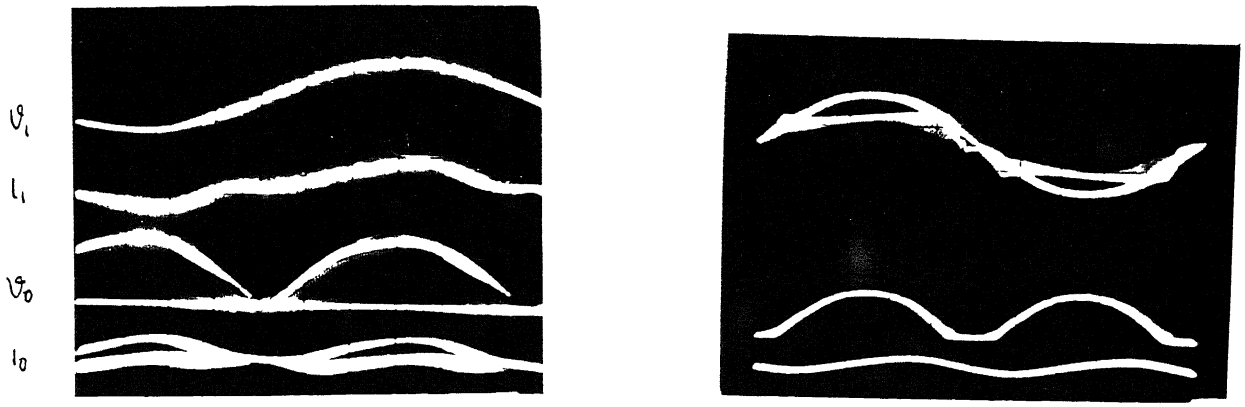

EPWM $m_a = 0.9$

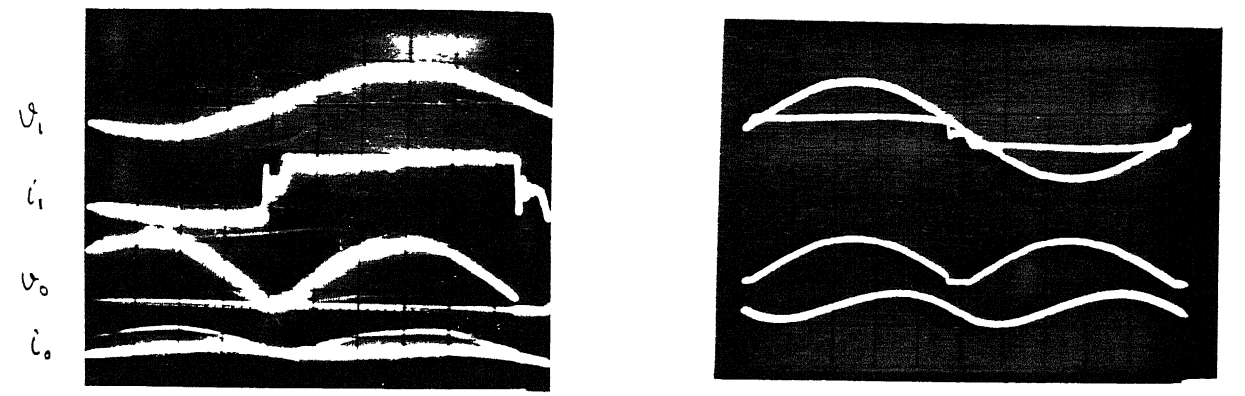

SEPWM $m_S = 0.9, m_E = 0.6$

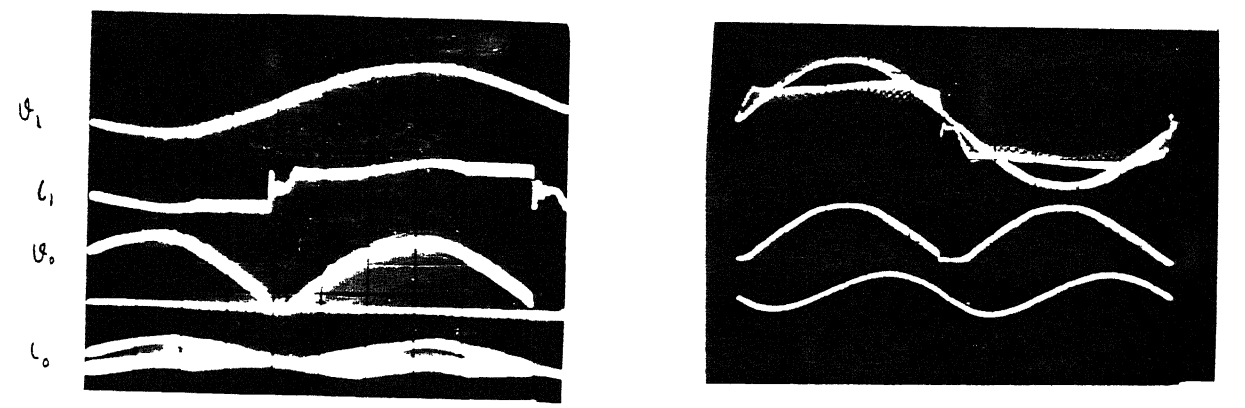

(a) (b)

Fig. 3.16 Input-Output waveforms of single-phase bridge converter.

(a) Without filter capacitor

0.9, m_E = 0.6 for SPWM. Fig. 3.16(a) shows the input-output waveforms without filter capacitor in the load circuit. The same waveforms with filter capacitor in the load circuit is shown in Fig. 3.16(b). It is evident from all the oscillograms that the input displacement angle ϕ is zero in all the three PWM schemes. The waveforms are improved with output filter capacitor.

Fig. 3.17 shows the frequency spectra of line voltage, line current and Fig. 3.18 shows the dc voltage and dc current for SPWM, EPWM and SEPWM control schemes.The experimental results of each EPWM and SPWM control scheme is taken at the modulation ratio of 0.9. The experiment of SEPWM control scheme with constant dc voltage at modulation ratio of 0.6 and rectified sinusoidal voltage at modulation ratio at 0.9, is carried out. The input voltage has only the fundamental component since it is sinusoidal. This evident from the frequency spectra. The same trend is observed in frequency spectra of input line current with negligible harmonic currents.

The harmonics in the line current waveform appear as sidebands, centred around the switching frequency (10kHz) and its multiples in SPWM scheme. In EPWM and SEPWM schemes, besides these sidebands, the low order odd harmonics with very small magnitudes are also present in the frequency spectra. In SEPWM the magnitudes of these order harmonics are lower than that in EPWM which is evident from Fig. 3.17(b). The frequency spectra of output voltage for these schemes (Fig. 3.17(a)) appears as sidebands centred around the switching frequency (10 kHz) and its

SPWM $m_a = 0.9$

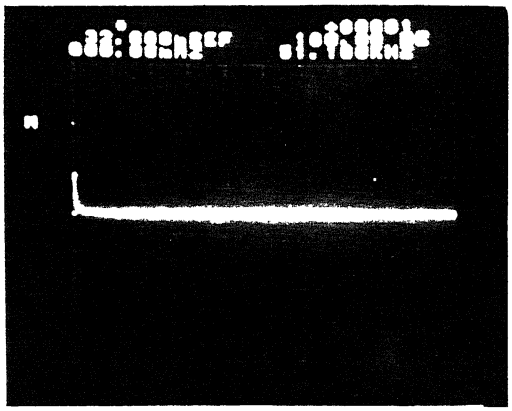

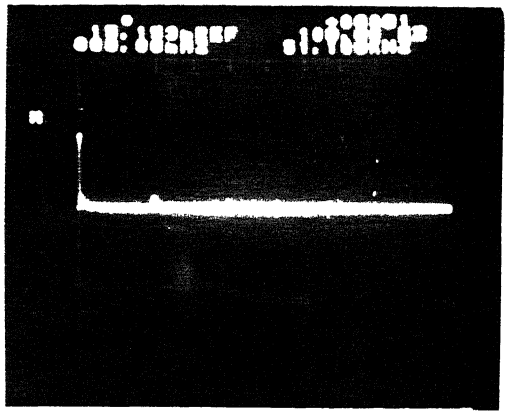

EPWM $m_a = 0.9$

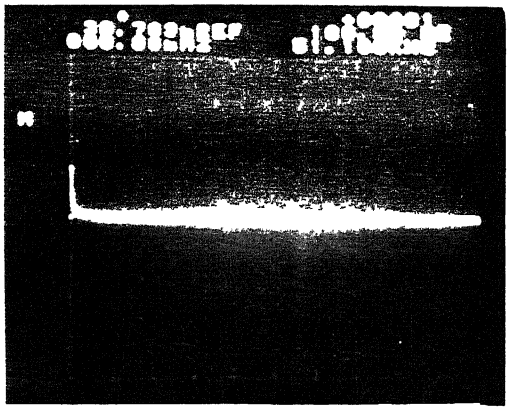

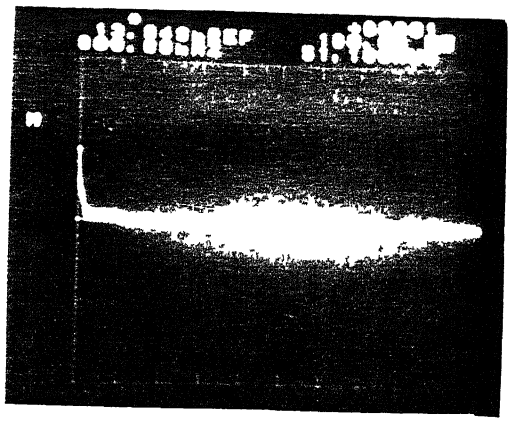

SEPWM $m_s = 0.9$, $m_\epsilon = 0.6$

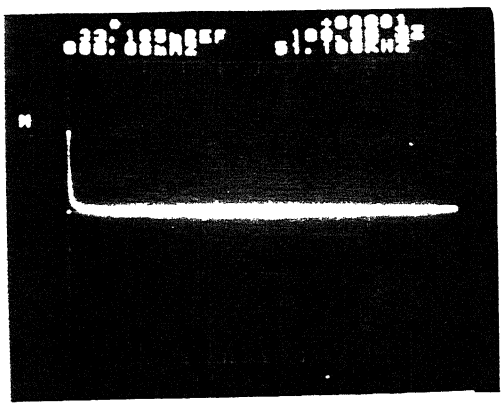

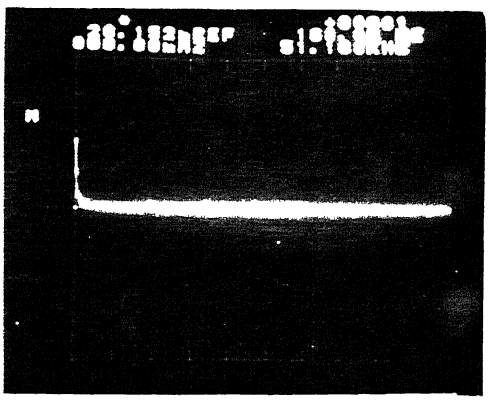

(a)

(b)

Fig. 3.17 Frequency spectra of

(a) Input line voltage (b) Input line current

SPWM $m_a = 0.9$

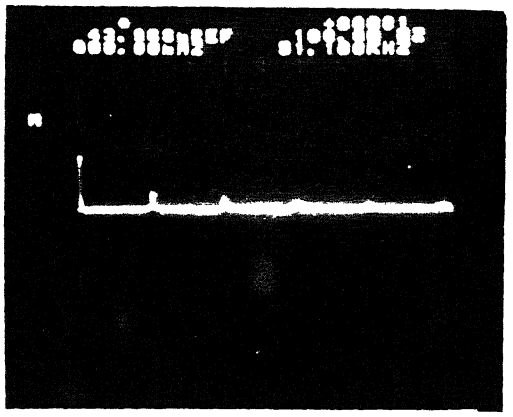

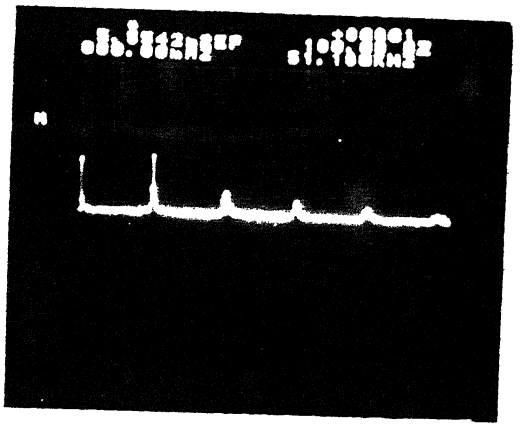

EPWM $m_a = 0.9$

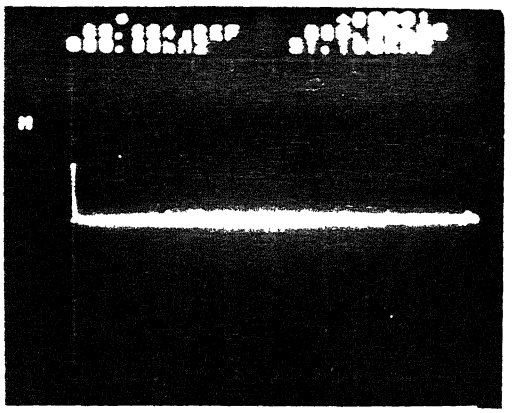

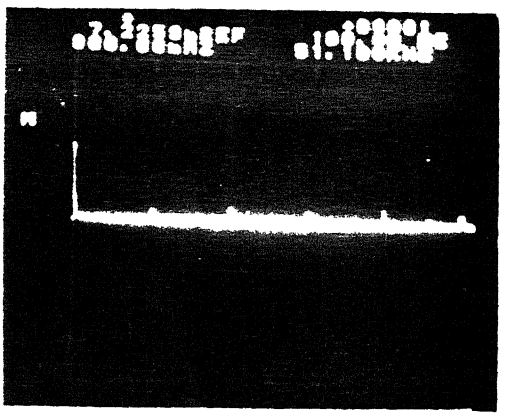

SEPWM $m_s = 0.9$, $m_E = 0.6$

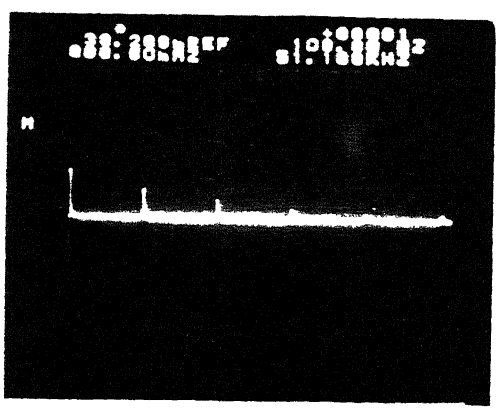

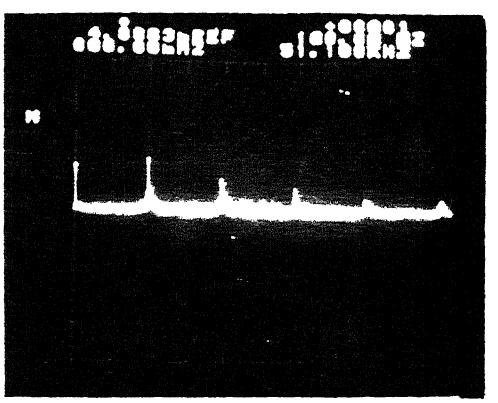

(a) (b)

Fig. 3.18 Frequency spectra of

(a) Output dc voltage (b) Output load current

multiples. The magnitudes of sidebands are more prominent in SEPWM than SPWM and EPWM. The magnitudes of sidebands in case of EPWM are negligibly small and odd ordered harmonics with very low magnitudes are spread throughout in the frequency spectra. Fig. 3.18(b) shows the frequency spectra of the load current in SPWM, EPWM and SEPWM. The harmonics in the load current appear as sidebands centred around the switching frequency. The magnitudes of sidebands are quite significant in SPWM and SEPWM than in the EPWM. In EPWM scheme, intermediate sidebands lower order odd harmonics are also present and spread out thoroughout the frequency spectra. Unlike in EPWM, the magnitudes of sidebands of SPWM and SEPWM reduces rapidly with the increase in the order of sideband.

These results are in close agreement with the theory of PWM control scheme.

3.6 CONCLUSION

The comparative study of PWM schemes shows that EPWM provides linear relationship between output voltage and amplitude modulation ratio. The SEPWM control scheme combines the good features of EPWM and SPWM output voltage. It has the drawback of constant output voltage. The input power factor remaining high and almost constant throughout the range of m_a. The input current harmonic factor is lower than the other two PWM schemes and it decreases with an increase in the modulation index. In SEPWM based battery charging circuit, to meet the requirement of

continuously varying voltage till the battery is fully charged, the m_S is varied with m_E equal to zero. Once the battery is fully charged the SPWM is switched over to SEPWM control scheme for better power factor. Small-sized filter is sufficient to eliminate the higher order harmonics. The experimental results from the laboratory setup varifies the basic principles of pulsewidth modulation control schemes.

CHAPTER - 4

CONCLUSION

4.1 CONCLUSION

In this thesis the comparative performance studies are presented for certain phase-controlled thyristor based three-phase converters. The half controlled symmetrical converter has been found to offer best performance among the other converters considered. The presence of freewheeling action not only reduces the harmonics in the output voltage. But also reduces the critical value of inductance, and as a result, for a given inductor, the usable range of converter for continuous current condition is extended. The high displacement factor and power factor, and low reactance power requirement are the some of the features of this converter. With the proper size of filter, the low order harmonics in the input line can be eliminated. For the medium and high power battery charging circuits, the three-phase half controlled symmetrical converter appears to be a good choice.

The comparative study of single-phase PWM ac-dc bridge converter using EPWM, SPWM and SEPWM controlled schemes is carried out. The EPWM and SPWM are well known PWM schemes. Another pulsewidth modulation scheme, Sine-Equal Pulsewidth Modulation (SEPWM), is proposed in this thesis. It is like a two-in-one control scheme, combining the good features of both EPWM and SPWM schemes in single control scheme. The high and almost

constant output voltage and input power factor are some of the good features realized using SEPWM. The SEPWM based converter can be operated as SPWM or EPWM controlled converter to meet any specific feature of these two schemes. In the low power battery charging circuit, the single-phase SEPWM bridge can be a good choice.

4.2 SUGGESTIONS FOR FUTURE WORK

The application of SEPWM control scheme present in this thesis may be extended to power supply applications. A complete UPS may be developed using PWM converter-inverter set. Different modulation schemes may be explored to improve the dc link voltage. The effect of different/same type of control techniques in converter-inverter pair may be studied for the improvement the performance of the inverter.

REFERENCES

[1] JOHN, A.O., ALEXENDER, E.E., and DAVID, J.P., Current harmonics, voltage distribution and powers associated with electric vehicle battery chargers distributed on the residential power system, IEEE Trans. Ind. Appl. IA-20, 1984, pp. 727.

[2] HOLTZ, Z. and SCHWELLENBERG, U., A new fast response current control scheme for line controlled converters, IEEE Trans. Ind. Appl. IA-19, 1983, pp. 579.

[3] PATEL, B.K. and DORADLA, S.R., Operating diagrams and minimum inductance estimation for fully-controlled converters with half controlled characteristics, Journal of the Institution Engineers (India), Vol. 62, pt. EL4, Feb. 1982.

[4] BHAT, P.S. and DUBEY, G.K., 3-phase regenerative converter with controlled flywheeling, IEEE Trans. Ind. Appl. IA-21, 1985, pp. 1431.

[5] STEFANOVIC, V.R., Power factor improvement with a modified phase controlled converter, IEEE Trans. Ind. Appl. IA-15, 1979, pp. 193.

[6] STRATFORD, R.P., Rectifier harmonics in power systems, IEEE Trans. Ind. Appl. IA-6, 1980, pp. 271.

[7] PATEL, H.K. and DUBEY, G.K., Modified sequence control technique for imrpoving the performance of regenerative bridge converters, IEEE Trans. Ind. Appl. IA-19, 1983, pp. 682.

[8] BHAT, P.S. and DUBEY, G.K., Two-stage sequentially operated regenerative converters with controlled flywheeling, IEEE Trans. Ind. Appl. IA-21, 1985, pp. 1441.

[9] OHNISHI, T. and OKITSU, H., Bias voltage controlled 3-phase converter with high power factor, IEEE Trans. Ind. Appl. IA-16, 1980, pp. 700.

[10] SEN, P.C. and DORADLA, S.R., Symmetrical and extinction angle control of solid state series motor drive, IEEE Trans. IECI-23, 1976, pp. 31.

[11] KATAOKA, T., MIZUMACHI, K. and MIYAIEI, J., A pulsewidth controlled ac to dc converter to improve power factor and waveforms of ac line current, IEEE Trans. Ind. Appl. IA-15, 179, pp. 670.

[12] PARIKH, P.D. and DORADLA, S.R., Equal pulse-width modulation control strategy for an AC to DC converter, Int. J. Electronics, 1983, Vol. 55, No. 3, pp. 339.

[13] DURGA PRASAD, N.V.P.R., DORADLA, S.R. and MURTHY, Y.V.V.S., Versatile digital firing schemes for pulse-width modulation AC-DC converters, Conf. Rec. Annu. Meet. IEEE Ind. Appl. Soc., 1984, pp. 826.

[14] KHAN, B.H., DORADLA, S.R. and DUBEY, G.K., A three phase AC-DC GTO thyristor converter employing equal pulsewidth modulation, IEEE IAS Annual Meeting, Oct. 1989.

[15] FUKAO, T. and MIYARI, S., AC-DC converter with improved power factor and current waveforms on ac side, Electrical Engg. in JAPAN, Vol. 94, No. 4, 1974, p. 89.

[16] DORADLA, S.R., NAGMANI, C. and SANYAL, S., A sinusoidal pulsewidth modulated three-phase ac-to-dc converter-fed dc motor drive, IEEE Trans. Ind. Appl., IA-21, 1985, pp. 1394.

[17] TURNBULL, F.G., Selected harmonic reduction in static dc-ac inverter , IEEE Trans. Ind. Appl., IA-21, 1985, pp. 562.

[18] PATEL, H.S. and HOFT, R.G., Generalized techniques of harmonics elimination and voltage control in thyristor inverters, Part I - harmonic elimination, IEEE Trans. Ind. Appl., IA-9, 1973, pp. 310.

[19] BROD, D.M. and NOVOTNY, D.W., Current control of VSI-PWM inverters, IEEE Trans. Appl., IA-21, 1985, pp. 562.

[20] PENKOWSKI, L.F. and PRUZINSY, E.K., Fundamentals of pulsewidth modulated power circuits, IEEE Trans. Appl., IA-8, 1972, pp. 584.

[21] BOOST, M.A. and ZIOGAS, P.D., State-of-the-art carrier PWM techniques; A critical evaluation, IEEE Trans. Appl., IA-24, 1988, pp. 271.

[22] BOSE, B.K., Evaluation of modern power semiconductor devices and future trend of converters, IEEE Trans. Appl., IA-25, 1989,pp. 790.

[23] DUBEY, G.K., DORADLA, S.R., JOSHI, A., and SINHA, R.M.K., Thyristorized power controllers, Wiley Eastern, 1986.

[24] DUBEY, G.K., Power semiconductor controlled drives, Prentice-Hall, 1989.

[25] MOHAN, N., UNDERLAND, T.M., and ROBBINS, W.P., Power electronics, John Wiley and Sons, 1989.

[26] PELLY, B.R., Thyristor phase-controlled converters and cycloconveters operation, control and performance, Wiley Inter-science, 1971.

[27] SEN, P.C., Thyristor DC drive, Wiley Inter-science, 1981.

APPENDIX - A

ROMBERG INTEGRATION METHOD

This method is used to evaluate numerically the integral

$$\int_a^b f(x)\,dx \qquad (1)$$

where f(x) is any single-valued function and a and b are finite. First it used the trapezoidal rule

$$T_{0,1} = (b-a)\left[\, f(a) + f(b) \,\right]/2$$

followed by repeated interval halving using the recursion relation

$$T_{N,1} = \frac{1}{2}\left\{ T_{N-1\ 1} + \frac{(b-a)}{2^{N-1}} \sum_{\substack{i=1 \\ \Delta i=2}}^{2^{N-1}} f\left[\, a + \frac{(b-a)}{2^N}\ i\ \right] \right\}$$

Then the Romberg sequence $\{ T_{N,J} \}$ are computed from the general extrapolation formula

$$T_{N,J} = \frac{4^{J-1}\ T_{N+1,j-1} - T_{N,J-1}}{4^{J-1} - 1}\ ,\ \text{for all } J \le J_{max},$$

$$\text{with } N = 0,1,\ldots,N_{max} - J+1$$

These Romberg sequences are arranged in simple tabular form as follows :

$$
\begin{array}{llllll}
T_{0,1} & T_{0,2} & T_{0,3} & T_{0,4} & T_{0,5} & \cdots\cdots\ T_{0,J} \\
T_{1,1} & T_{1,2} & T_{1,3} & T_{1,4} & T_{1,5} & \\
 & & & \vdots & \vdots & \\
T_{2,1} & T_{2,2} & T_{2,3} & & & \\
\vdots & \vdots & \vdots & & & \\
T_{N-2,1} & T_{N-2,2} & T_{N-2,3} & & & \\
T_{N-1,1} & T_{N-1,2} & & & & \\
T_{N,1} & & & & &
\end{array}
$$

Each of the sequences would converge to the true integral. The entry in the last column and last row is the most accurate approximation of true value.

Here the Romberg integration method is used to evaluate the coefficients of the Fourier expansion for a periodic function g(x). The Fourier expansion may be written

$$g(x) = g_o + \sum_{m=0}^{\infty} a_m \cos mx \quad \sum_{m=0}^{\infty} b_m \sin mx, \quad m = 0.1....,m_{max} \qquad (2)$$

where

$$g_o = \frac{p}{2\pi} \int_a^b g(x)\, dx \qquad (3)$$

$$a_m = \frac{p}{\pi} \int_a^b g(x) \cos mx\, dx \qquad (4)$$

$$b_m = \frac{p}{\pi} \int_a^b g(x) \sin mx \, dx \qquad (5)$$

where a and b are limits of integration, p number of pulses present in output during 2π.

The integrands for the integrals of (3), (4) and (5)

$$f_o(x) = p \, [\, g(x) \,]/2\pi$$

$$f_a(x) = p \, [\, g(x) \cos mx \,]/\pi$$

$$f_b(x) = p \, [\, g(x) \sin mx \,]/\pi$$

Therefore the integral (3), (4) and (5) can be written as

$$g_o = \int_a^b f_o(x) \, dx$$

$$a_m = \int_a^b f_a(x) \, dx$$

$$b_m = \int_a^b f_b(x) \, dx$$

The a_m and b_m are evaluated for $m = 0, 1, \ldots, m_{max}$ by repeatedly calling Romberg integration subroutine.

APPENDIX - B

EQUATIONS FOR NORMALIZED OUTPUT CURRENT FOR THREE-PHASE CONVERTER

(i) Fully-controlled bridge converter

$$i_N(\omega t) = \sin(\omega t-\phi) - \frac{m}{\cos\phi} + \left[\frac{m}{\cos\phi} - \sin\left(\frac{\pi}{3} + \alpha - \phi\right)\right] x$$

$$\exp\left\{\left[\alpha + \frac{\pi}{3} - \omega t\right]/\tan\phi\right\}$$

$$\alpha + \frac{\pi}{3} < \omega t \leq \alpha + \frac{2\pi}{3}$$

(ii) Half-controlled symmetrical bridge converter

mode 1 $\quad 0 \leq \alpha \leq 60^\circ$

$$i_N(\omega t) = \sin(\omega t-\phi) - \frac{m}{\cos\phi} + \left[\frac{m}{\cos\phi} - \sin\left(\frac{\pi}{3} + \alpha - \phi\right)\right] x$$

$$\exp\left\{\left[\alpha + \frac{\pi}{3} - \omega t\right]/\tan\phi\right\}$$

$$\alpha + \frac{\pi}{3} < \omega t \leq \alpha + \frac{2\pi}{3}$$

$$i_N(\omega t) = \sin\left(\omega t - \frac{\pi}{3} - \phi\right) - \frac{m}{\cos\phi} + \left[\frac{m}{\cos\phi} + I_N - \sin\left(\frac{\pi}{3} - \phi\right)\right] x$$

$$\exp\left\{\left[\frac{\pi}{3} - \omega t\right]/\tan\phi\right\}$$

$$\frac{\pi}{3} < \omega t \leq \alpha + \pi$$

where $i_N(\omega t) = I_N$ at $\omega t = \frac{2\pi}{3}$

mode 2 : $60^\circ < \alpha \leq 180^\circ$

$$i_N(\omega t) = \sin(\omega t - \frac{\pi}{3} - \phi) - \frac{m}{\cos\phi} + \left[\frac{m}{\cos\phi} - \sin(\alpha - \phi)\right] \times$$

$$\exp\left\{\left(2 + \frac{\pi}{3} - \omega t\right)/\tan\phi\right\}$$

$$\alpha + \frac{\pi}{3} < \omega t \leq \alpha + \frac{4\pi}{3}$$

$$i_N(\omega t) = -\frac{m}{\cos\phi} + \left[\frac{m}{\cos\phi} + I_N\right] \exp\left\{\left(\frac{4\pi}{3} - \omega t\right)/\tan\phi\right\}$$

$$\frac{4\pi}{3} < \omega t \leq \alpha + \pi$$

where $i(\omega t) = I_N$ at $\omega t = \frac{4\pi}{3}$

(iii) Half-controlled asymmetric bridge converter with one diode

mode 1 : $0^\circ < \alpha \leq 60^\circ$

$$i_N(\omega t) = \sin(\omega t - \phi) - \frac{m}{\cos\phi} + \left[\frac{m}{\cos\phi} - \sin\left(\frac{\pi}{3} + \alpha - \phi\right)\right] \times$$

$$\exp\left\{\left(\alpha + \frac{\pi}{3} - \omega t\right)/\tan\phi\right\}$$

$$\alpha + \frac{\pi}{3} < \omega t \leq \alpha + \frac{2\pi}{3}$$

mode 2 : $60^\circ < \alpha \leq 120^\circ$

$$i_N(\omega t) = \sin(\omega t - \phi) - \frac{m}{\cos\phi} + \left[\frac{m}{\cos\phi} - \sin\left(\alpha + \frac{\pi}{3} - \phi\right)\right] \times$$

$$\exp\left\{\left(\alpha + \frac{\pi}{3} - \omega t\right)/\tan\phi\right\}$$

$$\alpha + \frac{\pi}{3} < \omega t \leq \alpha + \pi$$

$$i_N(\omega t) = -\frac{m}{\cos\phi} + \left[\frac{m}{\cos\phi} + I_N\right] \exp\left\{\left[\pi - \omega t\right]/\tan\phi\right\}$$

$$\pi < \omega t \leq \alpha + \frac{2\pi}{3}$$

Where $i_N(\omega t) = I_N$ at $\omega t = \pi$.

(iv) Half-controlled asymmetric bridge converter with two diodes

mode 1 $0^\circ \leq \alpha \leq 30^\circ$

$$i_N(\omega t) = \sin(\omega t - \phi) - \frac{m}{\cos\phi} + \left[\frac{m}{\cos\phi} - \sin\left(\frac{\pi}{3} + \alpha - \phi\right)\right] x$$

$$\exp\left\{\left[\alpha + \frac{\pi}{3} - \omega t\right]/\tan\phi\right\}$$

$$\alpha + \frac{\pi}{3} < \omega t \leq \alpha + \frac{2\pi}{3}$$

mode 2 : $30^\circ < \alpha \leq 90^\circ$

$$i_N(\omega t) = \sin(\omega t - \phi) - \frac{m}{\cos\phi} + \left[\frac{m}{\cos\phi} - \sin\left(\frac{\pi}{3} + \pi - \phi\right)\right] x$$

$$\exp\left\{\left[\alpha + \frac{\pi}{3} - \omega t\right]/\tan\phi\right\}$$

$$\alpha + \frac{\pi}{3} < \omega t \leq \alpha + \frac{5\pi}{6}$$

$$i_N(\omega t) = \frac{1}{\sqrt{3}} \sin\left(\omega t - \frac{\pi}{6} - \phi\right) - \frac{m}{\cos\phi} + \left[\frac{m}{\cos\phi} + I_N - \frac{1}{\sqrt{3}} \sin\left(\frac{2\pi}{3} - \phi\right)\right] x$$

$$\exp\left\{\left[\alpha + \frac{5\pi}{3} - \omega t\right]/\tan\phi\right\}$$

$$\frac{5\pi}{6} < \omega t \leq \alpha + \frac{2\pi}{3}$$

where $i_N(\omega t) = I_N$ at $\omega t = \frac{5\pi}{6}$

mode 3 : $90^\circ < \alpha \leq 150^\circ$

$$i_N(\omega t) = \frac{1}{\sqrt{3}} \sin(\omega t - \frac{\pi}{6} - \phi) - \frac{m}{\cos\phi} + \left[\frac{m}{\cos\phi} - \frac{1}{\sqrt{3}} \sin\left[\alpha + \frac{\pi}{6} - \phi\right]\right] x$$

$$\exp\left\{\left[\alpha + \frac{\pi}{3} - \phi\right]/\tan\phi\right\}$$

$$\alpha + \frac{\pi}{6} < \omega t \leq \frac{7\pi}{6}$$

$$i_N(\omega t) = -\frac{m}{\cos\phi} + \left[\frac{m}{\cos\phi} + I_N\right] \exp\left\{\left[\frac{7\pi}{6} - \omega t\right]/\tan\phi\right\}$$

$$\frac{7\pi}{6} < \omega t \leq \alpha + \frac{2\pi}{3}$$

where $i_N(\omega t) = I_N$ at $\omega t = \frac{7\pi}{6}$.

APPENDIX - C

MANUFACTURER'S SPECIFICATION FOR POWER MOSFET IRFPE 50

$V_{(BR)DSS}$	800	Volts
$I_{DSS(max)}$	8.1	Amps
$P_{D(max)}$	180	Watts
$R_{DS(on)}$	1	Ohm
$g_{FS(min)}$	6.7	Mho
$V_{GS(th)}$	4.0	Volts
$C_{iss(max)}$	3.0	nfd
t_r	110	nsec
t_f	95	nsec

E - 1993 - M - BAI - STU